

T-3507

HYDRAULIC FRACTURE FLUID LEAKOFF ANALYSIS

by
Claude H. Joseph

**ARTHUR LAKES LIBRARY
COLORADO SCHOOL of MINES
GOLDEN, COLORADO 80401**

ProQuest Number: 10782980

All rights reserved

INFORMATION TO ALL USERS

The quality of this reproduction is dependent upon the quality of the copy submitted.

In the unlikely event that the author did not send a complete manuscript and there are missing pages, these will be noted. Also, if material had to be removed, a note will indicate the deletion.



ProQuest 10782980

Published by ProQuest LLC (2018). Copyright of the Dissertation is held by the Author.

All rights reserved.

This work is protected against unauthorized copying under Title 17, United States Code
Microform Edition © ProQuest LLC.

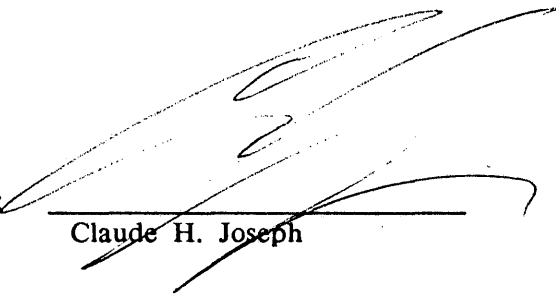
ProQuest LLC.
789 East Eisenhower Parkway
P.O. Box 1346
Ann Arbor, MI 48106 – 1346

T-3507

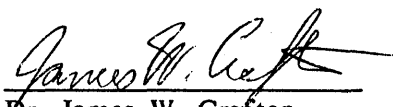
A thesis submitted to the Faculty and the Board of Trustees of the Colorado School of Mines in partial fulfillment of the requirements for the degree of Master of Science (Petroleum Engineering).

Golden, Colorado

Date: April 13, 1988

Signed: 

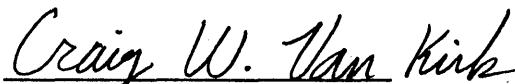
Claude H. Joseph

Approved: 

Dr. James W. Crafton
Thesis Advisor

Golden, Colorado

Date: April 13, 1988



Dr. Craig W. Van Kirk
Professor and Head,
Petroleum Engineering Department

Abstract

Hydraulic fracture fluid leakoff is a problem involving the flow of filtered non-Newtonian fluids through a dynamic filter cake into the reservoir rock. Prior studies have used simplified flow equations, derived by assuming static filtration and piston-like fluid displacement in the formation. These oversimplify the relation between flow through the filter cake and into the formation.

A new equation was developed in this inquiry to describe flow through a dynamically changing filter cake, from initial "spurt" through a period of cake maturation to pseudo-steady state flow. The equation describing cake flow was then linked to a two-phase, one-dimensional Implicit Pressure/Explicit Saturation (IMPES) reservoir simulator. This exploited the strengths of both procedures: a more accurate picture of cake flow drawn from a dynamic filtration experiment, and the description of two-phase flow given by reservoir simulation.

Rock and fluid properties were shown to have a much greater impact on leakoff than suggested by the literature. While the shallow depth of filtrate penetration validates the assumption of piston-like displacement, the pressure wave reaches far into the reservoir. This implies that leakoff is controlled more by the fluids resident in the formation than those imbibed during leakoff. It was found that leakoff is typically less than that predicted by traditional methods. This suggests the possibility that sandouts are caused by excessive leakoff into micro-fractures present in the reservoir.

Table of Contents

	<u>Page</u>
ABSTRACT	iii
LIST OF FIGURES	vi
LIST OF TABLES	viii
ACKNOWLEDGEMENTS	ix
CHAPTER 1	
Literature Review	1
1.1 Classical Leakoff Theory	1
1.2 Newer Leakoff Formulations	10
CHAPTER 2	
Theoretical Model	12
2.1 Fluid Flow in the Filter Cake	12
2.2 Fluid Flow in the Reservoir	13
CHAPTER 3	
Investigative Procedure	14
3.1 Fluid Flow in the Cake	15
3.2 Fluid Flow in the Reservoir	27
3.3 Cake/Reservoir Linkage	31
CHAPTER 4	
Results	33
CHAPTER 5	
Conclusions	58

	<u>Page</u>
CITED REFERENCES	62
UNCITED REFERENCES	64
NOMENCLATURE	67
APPENDIX A	
Derivation of Traditional Leakoff Formulation	70
APPENDIX B	
Derivation of New Leakoff Formulation	73
APPENDIX C	
Derivation of IMPES Formulation	76
APPENDIX D	
Derivation of Least Squares Regression	82
APPENDIX E	
Coefficient Regression Program Listing	84
APPENDIX F	
Leakoff Simulation Program Listing	86

List of Figures

	<u>Page</u>
Figure 1 - Howard and Fast	4
Figure 2 - Hall and Dollarhide	6
Figure 3 - Howard and Fast, Various Models	16
Figure 4 - Hall and Dollarhide, Various Models	17
Figure 5 - Gulbis, Various Models	18
Figure 6 - McDaniel, et al, Various Models	19
Figure 7 - McDaniel, et al, Data Extrapolation	20
Figure 8 - Penny, et al, Various Models	21
Figure 9 - Roodhart, Various Models	22
Figure 10 - Roodhart, Data Extrapolation	23
Figure 11 - Sinha, Various Models	24
Figure 12 - Williams, Various Models	25
Figure 13 - Geometric Mesh Spacing	28
Figure 14 - Relative Permeability Curves	30
Figure 15 - Capillary Pressure Curve	31
Figure 16 - Leakoff Comparison: Various Equations	34
Figure 17 - Leakoff Comparison: Including Reservoir Effects	35
Figure 18 - Base Case: Pressure Wave	37
Figure 19 - Base Case: Water Saturation Front	38
Figure 20 - Base Case: Leakoff Rate	39
Figure 21 - Base Case: Leakoff Volume	40

		<u>Page</u>
Figure 22	- Base Case: Mass Balance	41
Figure 23	- Water Viscosity Effect on Leakoff Volume	43
Figure 24	- Water Viscosity Effect on Pressure Wave	44
Figure 25	- Oil Viscosity Effect on Leakoff Volume	45
Figure 26	- Oil Viscosity Effect on Pressure Wave	46
Figure 27	- Total Compressibility Effect on Leakoff Volume	47
Figure 28	- Total Compressibility Effect on Pressure Wave	48
Figure 29	- Initial Water Saturation Effect on Leakoff Volume	49
Figure 30	- Initial Water Saturation Effect on Pressure Wave	50
Figure 31	- Permeability Effect on Leakoff Volume	52
Figure 32	- Permeability Effect on Pressure Wave	53
Figure 33	- Porosity Effect on Leakoff Volume	54
Figure 34	- Porosity Effect on Pressure Wave	55
Figure 35	- Initial Pressure Drop Effect on Leakoff Volume	56
Figure 36	- Initial Pressure Drop Effect on Pressure Wave	57

List of Tables

	<u>Page</u>
Table 1 - Comparison of values found by regression on Equation B.6	60
Table 2 - Simulation Input Data	61

Acknowledgements

With much appreciation for the efforts of my committee members; Dr. James W. Crafton, Dr. John D. Wright and Dr. Ramona M. Graves. Thanks also to Dr. Crafton for suggesting this topic and supporting my efforts at developing a new approach to fracture fluid leakoff. A great deal of gratitude for the guidance of Dr. Craig W. Van Kirk and to the Tenneco, Pennzoil, Shell, Standard Oil and Union Pacific companies for their support over the last several years.

Many thanks to my wife Nancy, who endured through all the sightseeing along the road to completion of this work. This thesis is dedicated to Charlotte Rachel Joseph and Hannah Frances Joseph who are my future, Rosemarie Joseph and Hans Hugo Joseph who were my inspiration.

Chapter 1
Literature Review

1.1 Classical Leakoff Theory

The pioneering work in hydraulic fracture fluid leakoff was done by Howard and Fast in 1957¹. They introduced three "fracture fluid coefficients" representing the perceived dominant mechanisms of filtrate leakoff: 1) viscosity and relative permeability effects of the fracture fluid; 2) viscosity and compressibility effects of the reservoir fluid; and 3) wall building effects of the fracture fluid.

They asserted that the processes could in reality act together through an inverse combination of coefficients. Later Smith² proposed use of the analogy to parallel resistors. Without theoretical basis, he suggested that:

$$\frac{1}{C_{\text{eff}}} = \frac{1}{C_{\text{I}}} + \frac{1}{C_{\text{II}}} + \frac{1}{C_{\text{III}}} \quad (1.1)$$

The coefficients as defined by Howard and Fast¹ are shown below. The first two coefficients may be calculated from known fluid and reservoir properties:

Relative Permeability Coefficient -

$$C_{\text{I}} = 0.0469 \left[\frac{k \delta P \phi}{\mu} \right]^{\frac{1}{2}}, \text{ ft/min}^{\frac{1}{2}} \quad (1.2)$$

Compressibility Coefficient -

$$C_{II} = 0.0374 \delta P \left[\frac{k \phi c}{\mu} \right]^{\frac{1}{2}}, \text{ ft/min}^{\frac{1}{2}} \quad (1.3)$$

Wall Building Coefficient -

The third coefficient, related to wall building, must be determined by laboratory experimentation:

$$C_{III} = 0.0328 \left[\frac{m}{2A_c} \right], \text{ ft/min}^{\frac{1}{2}} \quad (1.4)$$

Howard and Fast used a static filtration experiment to simulate filter cake buildup, which led to the familiar relationship that cumulative fluid throughput is proportional to the square root of time elapsed:

$$V = m \sqrt{t} + V_{sp} \quad (1.5)$$

The experimental data was collected by filtration of three types of refined oils as well as two proprietary fluid-loss additives in paraffin-base and mixed-base crude oils. The refined oils ranged from 30 - 500 cp and the crude oils from 1.4 - 4.0 cp. Core wafers were cut with a cross-sectional area of 18.4 sq cm and 0.5 cm in thickness and varied in permeability from 0.75 - 99.2 md.

The experimental apparatus consisted of a core wafer locked into the bottom of the pressure cell, which was then filled with fluid and sealed. Pressure was applied to the top of the static fluid column in the cell, and filtrate collected

from the bottom. The analysis was conducted at the estimated bottom hole treating temperature (125 degrees Fahrenheit) and differential pressure (from 100 to 900 psi).

Some results of Howard and Fast's experimental work are presented in Figure 1 for one of the above-mentioned paraffin-base fluid systems. The filtration data approximates the expected straight line behavior when plotted against the square root of elapsed time.

It was over 25 years later that Settari³ presented a theoretical derivation describing the process of flow through a growing filter cake, as presented in Equation 1.3 above (see Appendix A). Among the chief assumptions made was the supposition that cake buildup is directly proportional to the throughput volume. This is the primary characteristic of a static test, ie. - infinite, steady state deposition of fluid-loss additives on the filter.

As seen in Figure 1, the assumption of infinite cake buildup may not always be entirely valid for a static test, even less so in dynamic situations. Concern for an accurate representation of downhole conditions led to much discussion about static versus dynamic drilling fluid filtration^{4,5}. In this research, it was found that there was a very large difference between the two, largely attributed by Outmans⁵ to limitations on cake deposition by shear stresses.

Hall and Dollarhide^{6,7} proposed the dynamic filtration experiment to simulate fracturing conditions more realistically. Fracture fluid was circulated outside a

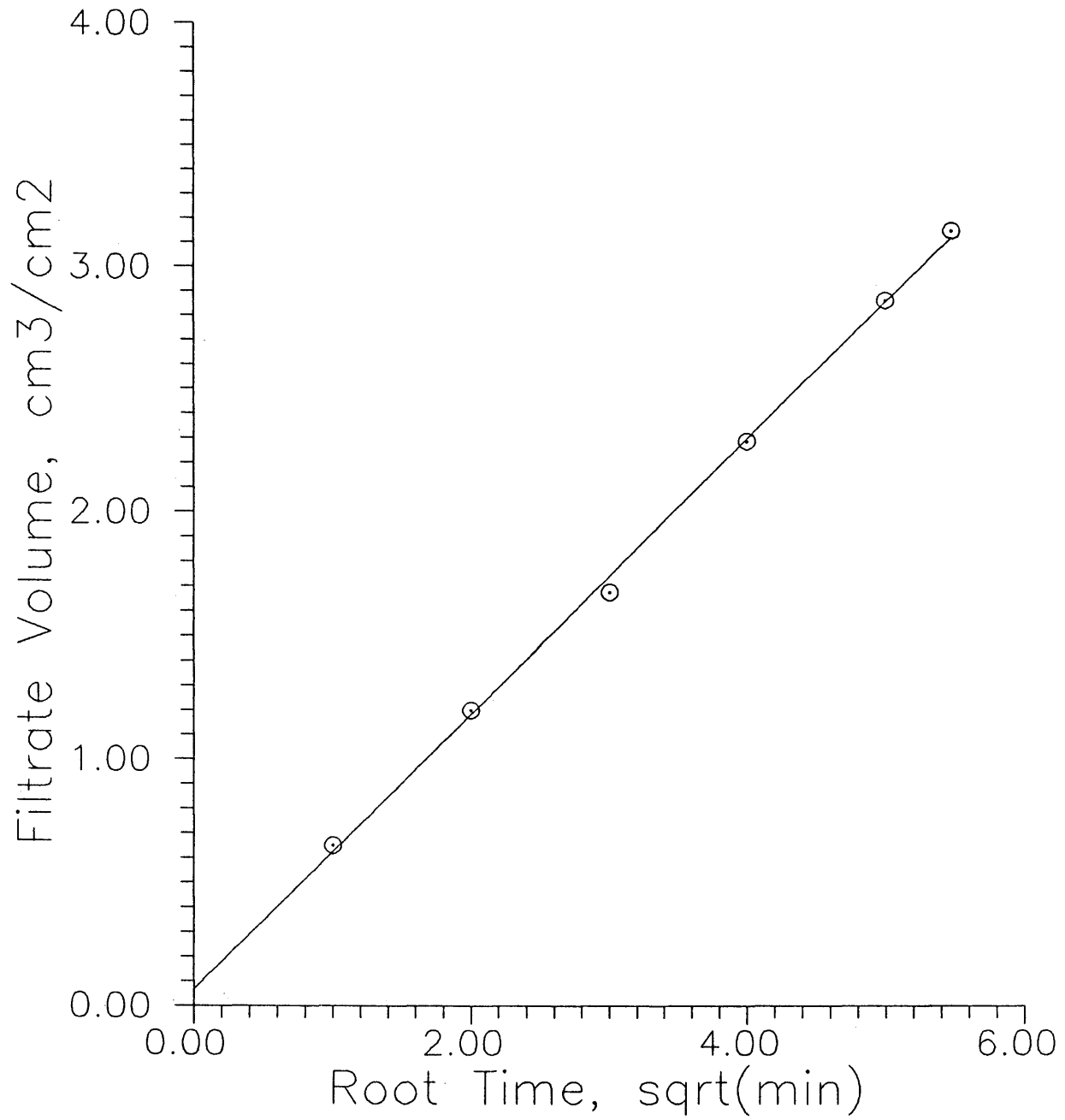
Figure 1 - Howard and Fast

Figure 1 - Filtrate volume versus square root of time for data of Howard and Fast¹.

hollow core at simulated reservoir conditions, and filtrate collected from the center of the core. Their experiments showed three distinct phases of filter cake performance: initiation, buildup, and limitation.

The first phenomenon involves the extremely high leakoff rate before enough material has been deposited to control flow, thus leakoff occurs as if there were no fluid-loss additives present. The buildup phase occurs when the rate of deposition is directly proportional to volume throughput, and is analogous to the static leakoff described by Howard and Fast¹. The third stage occurs when cake growth is limited by the shear rate imposed by the fluid velocity in the fracture.

The first two occur in common with the static laboratory test. In the dynamic test, buildup was in a constant state of transition with the third stage, of cake limitation. Results from one of the Hall and Dollarhide tests on Bandera sandstone are presented in Figure 2, along with the straight line approximation proposed by the authors.

Dynamic fluid-loss testing was investigated further by Williams⁸ in 1970. He recognized the above three flow regimes, and presented equations for fluid-loss velocity:

Before Cake Formation -

$$v = \frac{V_{sp}}{t_{sp}} \quad (\text{control by reservoir properties}) \quad (1.6)$$

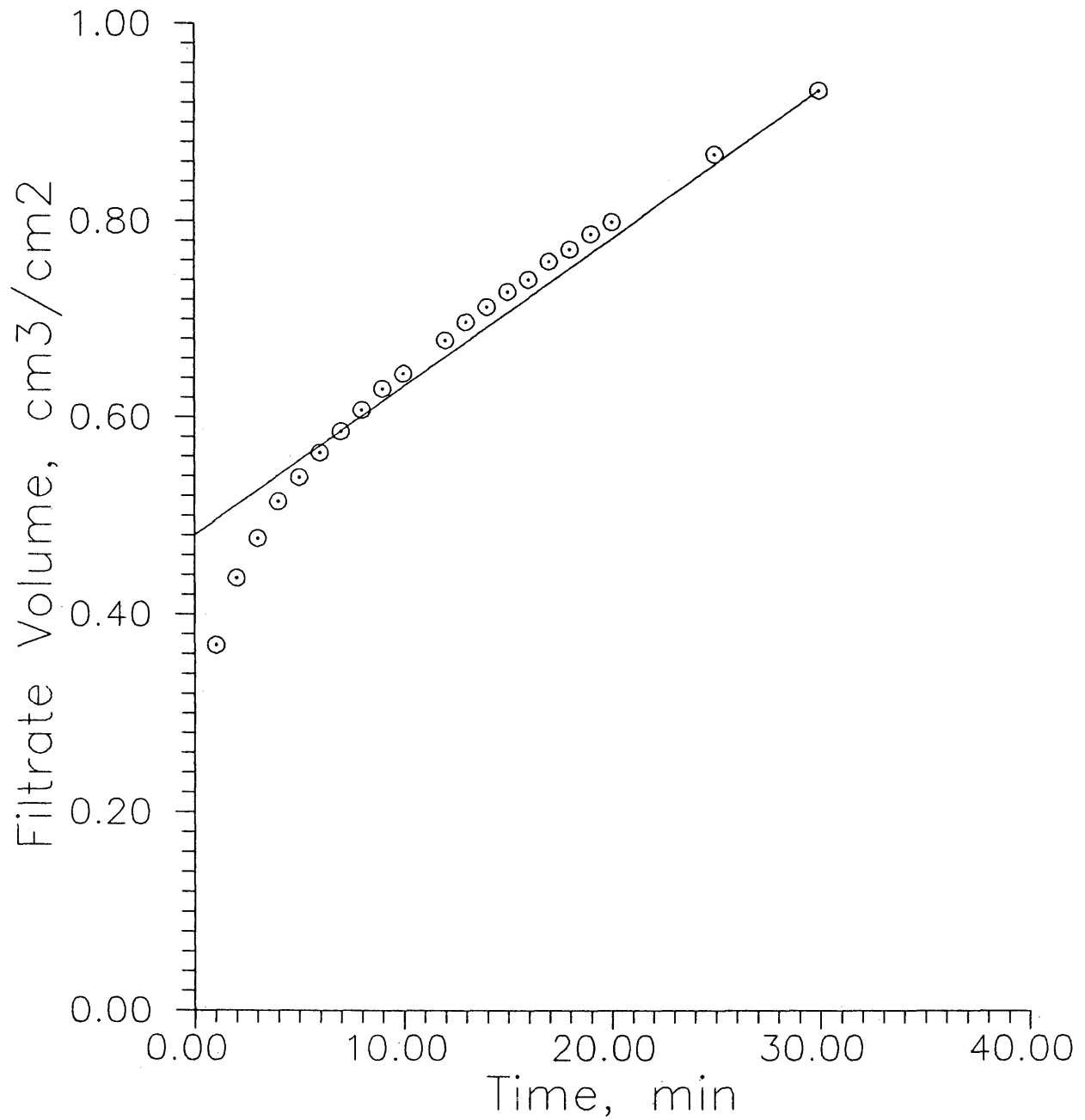
Figure 2 - Hall and Dollarhide

Figure 2 - Filtrate volume versus time for data of Hall and Dollarhide⁶. Straight line approximation given by the authors.

During Cake Formation -

$$v = \frac{C_{vc}}{\sqrt{t}} \quad \text{(control by reservoir properties and filter cake)} \quad (1.7)$$

After Cake Formation -

$$v = \text{constant} \quad \text{(control by steady-state filter cake)} \quad (1.8)$$

Williams used the equations developed by Kristianovich and Zeltov to describe fracture geometry, integrating them with the two zones he speaks of as being present in a fracturing treatment: 1) fracture portion open long enough for filter cake to have formed and control flow, and 2) the fracture tip, where leakoff is controlled by fluid and reservoir properties. He suggested, in effect, combining the static equations of Howard and Fast¹ and the dynamic equations of Hall and Dollarhide^{6,7} to achieve a more realistic model of fracture leakoff simulation.

The next paper to address the problem was written by Sinha⁹. He was the first to deviate from modelling a physical phenomenon, and focused instead on the relationship between static and dynamic tests. It was his contention that, contrary to previous investigations, dynamic fluid-loss was less than or equal to static loss. He suspected more efficient plugging of the pores in a dynamic test, while more highly permeable bridges could be permitted to form in a static test.

The heart of the research by Sinha was an experimental setup that allowed for both static and dynamic tests to be run. Virtually all of the conclusions drawn from the inquiry concern the impact of the equipment on the experiment.

Gulbis¹⁰ noted that the fluid rheology plays an important part in leakoff behavior, and questioned the resemblance between fluids mixed in a lab blender and those flowing in a hydraulic fracture. An empirical relationship was used to describe dynamic fluid leakoff phenomena, a variation of Equation 1.5 (the dependent variable in this case is time, not the square root of time):

$$V = m t + V_{sp} \quad (1.9)$$

McDaniel, et al¹¹ presented an experimental setup designed to perform both static and dynamic filtration tests at the pressure and temperature anticipated at fracturing conditions. The experiment also incorporated planar flow in a simulated fracture, rather than annular flow outside a core. They concluded that static and dynamic testing produced nearly identical leakoff results for Newtonian fluids, while dynamic testing was necessary to describe highly non-Newtonian fluids.

Penny, et al¹² also found that large discrepancies in laboratory filtration results could be attributed to core preparation and fluid mixing procedures. They concluded that, at low rates of shear, static and dynamic tests gave the same outcome. At higher shear rates and pressure drops, they proposed that:

$$V = m t^n + V_{sp} \quad (1.10)$$

Roodhart¹³ also found that static tests were misleading, due to the occurrence of fluid shear in a realistic fracture. He also looked at differential pressure across the cake formed and the effect of rock permeability. Roodhart concluded that the leakoff coefficient is not dependent on rock permeability (but that the spurt volume "...appears to be a function of the square root of permeability for all fluids tested.>").

Hagoort, et al¹⁴ studied waterflood-produced hydraulic fractures using a fluid-loss coefficient involving the square root of time. In 1983, Veatch^{15,16} mentions the work of Howard and Fast¹ and Settari³ regarding fluid loss coefficients, but gives tacit approval to the static fluid loss test by giving leakoff coefficient units in $\text{ft}/\text{min}^{\frac{1}{2}}$. Later in the paper he mentions the work of Hall and Dollarhide, etc. as being indicative of the need for further research into the discrepancy between static and dynamic testing.

Crawford¹⁷ observed the need to adjust the static leakoff test. He stated that one must "...multiply the laboratory C factor ... by 1.5, to provide a 50% safety factor." Since dynamic filtration should exhibit higher leakoff than a static one, this observation supports the dynamic nature of leakoff. Using this safety factor, Crawford reported successfully fracturing over 100 wells without any screenouts.

1.2 Newer Leakoff Formulations

A radically new formulation was proposed by Clark and Barkat¹⁸. Using an empirical relationship borrowed from biology, wherein the action of digestive enzymes on a substrate is characterized by¹⁹:

$$[V] = A_1 t + B_1 (1 - e^{-bt}) \quad (1.11)$$

The authors propose a modified equation for cumulative fluid leakoff volume:

$$V = u_d t + V_{sp} (1 - e^{-bt}) \quad (1.12)$$

This correlation has significance in that it is the first to combine what Hall and Dollarhide^{6,7} observed, ie. - initiation, buildup and limitation, into a single equation. At early times, during initiation and buildup, both terms are significant. As time increases the exponential term approaches zero, and the relationship becomes equal to Equation 1.9 above. It's main detractor is the empirical nature of the relationship, since the authors fail to derive the equation from any theory of fluid flow in porous media.

Settari³ proposed a model of flow through the filter cake with flow in the reservoir proper. He incorporated cake erosion, cake compaction and the viscosity effect due to differences between fracture and laboratory fluid rheologies. He also discussed relative permeability effects, the influence of capillary

pressure, along with dispersion and mixing in the invaded zone. He then solved the more complex equations by an iterative Newton-Raphson scheme on a very fine grid.

Chapter 2 - Theoretical Model

The model used in this study is a synthesis of the ideas presented by Settari³ and Clark and Barkat¹⁸, as well as new insights into leakoff behavior. The intent is to reevaluate the application of traditional static filtration results to field work. The relationship between the cake and reservoir flow is of particular interest. The dynamic filtration model appears to be the most complete representation of cake formation and fluid flow through the cake, given the constraints of laboratory experimentation. As for flow from the cake into the formation, the most appropriate model to use is a one dimensional, two phase flow reservoir simulator. The combination of these two models permits one to investigate the cake/reservoir flow relationships.

2.1 Fluid Flow in the Filter Cake

The literature recognizes various phenomena affecting cake formation, including; initial cake growth¹, cake erosion and compaction^{6,7}, and viscosity effects³. The dynamic laboratory test is recognized as coming closest to approximating actual filtrate leakoff under field conditions^{11,13}. The problem lies not in the experiment, but in its interpretation. While the traditional static test is interpreted with a square root of time relationship, the dynamic test is interpreted with a straight time relationship. In reality, the proper interpretation is a combination of the two.

At early times, as the cake is rapidly forming, the static model applies⁸. When the cake begins to stabilize, due primarily to the shear effects of the

fracture fluid flowing past, the dynamic model begins to better describe the leakoff⁸. A correlation has been developed in this thesis to describe the volumetric relationship (see Appendix B), in a format similar to that proposed by Clark and Barkat¹⁸. The new formulation for limited cake growth (Equation B.6) is not empirical, but based entirely upon Darcy's Law:

$$V = A \ln(t) + B t + C \quad (\text{B.6})$$

2.2 Fluid Flow in the Reservoir

A simple Implicit Pressure/Explicit Saturation (IMPES) one-dimensional, two-phase reservoir simulator is employed to describe fluid flow in the reservoir beyond the cake (see Appendix C). This method allows for the investigation of effects traditionally presumed to have negligible impact. These include the study of two phase flow in the invaded zone, capillary pressure effects, varying mobility ratios, and changing pressure at the fracture face.

The method first solves an "N x N" matrix for the average water pressure of each grid block at the next time level. This matrix is created by setting all pressure values in Equation C.19 (the Pressure Equation) to the new time level. This is the implicit part of the IMPES procedure. Once the new pressures are known the new water saturations may be calculated from Equation C.21 (the Saturation Equation) explicitly. This is possible since there is only one unknown in the Saturation Equation (Sw_i), while three are present in the one-dimensional Pressure Equation (the pressure at a node and its two neighbors - P_{i-1} , P_i , P_{i+1}).

Chapter 3 - Investigative Procedure

The approach involved a two step process. Filtration data were matched to a relationship which combines elapsed time, pressure drop across the filter cake and cumulative volume throughput (Equation B.6). The data were obtained from the work of Howard and Fast¹ (Figure 5), Hall and Dollarhide⁷ (Figure 4), Williams⁸ (Figure 13), Sinha⁹ (Figure 5), Gulbis¹⁰ (Figure 6), McDaniel, et al¹¹ (Figure 7), Penny, et al¹² (Figure 17), and Roodhart¹³ (Figure 1a). All presented dynamic filtration data with the exception of Howard and Fast¹. The only authors to submit actual data points were Howard and Fast¹ and Hall and Dollarhide⁷, the others simply offered curves representing cumulative leakoff volume versus elapsed time.

These curves, with or without data points shown, were enlarged on a copier until they could readily be digitized by using a straight edge to find the coordinates of a number of locations on each curve. The cumulative volume data were normalized in each case, dividing by the cross sectional area of the core (except in the case of McDaniel, et al¹¹, where the core dimensions were never specified). A least squares technique was employed to match these data sets to Equation B.6 (see Appendix D).

The second step used the one-dimensional, two-phase IMPES reservoir simulator to model the infinite-acting reservoir behavior. The two steps were then linked through the pressure/volume boundary condition comparisons.

3.1 Fluid Flow in the Cake

A procedure was developed to perform a least squares regression procedure on dynamic filtration data in order to solve for the constants A, B, and C in Equation B.6 (see Appendix D). The least squares regression was coded in FORTRAN and used to evaluate the coefficients from the work of the above listed authors. Results of the various matches are shown in Table 1 (Page 59). The sum of the squared residuals (a measure of the quality of the curve fit) ranged from a high of .156 for the data of McDaniel, et al (indicating a poor fit) to a low of .000026 for the data of Williams (indicating a good fit). (The fit of the McDaniel data is misleading, since the authors never provided a cross-sectional area for their core. This led to much higher numbers for filtrate volume in the matching process, since the units given are actually in cm^3 rather than cm^3/cm^2). Residuals from the fitting of the static leakoff equation are also presented. This shows that the new model provides a better match since the average residual, or error, is about 15% of the residual from the static equation.

The corresponding plots may be seen in Figures 3 - 12. The data presented in Figure 3 is from Howard and Fast, and the new equation does not significantly improve the fit obtained by the linear regression on a square-root-of-time plot, as in Figure 1. This seems reasonable for a static test. The remaining plots in Figures 4 - 12 represent dynamic filtration data from the above sources. In each case the data was fitted to the three different models: 1) Static (volume versus square root of time), 2) Dynamic (volume versus time), and 3) The new model (Equation B.6). In no case was the fit significantly improved to the naked eye by

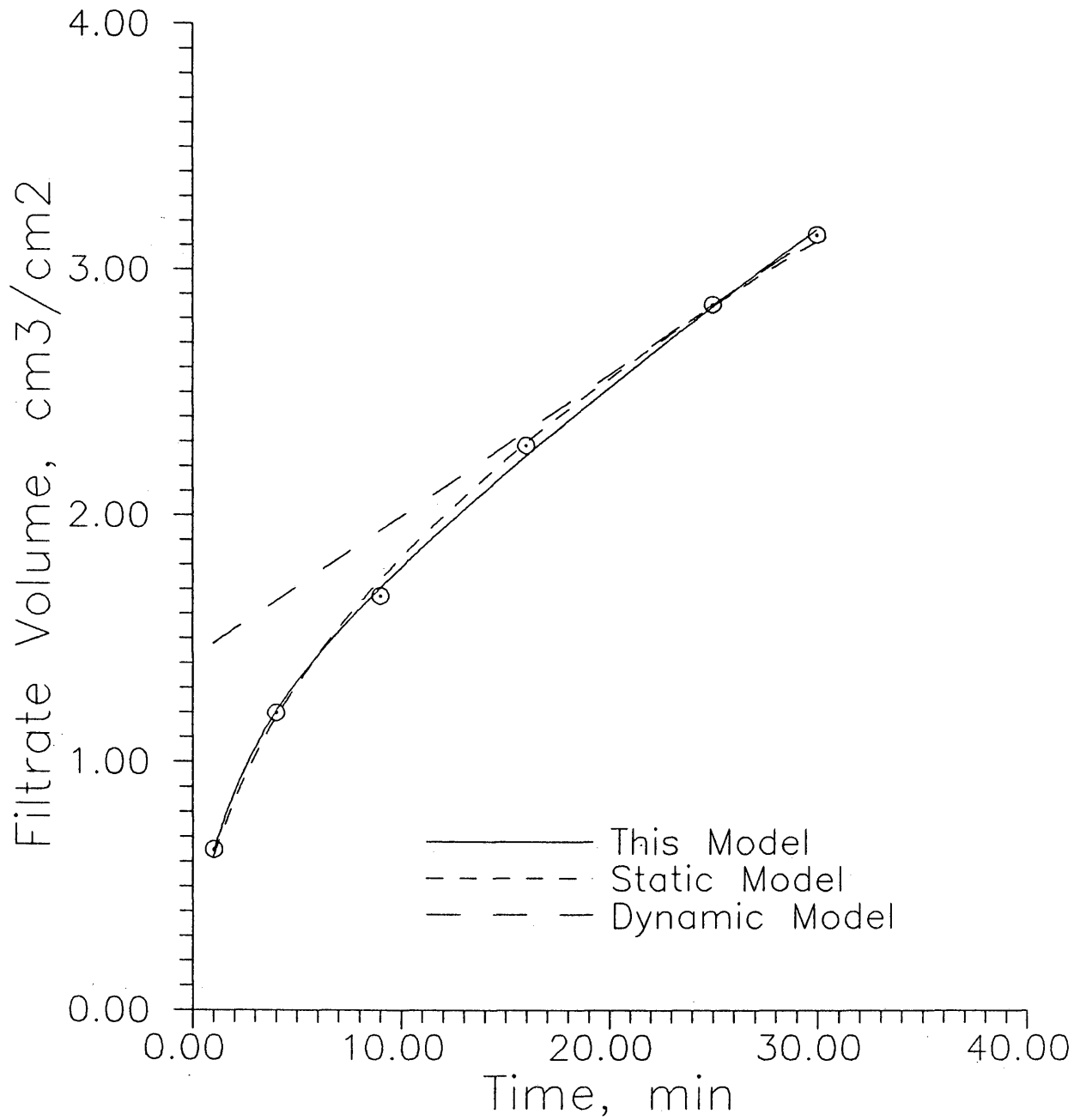
Figure 3 - Howard and Fast, Various Models

Figure 3 - Filtrate volume versus time for data of Howard and Fast¹. Data points fit with various models.

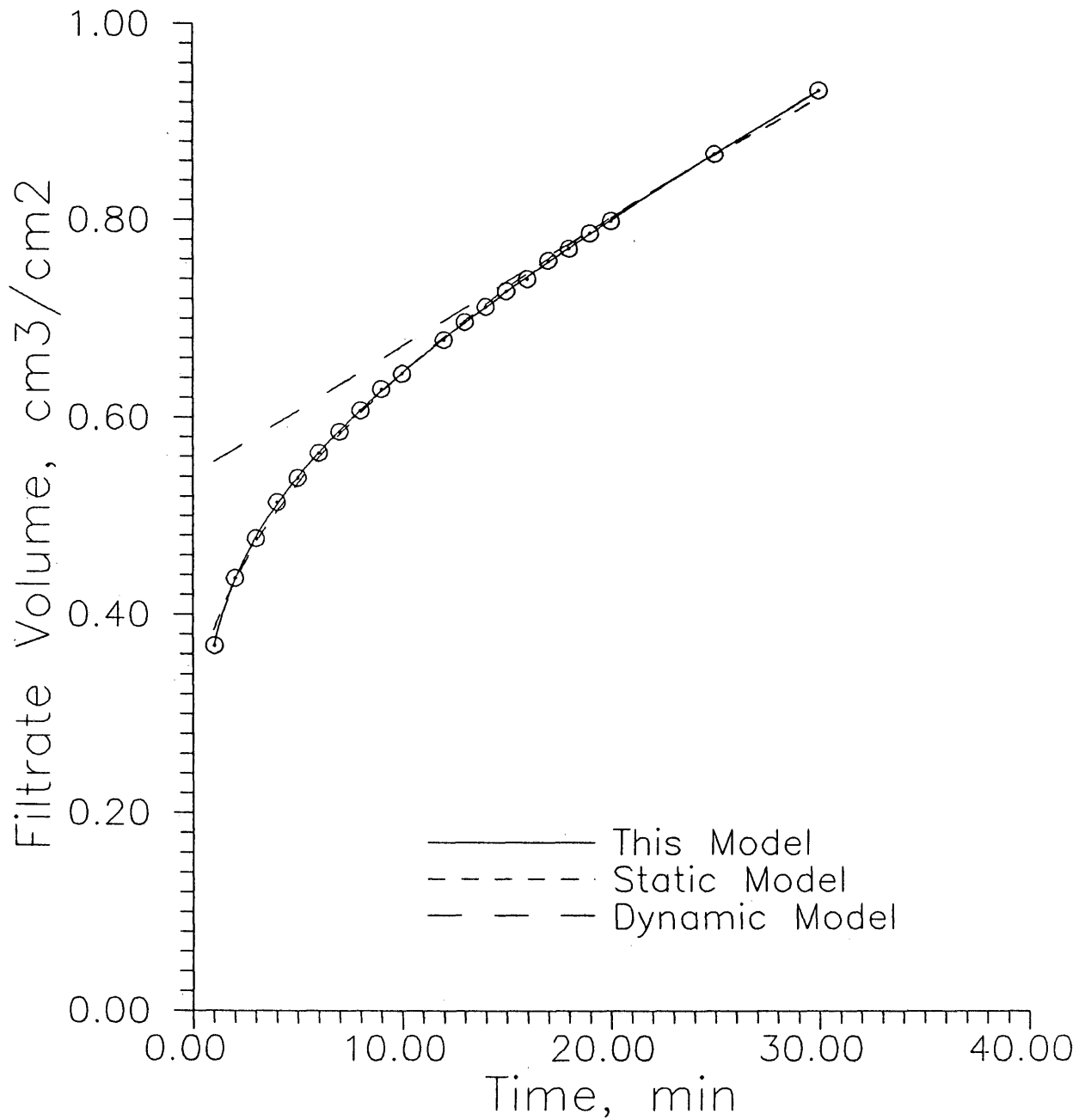
Figure 4 - Hall and Dollarhide, Various Models

Figure 4 - Filtrate volume versus time for data of Hall and Dollarhide⁶. Data points fit with various models.

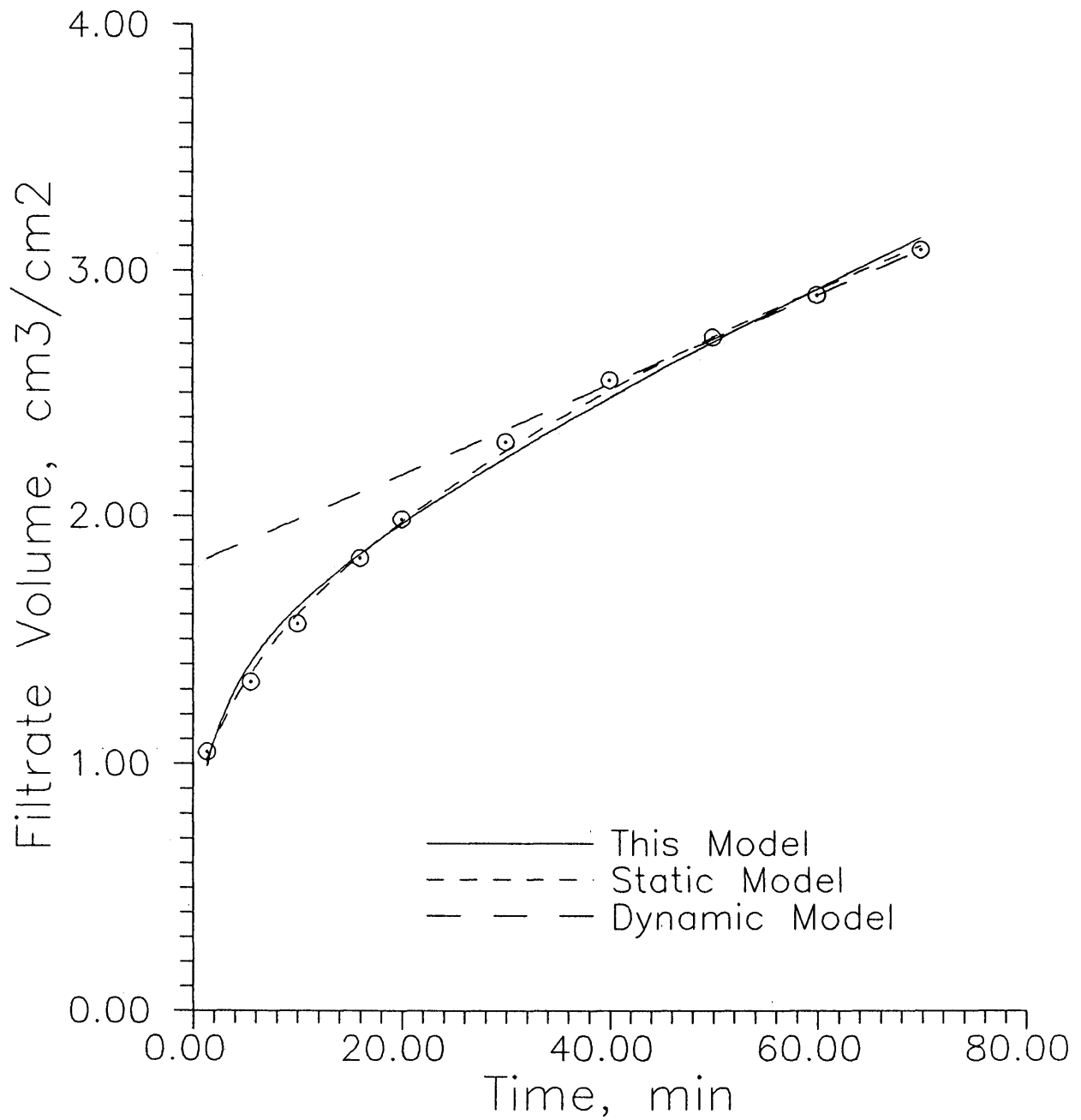
Figure 5 - Gulbis, Various Models

Figure 5 - Filtrate volume versus time for data of Gulbis¹⁰. Data points fit with various models.

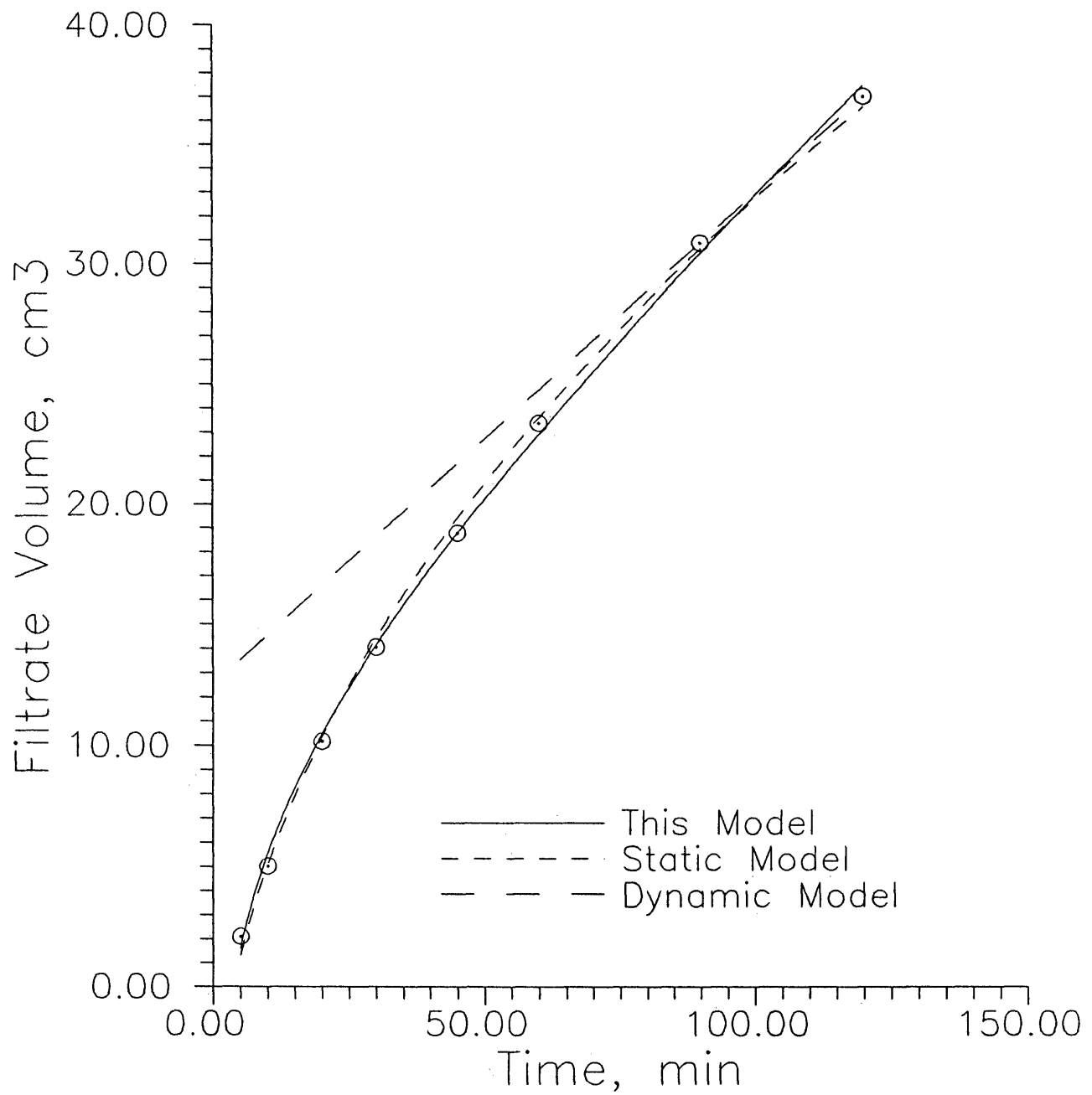
Figure 6 - McDaniel, et al, Various Models

Figure 6 - Filtrate volume versus time for data of McDaniel, et al¹¹. Data points fit with various models.

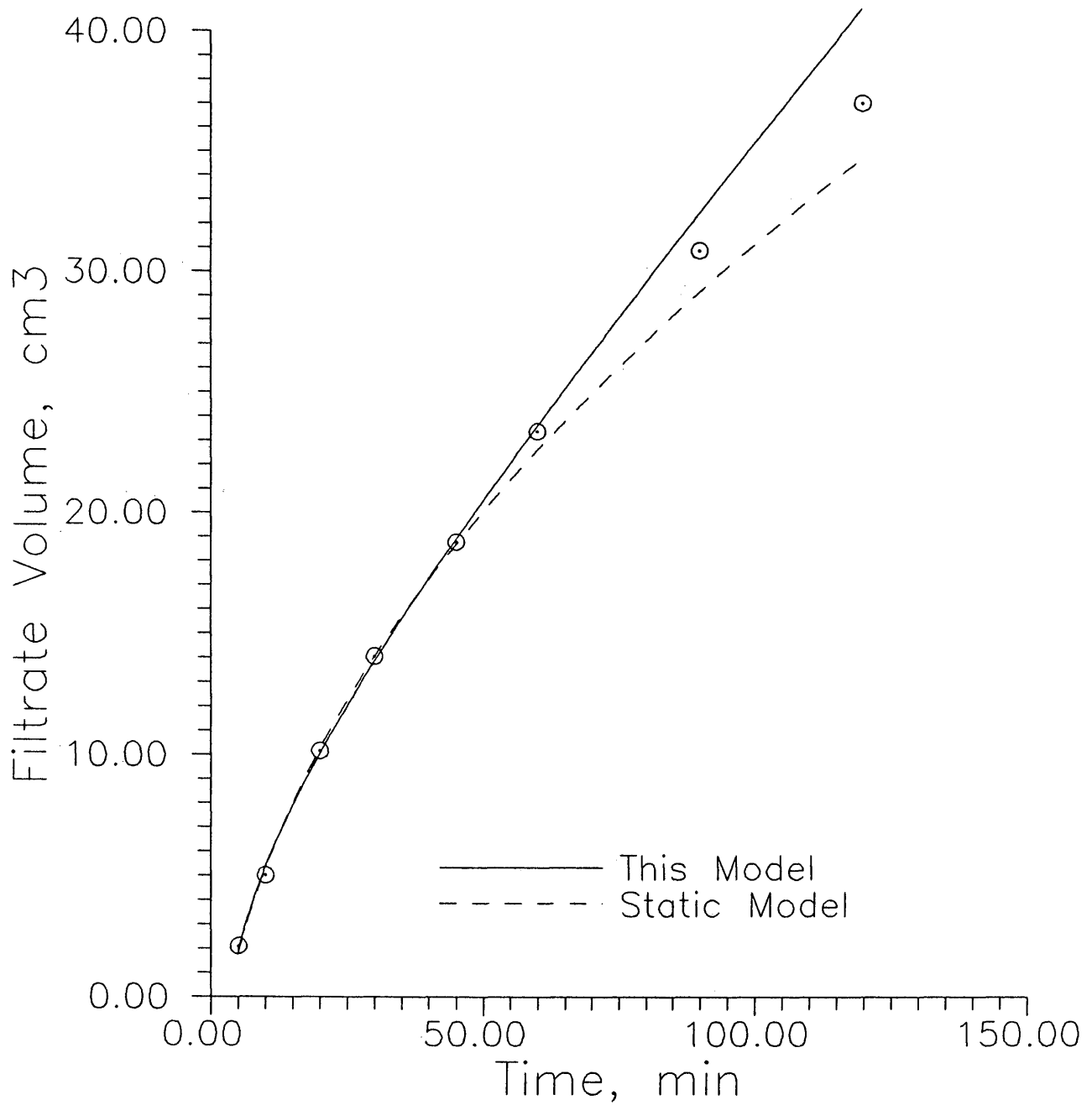
Figure 7 - McDaniel, et al, Data Extrapolation

Figure 7 - Filtrate volume versus time for data of McDaniel, et al¹¹. Extrapolated from data prior to 50 minutes.

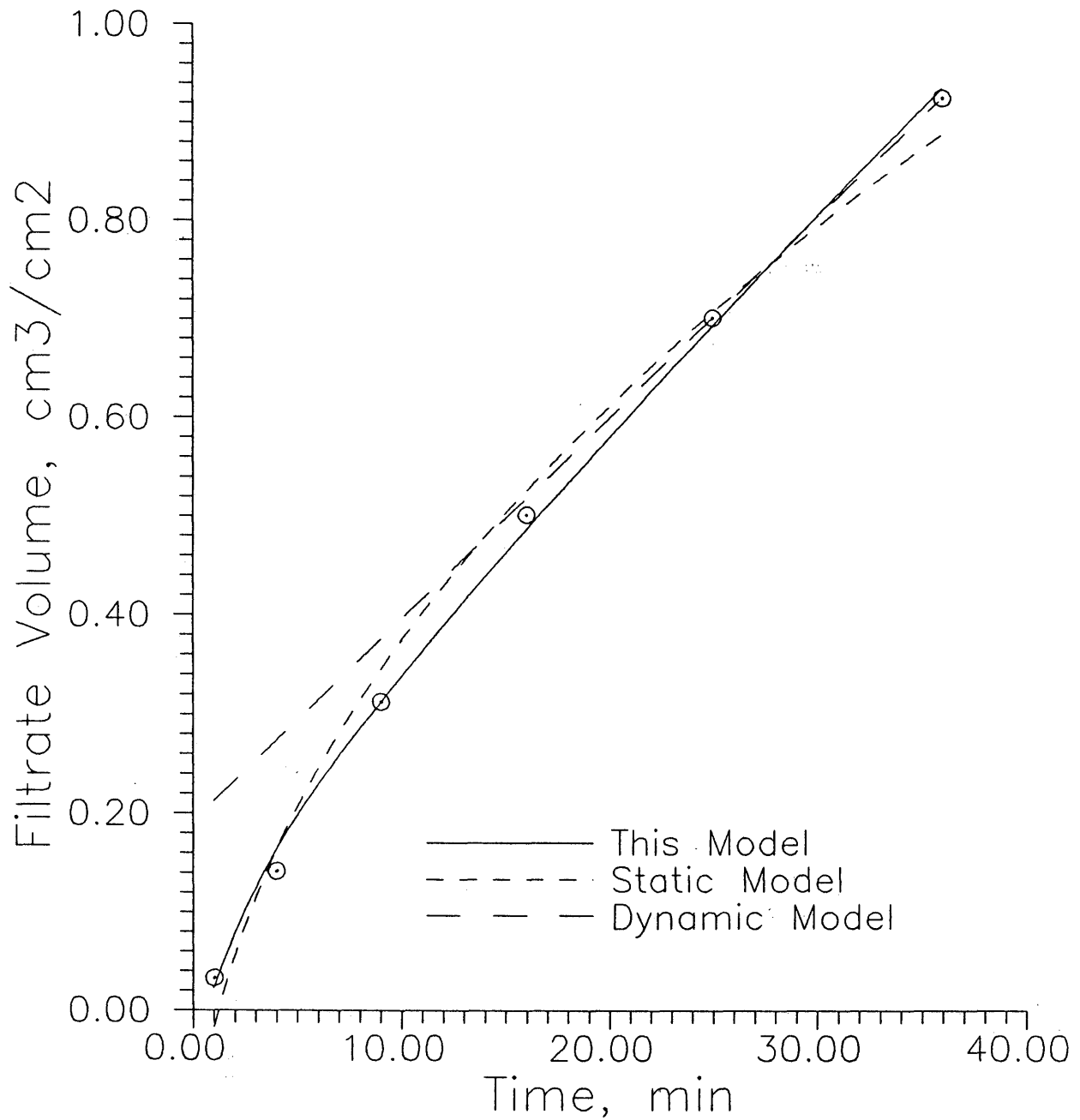
Figure 8 - Penny, et al, Various Models

Figure 8 - Filtrate volume versus time for data of Penny, et al¹². Data points fit with various models.

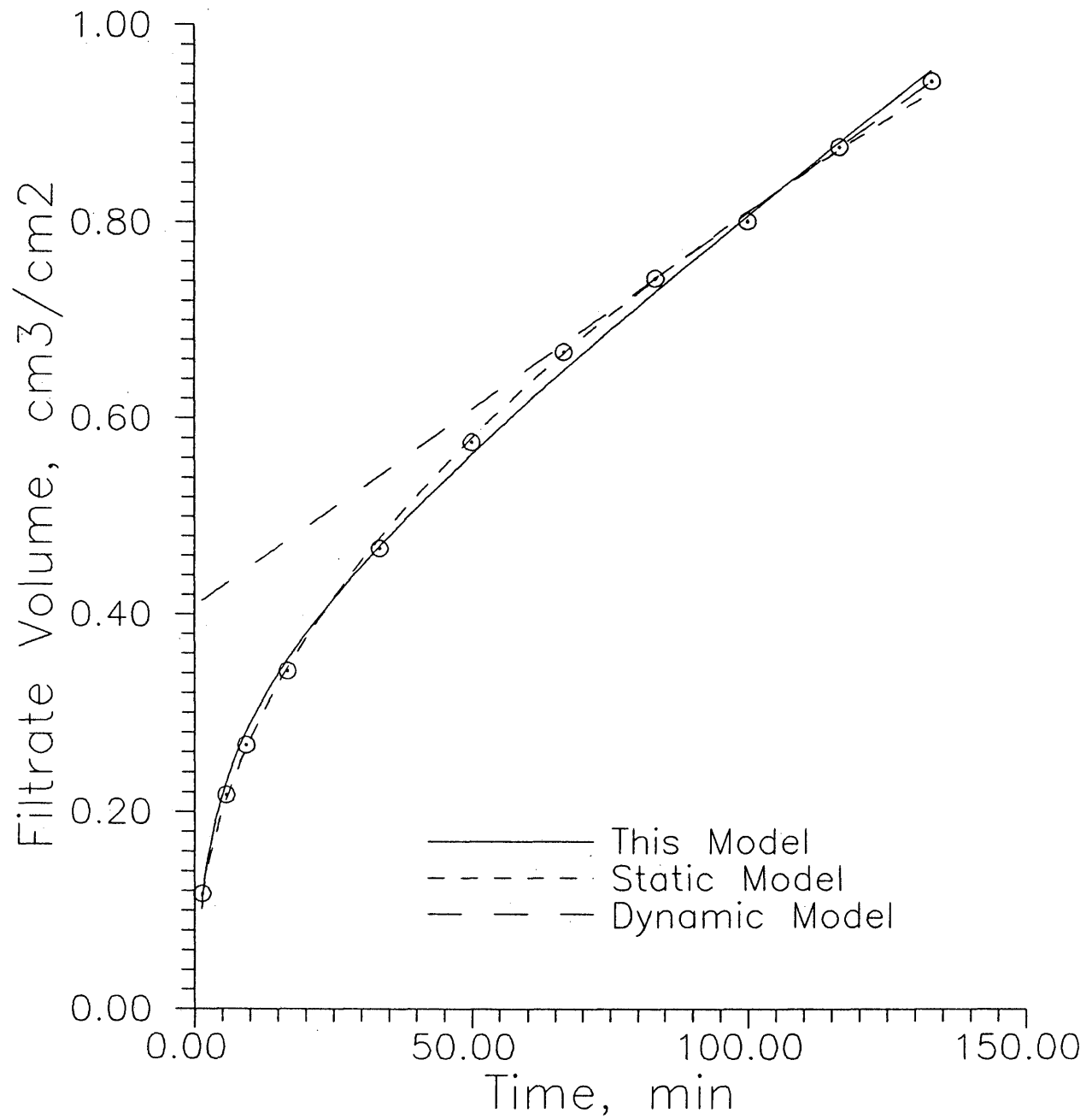
Figure 9 - Roodhart, Various Models

Figure 9 - Filtrate volume versus time for data of Roodhart¹³. Data points fit with various models.

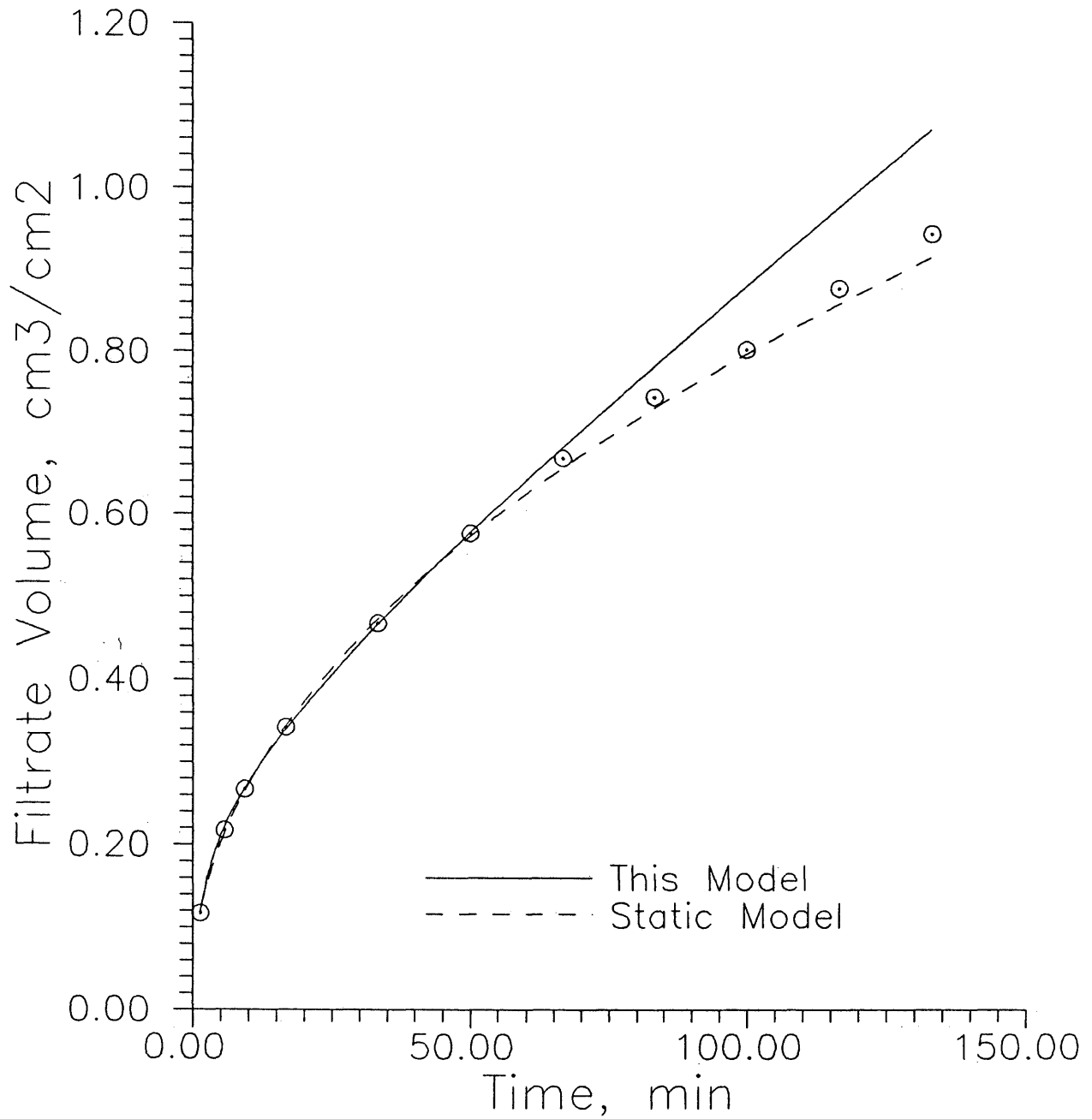
Figure 10 - Roodhart, Data Extrapolation

Figure 10 - Filtrate volume versus time for data of Roodhart¹³. Extrapolated from data prior to 50 minutes.

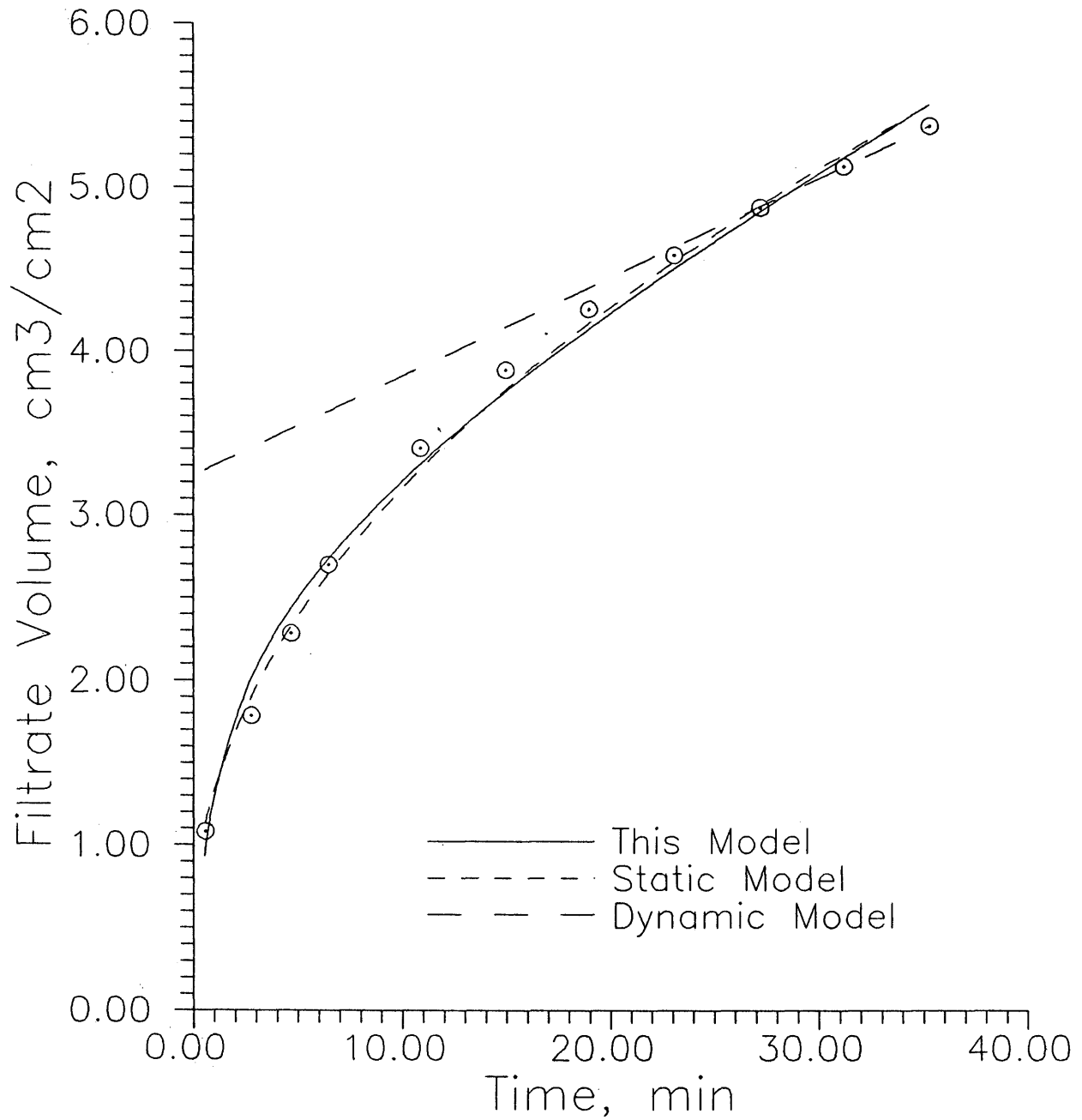
Figure 11 - Sinha, Various Models

Figure 11 - Filtrate volume versus time for data of Sinha⁹. Data points fit with various models.

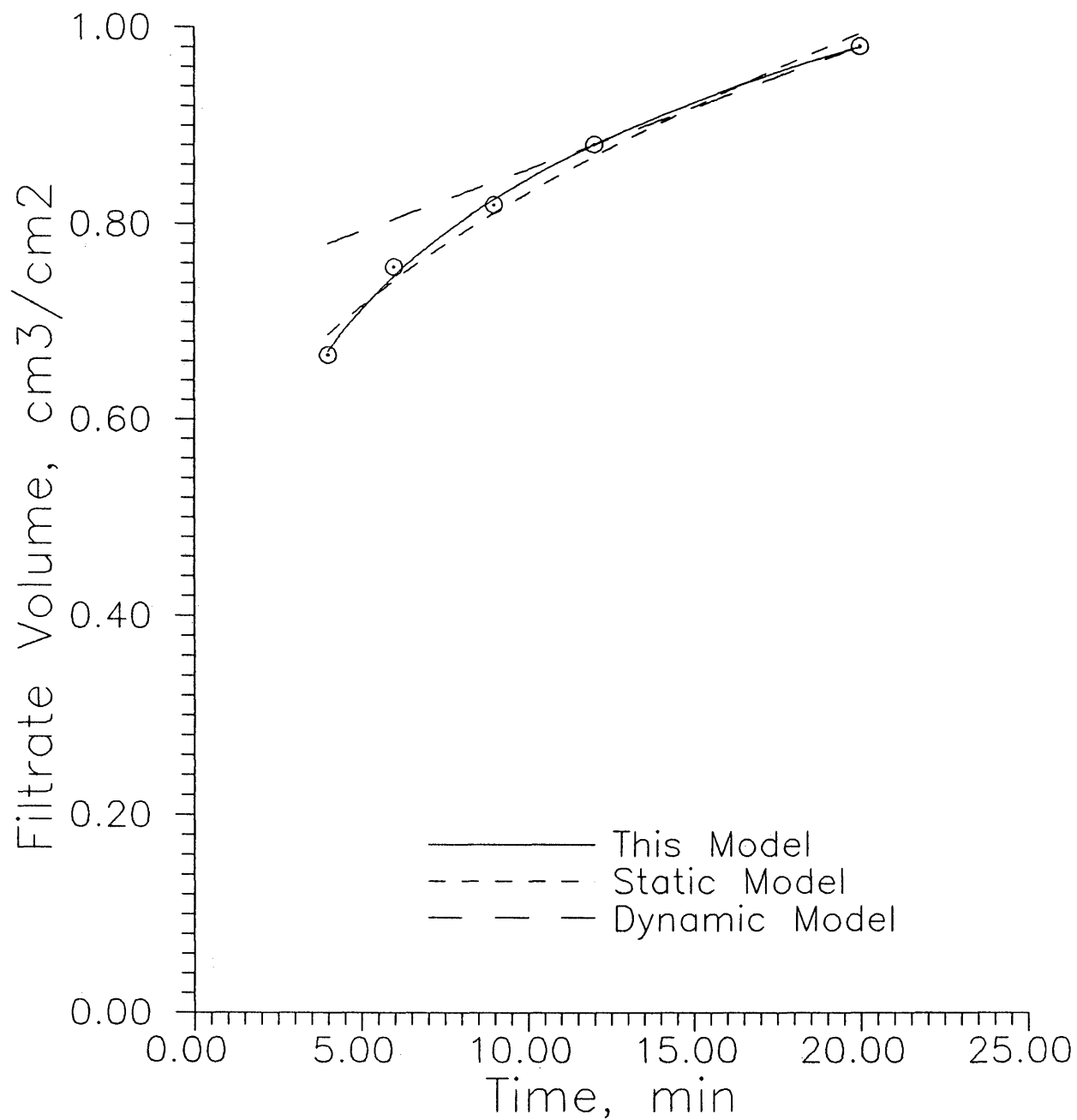
Figure 12 - Williams, Various Models

Figure 12 - Filtrate volume versus time for data of Williams⁸. Data points fit with various models.

using Equation B.6 over a static model. Figures 7 and 10 were created by fitting the model to early data (prior to 50 minutes), and extrapolating to the end of the test. Both graphs show the underestimation of the static model, caused by the assumption of infinite cake buildup. The new model overestimates the leakoff, indicating that cake buildup is occurring at a higher rate than anticipated by the model, a possible indication that the test was too short in duration to achieve pseudo-steady state behavior.

In every case other than Sinha and Williams (Figures 11 and 12) the square root of time relation provides less cumulative leakoff after two hours than the new model. This should be expected, as the new model does not permit infinite, steady state deposition of fluid-loss additives which would tend to limit flow.

The volume versus time relationship, however, overestimates the early flow due to its neglect of cake buildup. Additionally, the straight line deviates from actual data at the third from the last point in each case, indicating that cake stabilization had not occurred even at the end of the lab filtration.

Figures 3 - 12 are presented primarily to show that Equation B.6 may be used to describe all regions of a dynamic leakoff test with a higher degree of accuracy previously attained with a square root of time relationship. When filtration occurs from a fracture in reality, Equation B.6 may be more representative than either a time or root time relationship. This may be deduced since filter cake in a real fracture is not continually building at a constant rate, as assumed by the static test, nor does it stop growing altogether, as in a dynamic test.

3.2 Fluid Flow in the Reservoir

To model the transient, two-phase reservoir flow behavior the IMPES simulator is written with Neumann (ie. - constant rate) boundary conditions. The rate at the injection block is determined by the cake flow equation Equation B.2, the velocity equation. In order to accurately observe the fracture fluid invasion near the fracture face, as well as to simulate an infinite acting system, a geometric mesh spacing was used. This was done by setting the mesh size of the first block, and using a multiplier on each subsequent block. For example, if the first block was 1" thick and the multiplier was 2, then the second block was 2", the third 4", the fourth 8", etc. (see Figure 13a). The geometric mesh spacing requires that pore volumes be calculated separately for each block, as they are different. Additionally, the mass balance calculations must recognize the varying grid block size.

Based on the work of Buell²⁰, the fracture fluid inside the formation was taken to behave as Newtonian. He hypothesized that by the time the fluid passes through the filter cake it would be stripped of most of the initial polymer, which has adsorbed onto the cake itself.

In order to generate a set of relative permeability and capillary pressure curves, a generalized set of correlations for a water wet rock were used²¹. The following relationships were assumed (these are shown in Figures 14 and 15):

Figure 13 - Geometric Mesh Spacing

Figure 13a
Geometric Mesh Spacing

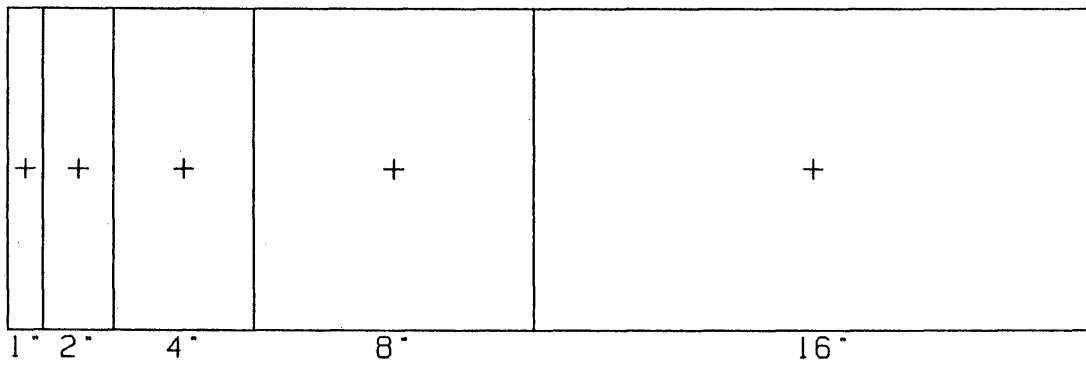
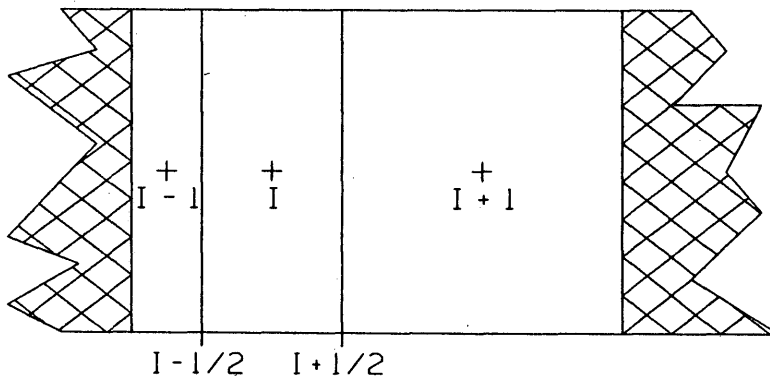


Figure 13b
Delta-x Subscripts



$$P_c = A (1.25 - 5/3 S_w) ^2 \quad (3.7)$$

$$K_{rw} = 0.2 (-.25 + 5/3 S_w) ^2 \quad (3.8)$$

$$K_{ro} = 1.0 (1.25 - 5/3 S_w) ^2 \quad (3.9)$$

which imply that:

$$S_{w_{irr}} = 0.15 \text{ and } S_{o_r} = 0.75 \quad (3.10)$$

3.3 Cake/Reservoir Linkage

The filter cake flow equation (Equation B.2) requires two defining coefficients A and B. One is the Darcy (pseudo-steady state) velocity, which includes the variable pressure drop across the cake. The other includes the Darcy velocity and the filter cake half-life, "a"

$$u = u_d [a/t + 1] = A/t + B \quad (B.2)$$

(Note: Equation B.2 is the 1st derivative of Equation B.6)

In order for a solution to be obtained at a given time step, the flow through the filter cake must equal the flow into the reservoir at the fracture face. This was accomplished in the following manner: The pressure under which the laboratory experiment was conducted is first divided out of the coefficients A and B. As a first approximation, it is assumed that the pressure drop across the cake equals

Figure 14 - Relative Permeability Curves

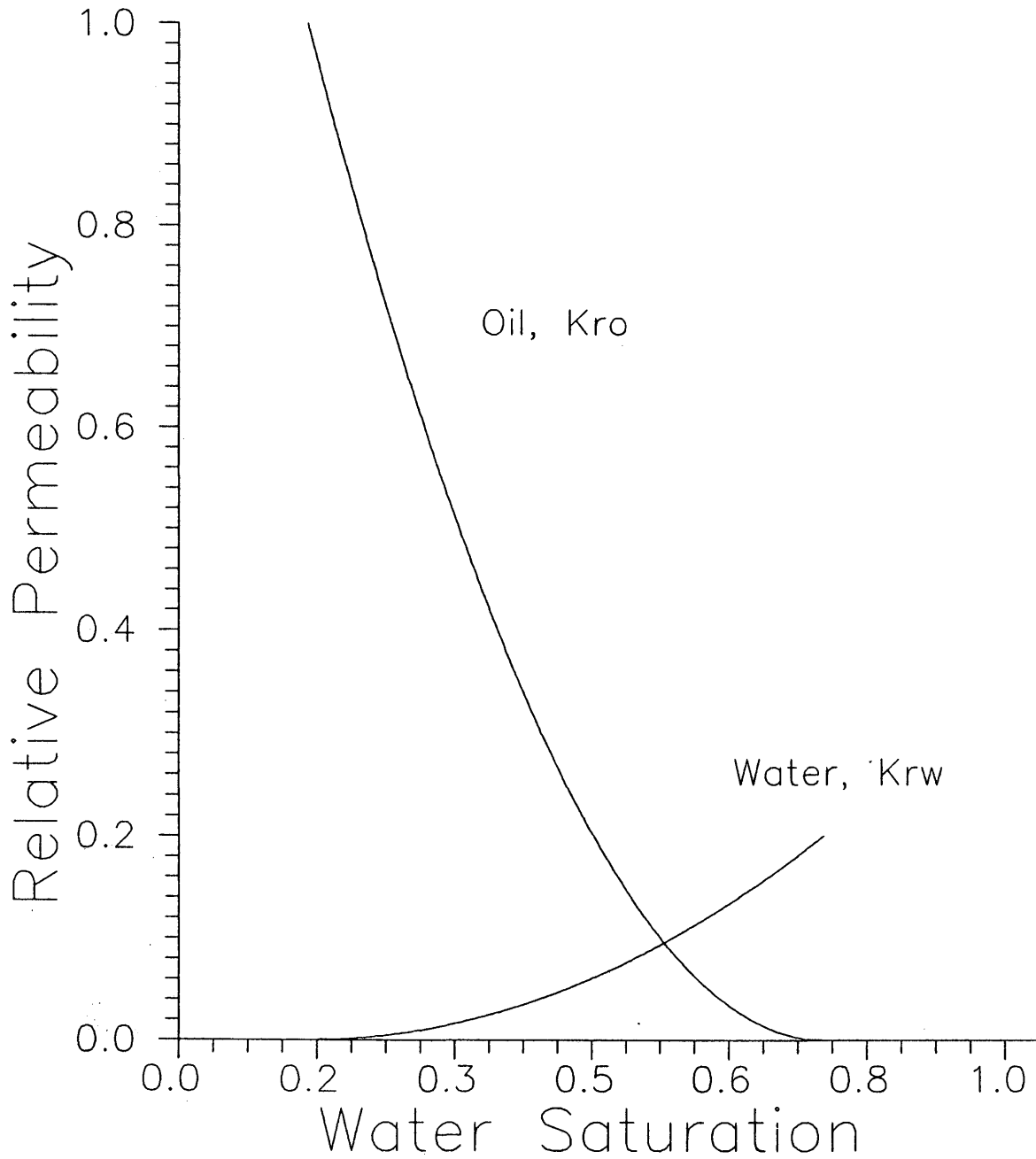


Figure 14 - Oil and water relative permeability versus water saturation.

Figure 15 - Capillary Pressure Curve

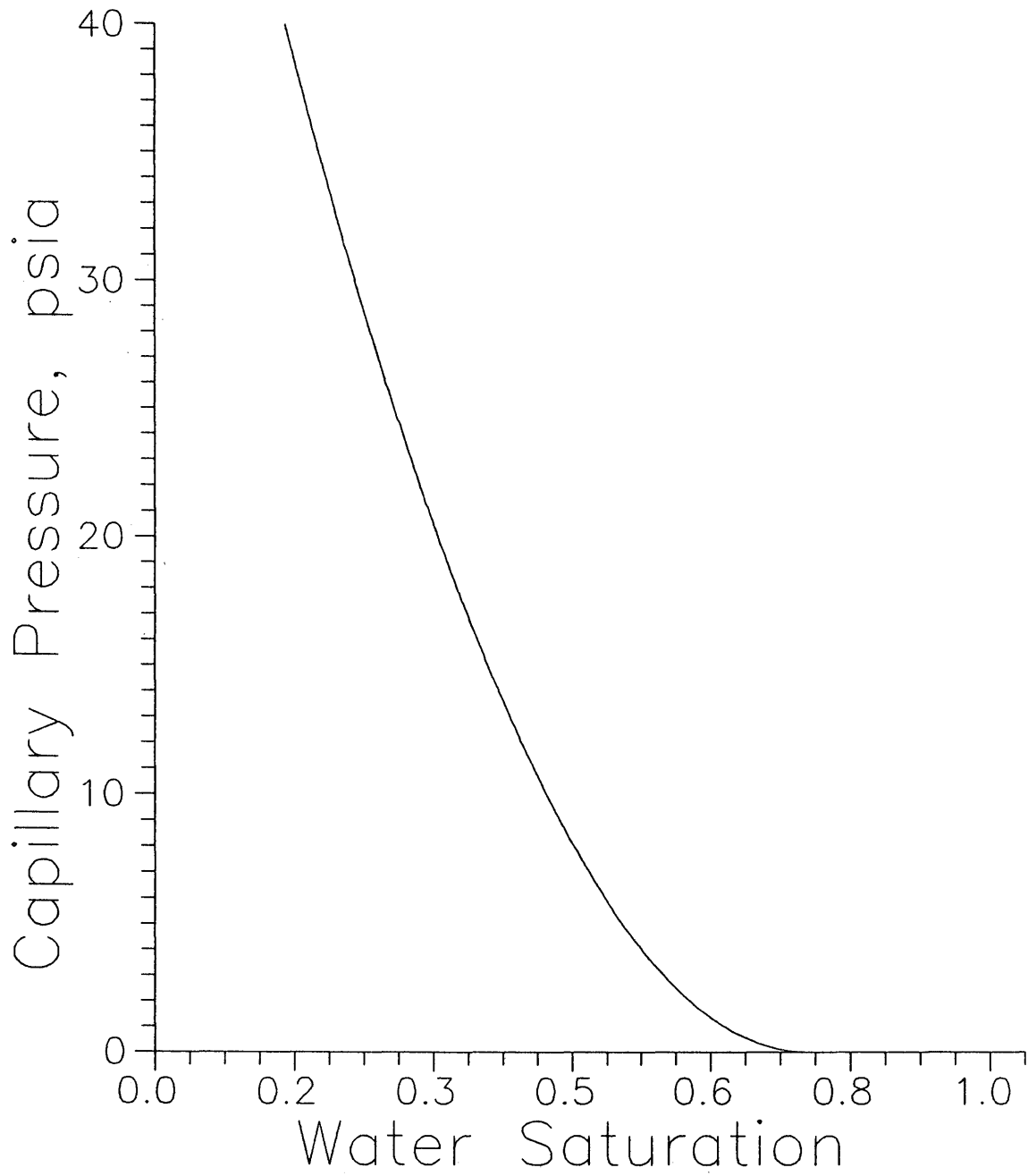


Figure 15 - Capillary pressure versus water saturation.

the pressure inside the fracture less the reservoir pressure at the fracture face from the previous time step. This gives a very high initial rate which may approximate the spurt loss phase.

From this pressure drop two new coefficients are calculated (A' and B') which have been adjusted to account for the variation from the laboratory pressure drop. Equation B.2 then gives the injection rate at the first block. This rate is fed into the IMPES simulator, and the resulting pressure at the first node is extrapolated back one half mesh space to the fracture face between the reservoir and the cake. This is compared to the value of pressure obtained by subtracting the pressure drop across the cake from the fracture pressure. If the two values agree to within 0.01 psi the program continues to the saturation equation and eventually the next time step. If not, the pressure drop across the cake is recomputed, and the process is repeated. For future time steps the initial guess for the pressure drop across the cake is taken as the fracture pressure less the pressure at the fracture wall, half a grid block from the first node.

As long as the formation volume factor changes little with time, the IMPES formulation is stable. Convergence occurs after two or three iterations as the model iterates toward a solution at a given time step. This occurs when the filtrate volume through the cake is equal to the volume necessary to be injected at the fracture face to cause the appropriate pressure at the face. Material balance errors from the IMPES simulation are on the order of 1 to 2 percent.

Chapter 4 - Results

Figures 16 and 17 compare classical leakoff with this study. Figure 16 shows the potential problem when extrapolating data from a 30 minute laboratory test to a two hour field situation. The upper curve uses the cumulative volume equation (Equation B.6) developed in this paper, while the middle curve is a regressed square root of time fit to the laboratory data. The two models, this paper's and the static model, overlies each other until 30 minutes, but are 25% in error after two hours.

The bottom curve represents the same square root of time graph as the middle curve, but neglects the initial spurt loss. Now the difference between Equation B.6 and this curve approaches a 50% error, and the two square root of time curves differ by a consistent 1000 cubic feet. This is significant, since the incorporation of leakoff into a fracture area calculation typically does not include spurt loss. This is very important, as the under-estimation of leakoff may lead to sandouts.

A set of results from a simulation run on data provided in examples by Howard and Fast is presented in Figure 17, which represents the incorporation of reservoir behavior into the leakoff picture. Howard and Fast actually did calculate an effective leakoff coefficient according to Smith², shown in the graph. The other curve is a result of this study, the new equation combined with a simulation. The non-linear combination of coefficients apparently overestimates the actual leakoff when taking into account the interaction of the reservoir. This

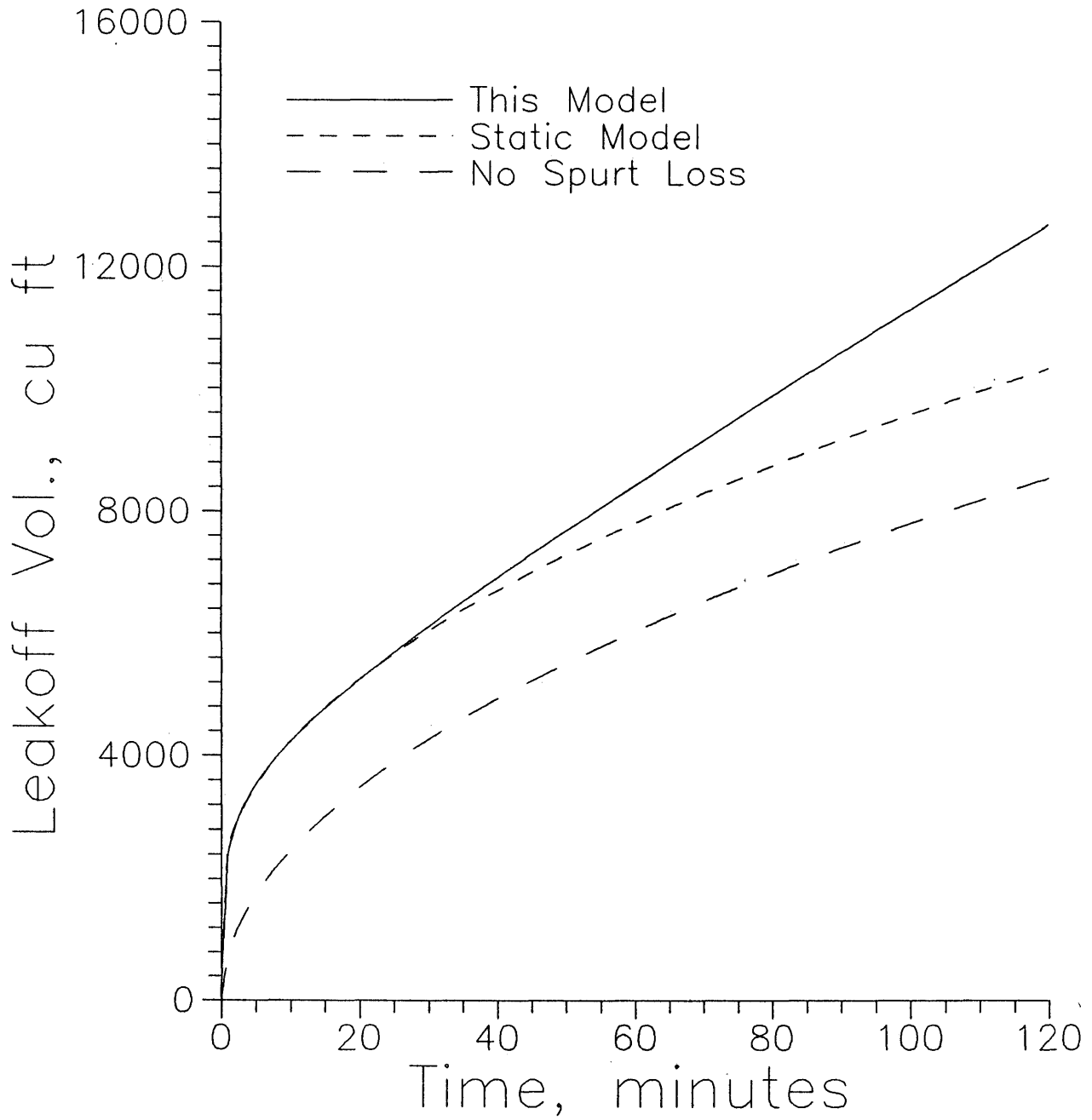
Figure 16 - Leakoff Comparison: Various Equations

Figure 16 - A comparison between the new equation, the static model, and the static model neglecting spurt loss.

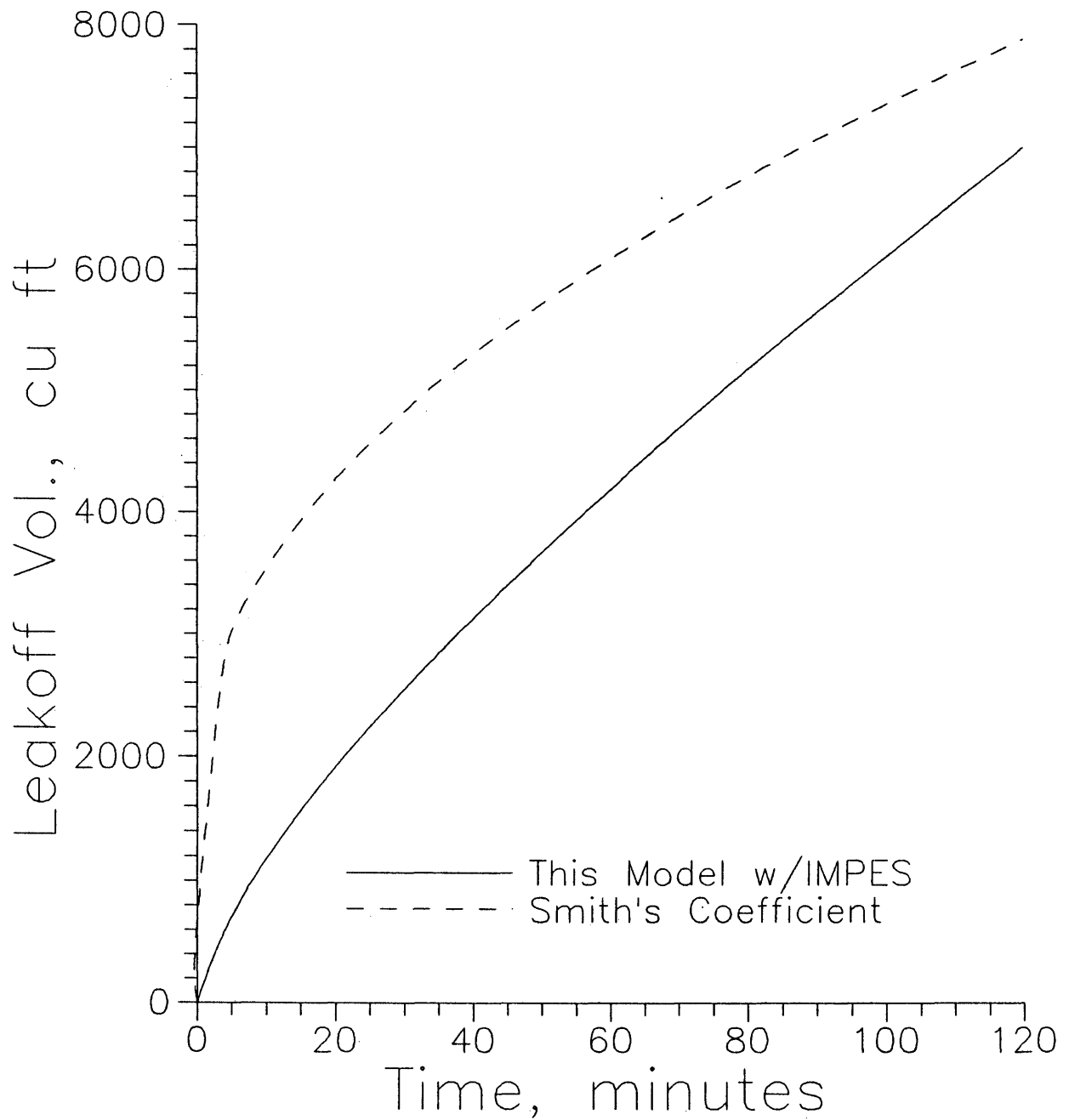
Figure 17 - Leakoff Comparison: Including Reservoir Effects

Figure 17 - A comparison between the new equation (including IMPES simulation) and the Smith coefficient, Ceff.

is due to a combination of effects, but primarily the Smith coefficient does not account for the decreasing pressure drop with time.

Using the matched leakoff coefficients obtained from the work of Hall and Dollarhide⁷ different cases were run with varying mobility ratios, permeabilities, compressibilities, differential pressures, initial water saturations, and porosities. A representative base case is given by:

Equation B.6 Coefficients:

$$A = 0.08104885 \quad B = 0.00985819 \quad C = 0.35906170$$

Rock and Fluid Properties:

$\mu_w =$	4 cp	$\mu_o =$	1 cp
$\Delta t =$	5 min	$T_{max} =$	120 min
$k =$	10 md	$\phi =$	0.15
$P_f =$	2000 psia	$P_i =$	1000 psia
$c_w =$	10 E-6 1/psi	$c_o =$	10 E-6 1/psi
$IMAX =$	50	$Area =$	20,000 sq ft
$S_{wi} =$	0.15		

Results are given in Figures 18 - 22. Figure 18 shows that the pressure wave has travelled about 200 feet from the fracture face in two hours, while Figure 19 indicates that the saturation front is only two feet into the formation. This may be a consequence of the relative permeability curves (Figure 14), since at the initial water saturation of 15% the injected water is barely mobile and hard to introduce into the system. Leakoff rate, shown in Figure 20, starts high at about 25 BPM, then appears to level at around 7 BPM after two hours. The leakoff volume in Figure 21 reaches 6400 cubic feet (1100 barrels) after two hours. The plot in Figure 22 shows the ratio of mass accumulated to mass injected close to a

Figure 18 - Base Case: Pressure Wave

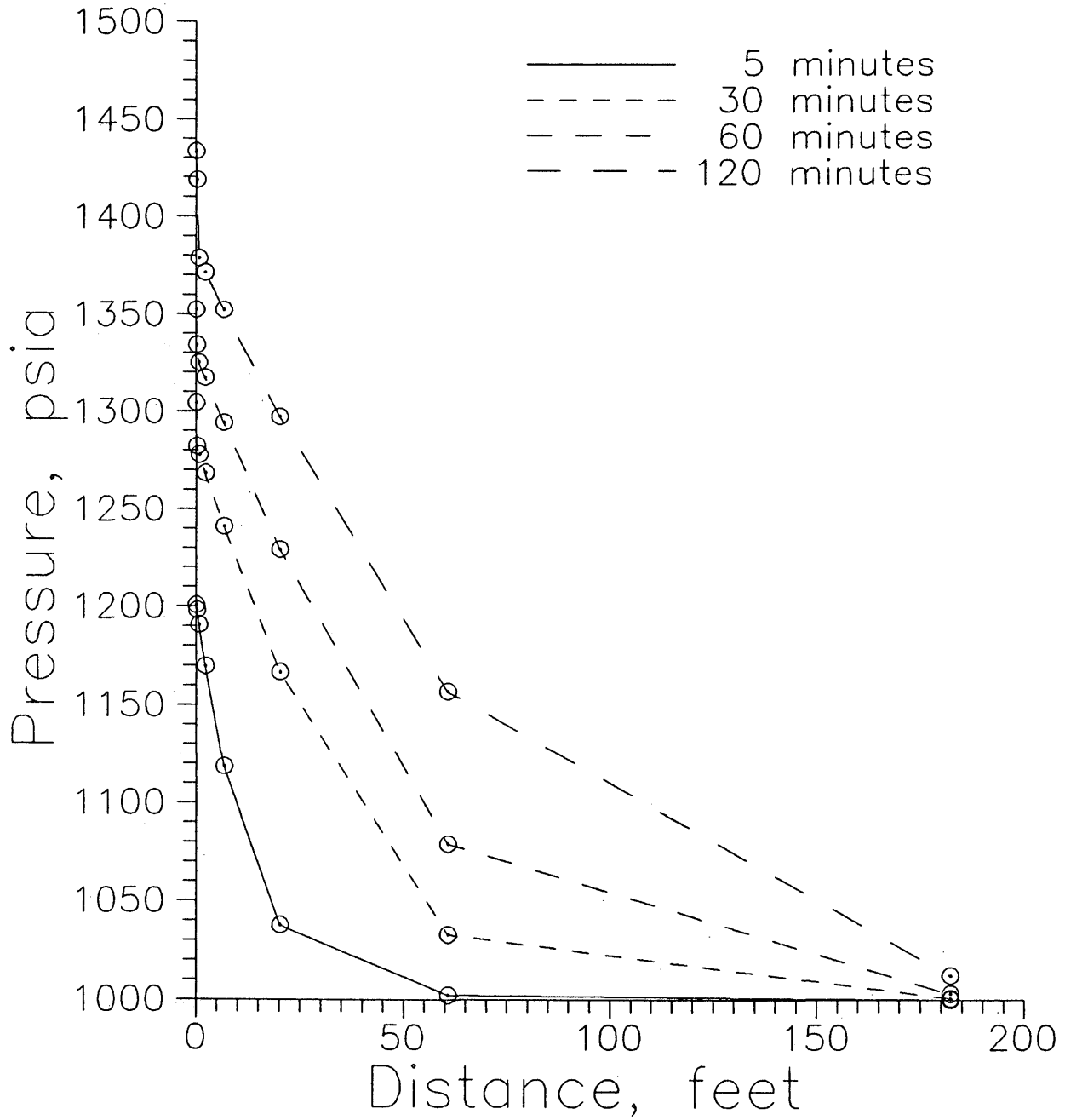


Figure 18 - Pressure versus distance at various times.

Figure 19 - Base Case: Water Saturation Front

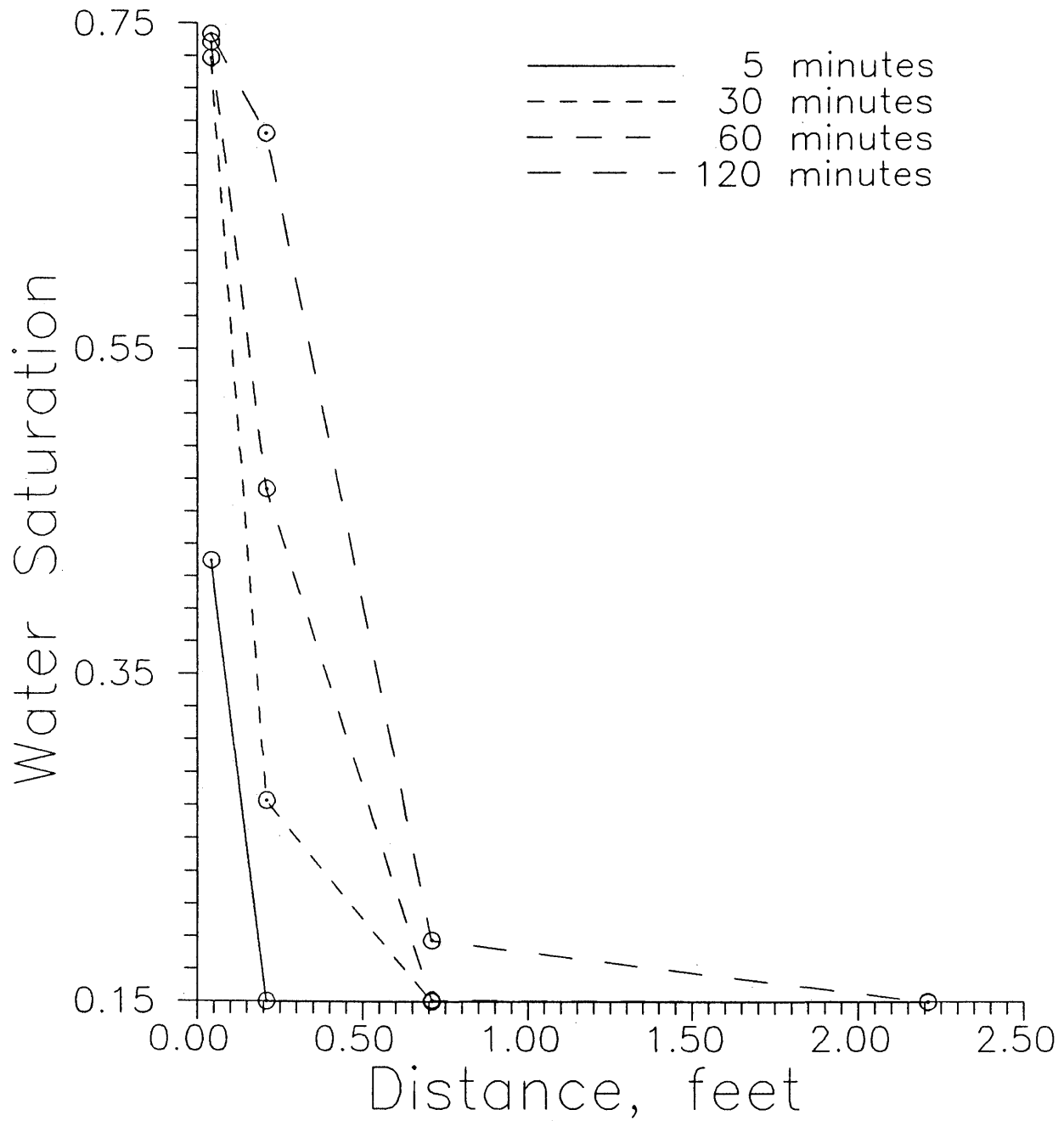


Figure 19 - Water saturation versus distance at various times.

Figure 20 - Base Case: Leakoff Rate

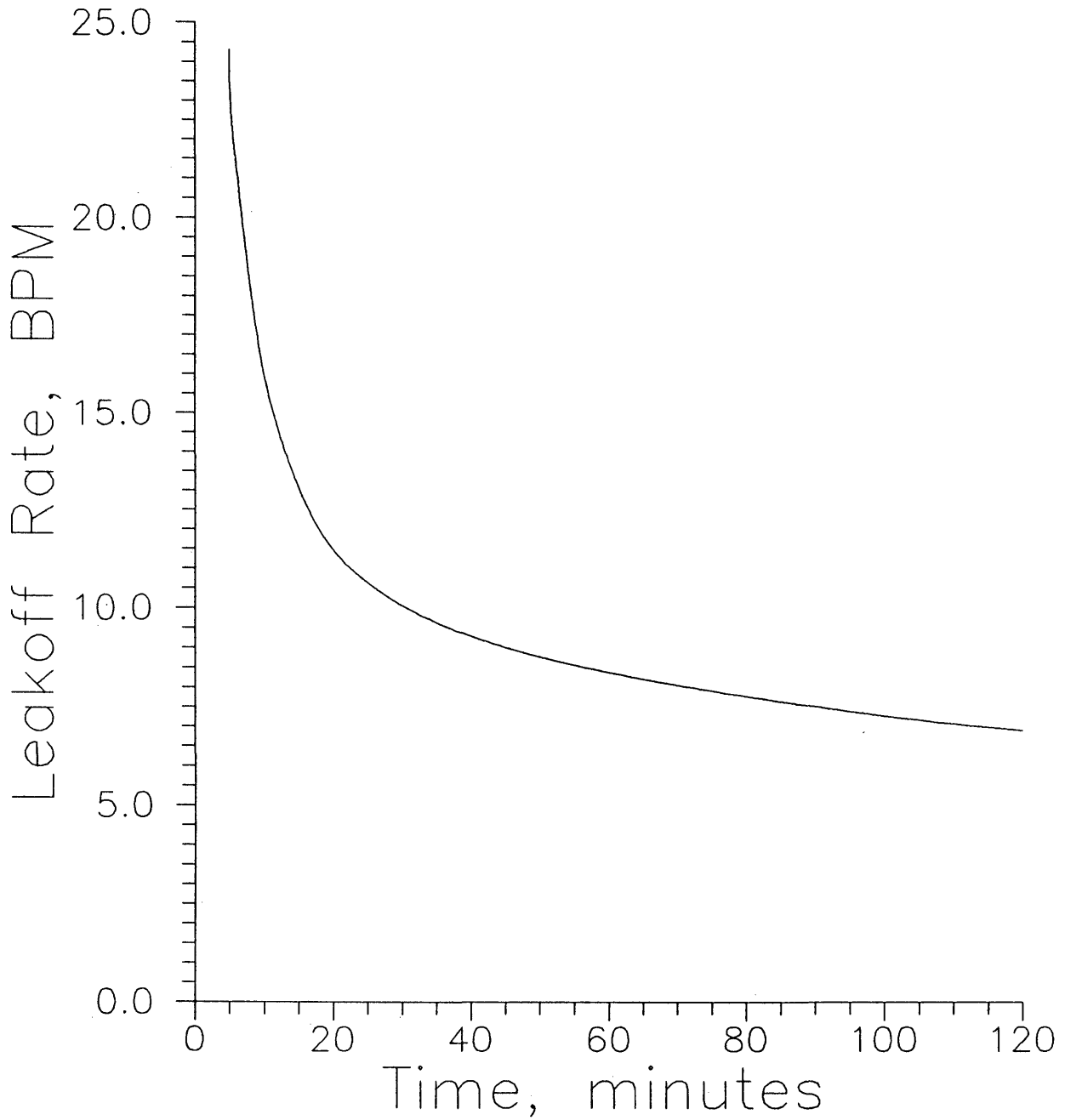


Figure 20 - Filtrate leakoff rate versus time.

Figure 21 - Base Case: Leakoff Volume

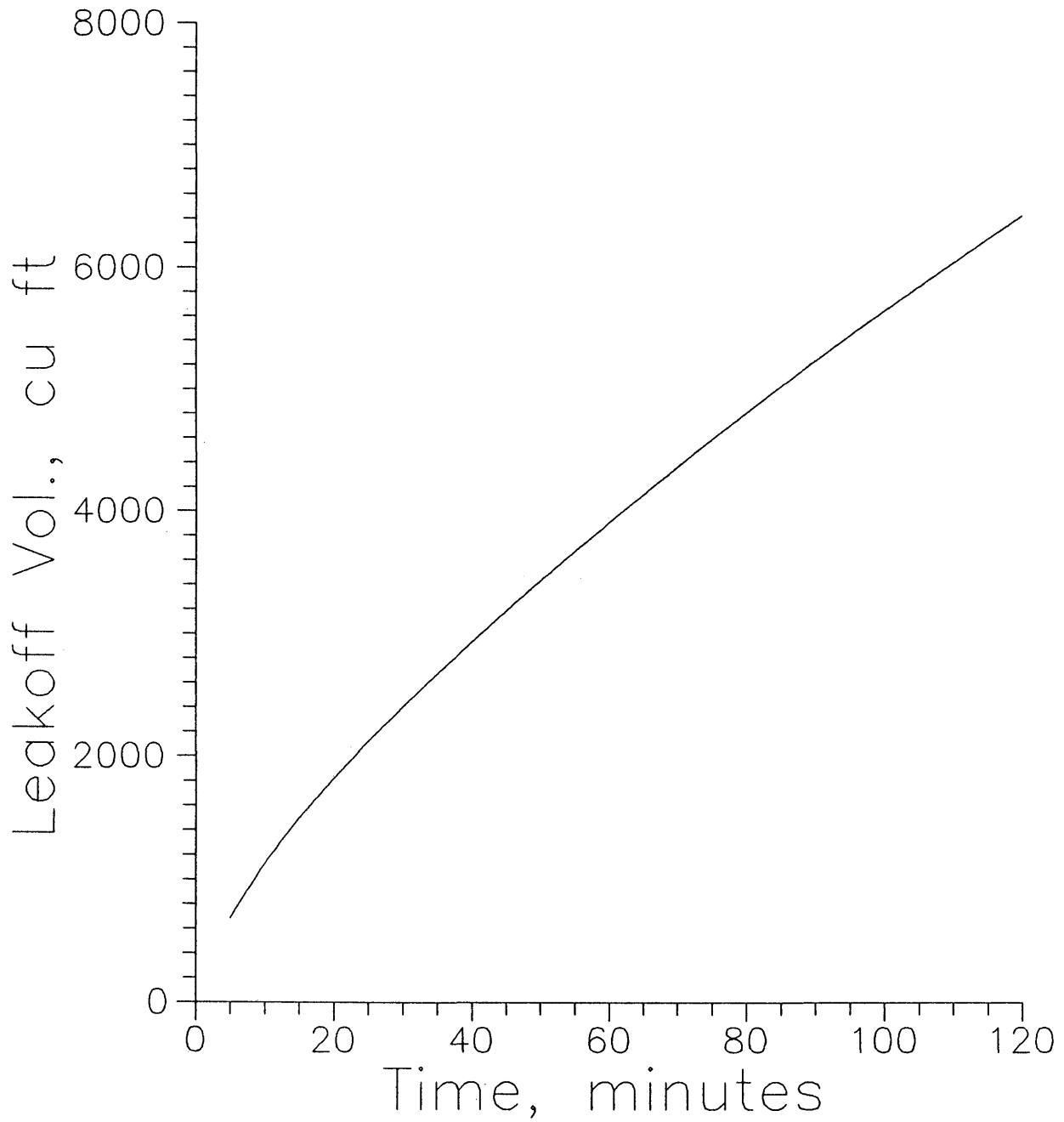


Figure 21 - Cumulative filtrate leakoff volume versus time.

Figure 22 - Base Case: Mass Balance

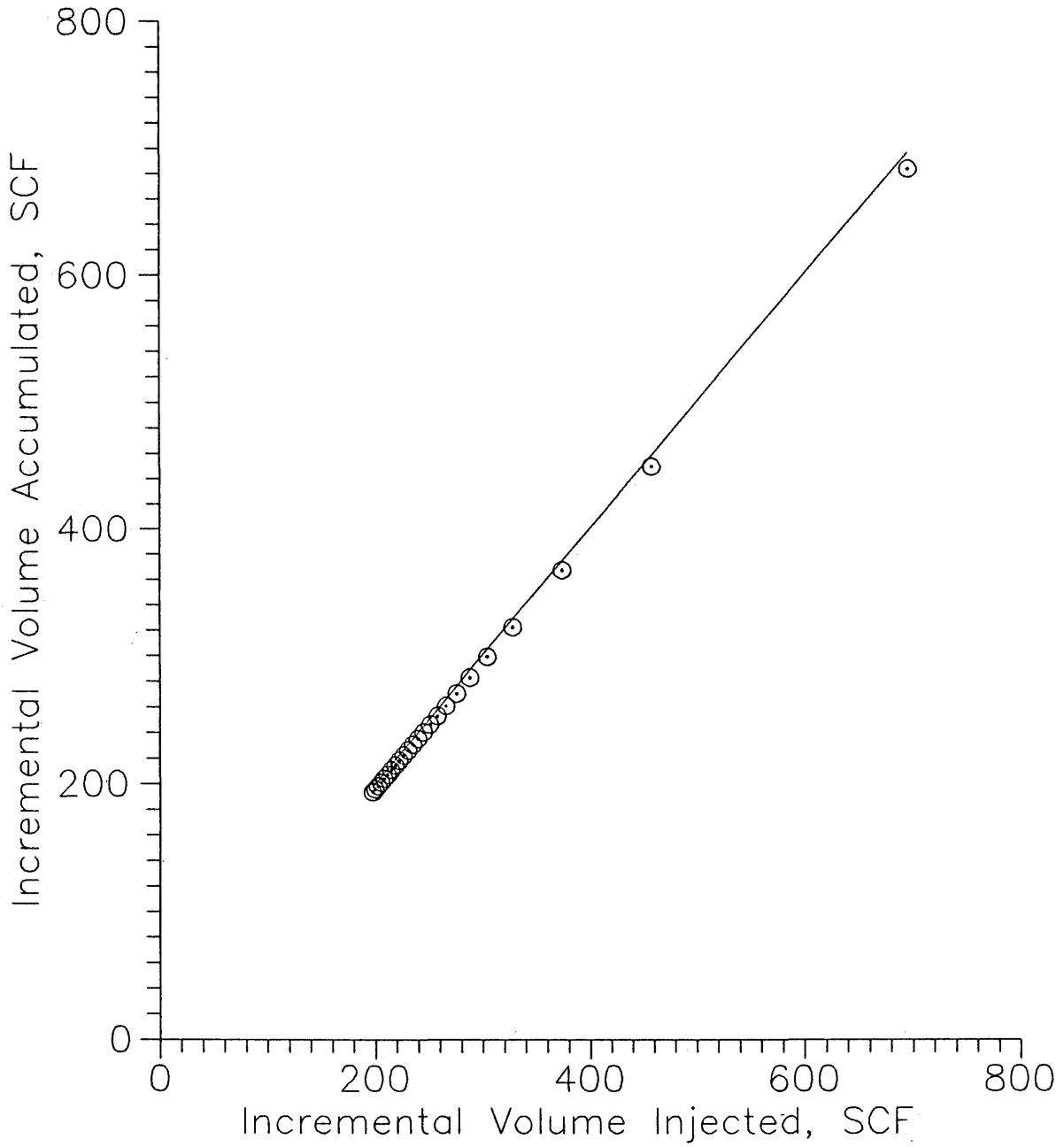


Figure 22 - Incremental mass injected versus mass accumulated in the system.

slope of unity (actually about 98%), which would indicate a good material balance in the model.

A series of runs were made to investigate the effect of changes in rock and fluid properties for a given set of matched cake coefficients. The variables investigated were: initial pressure drop from fracture into reservoir, water and oil viscosities, compressibility, permeability, porosity and initial water saturation. The values used are found in Table 2 (Page 60), and the corresponding plots showing cumulative leakoff volume and the corresponding pressure wave after two hours are found in Figures 23 through 36.

Figures 23 through 26 show the effect of changing oil and water viscosities. As might be expected from the shallow depth of filtrate penetration, changing the water viscosity had a very small effect, while a difference in oil viscosity showed a pronounced change in both the leakoff volume and distance of the pressure wave after two hours. Figures 27 and 28 show that increasing or decreasing the total system compressibility will have a directly proportional effect on the cumulative leakoff volume. This was accomplished by changing both the water and oil compressibilities equally.

The consequence of initial water saturation is shown in Figures 29 and 30, where the results are not at all intuitive. (Larger pad volumes, for example, might lead to elevated initial water saturations). One might expect an increase in the initial water saturation to increase the system mobility. In this situation the

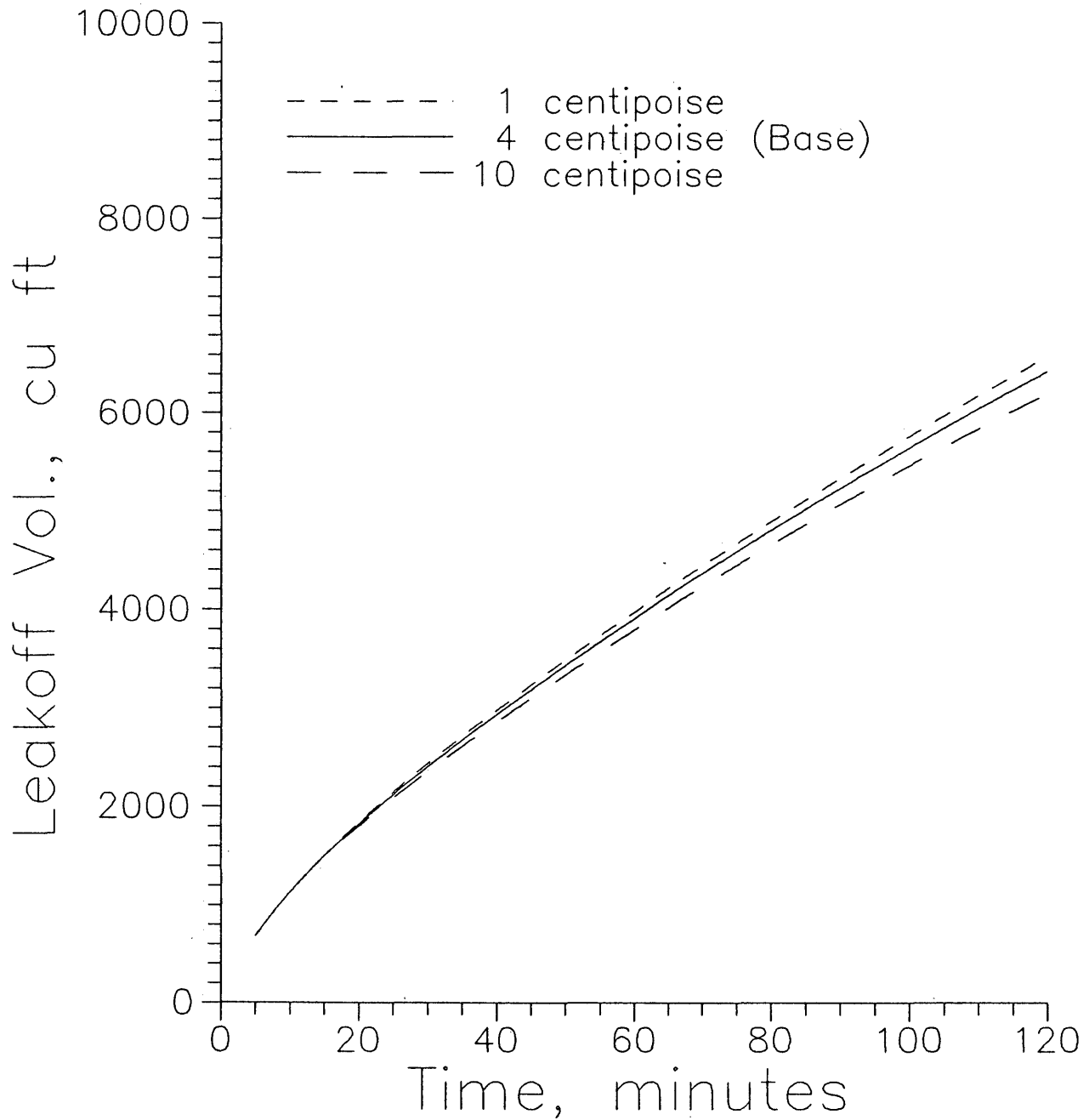
Figure 23 - Water Viscosity Effect on Leakoff Volume**Figure 23 - Cumulative leakoff volume versus time for different values of water viscosity.**

Figure 24 - Water Viscosity Effect on Pressure Wave

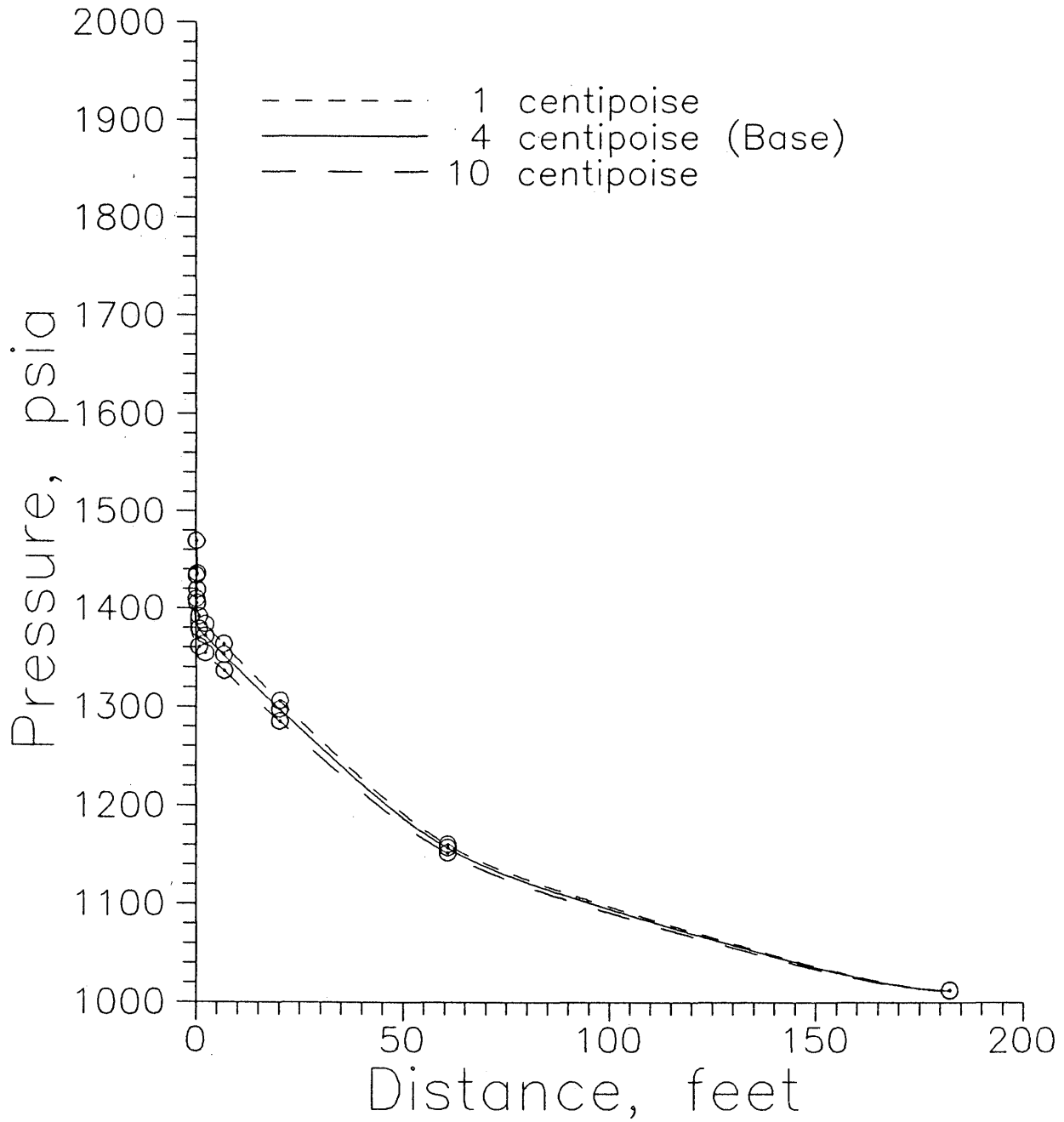


Figure 24 - Pressure versus distance for different values of water viscosity.

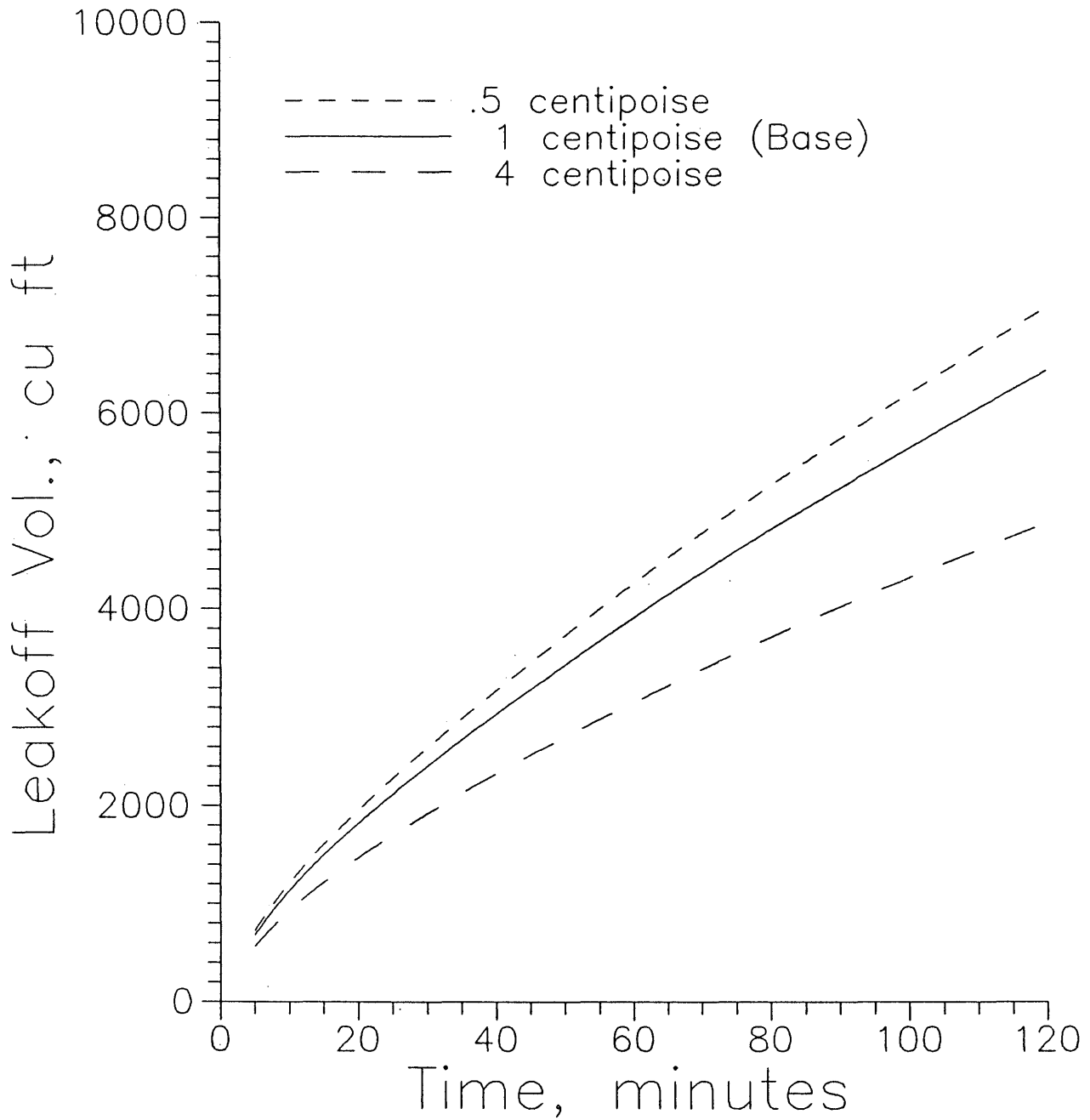
Figure 25 - Oil Viscosity Effect on Leakoff Volume**Figure 25 - Cumulative leakoff volume versus time for different values of oil viscosity.**

Figure 26 - Oil Viscosity Effect on Pressure Wave

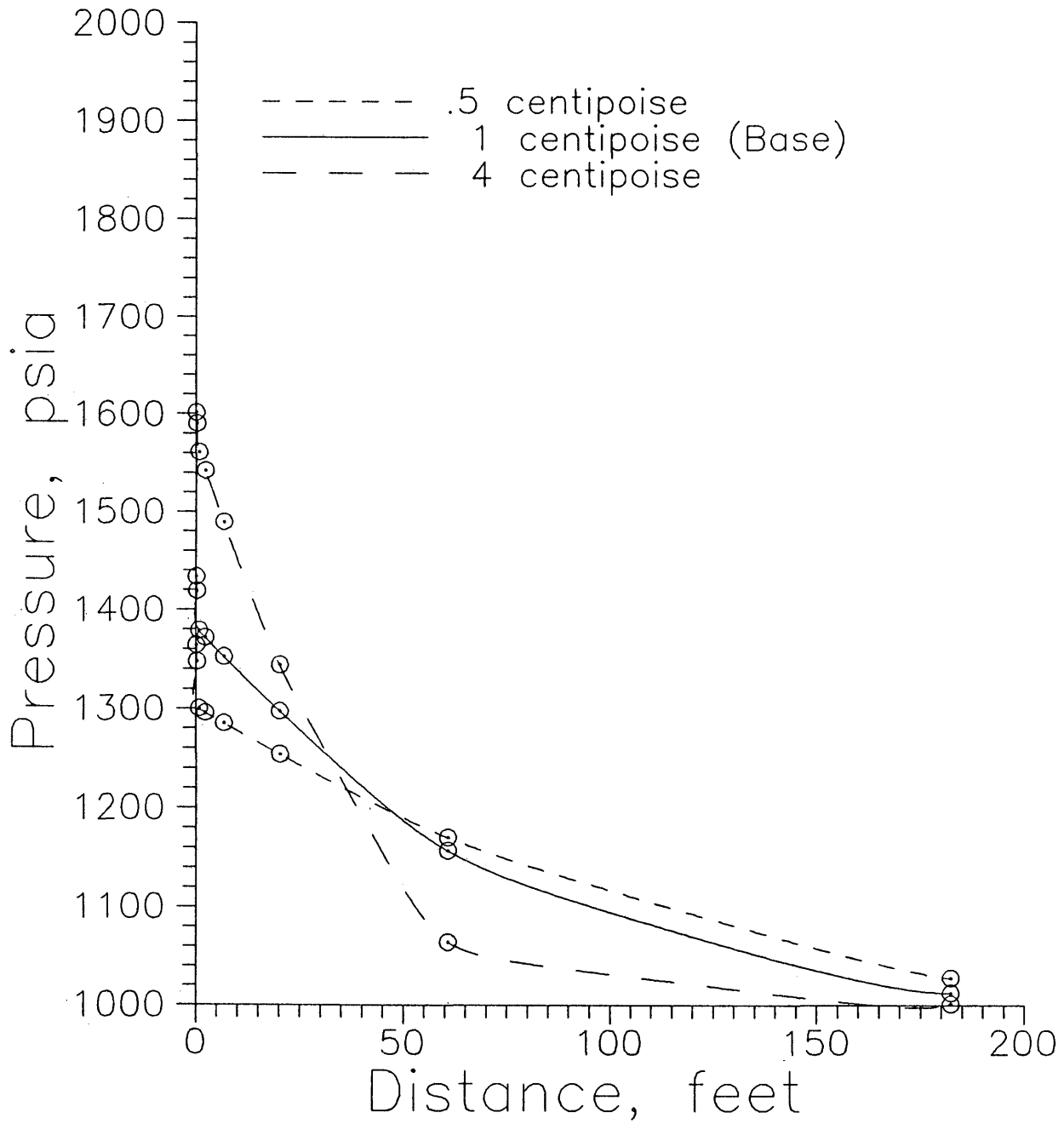


Figure 26 - Pressure versus distance for different values of oil viscosity.

Figure 27 - Total Compressibility Effect on Leakoff Volume

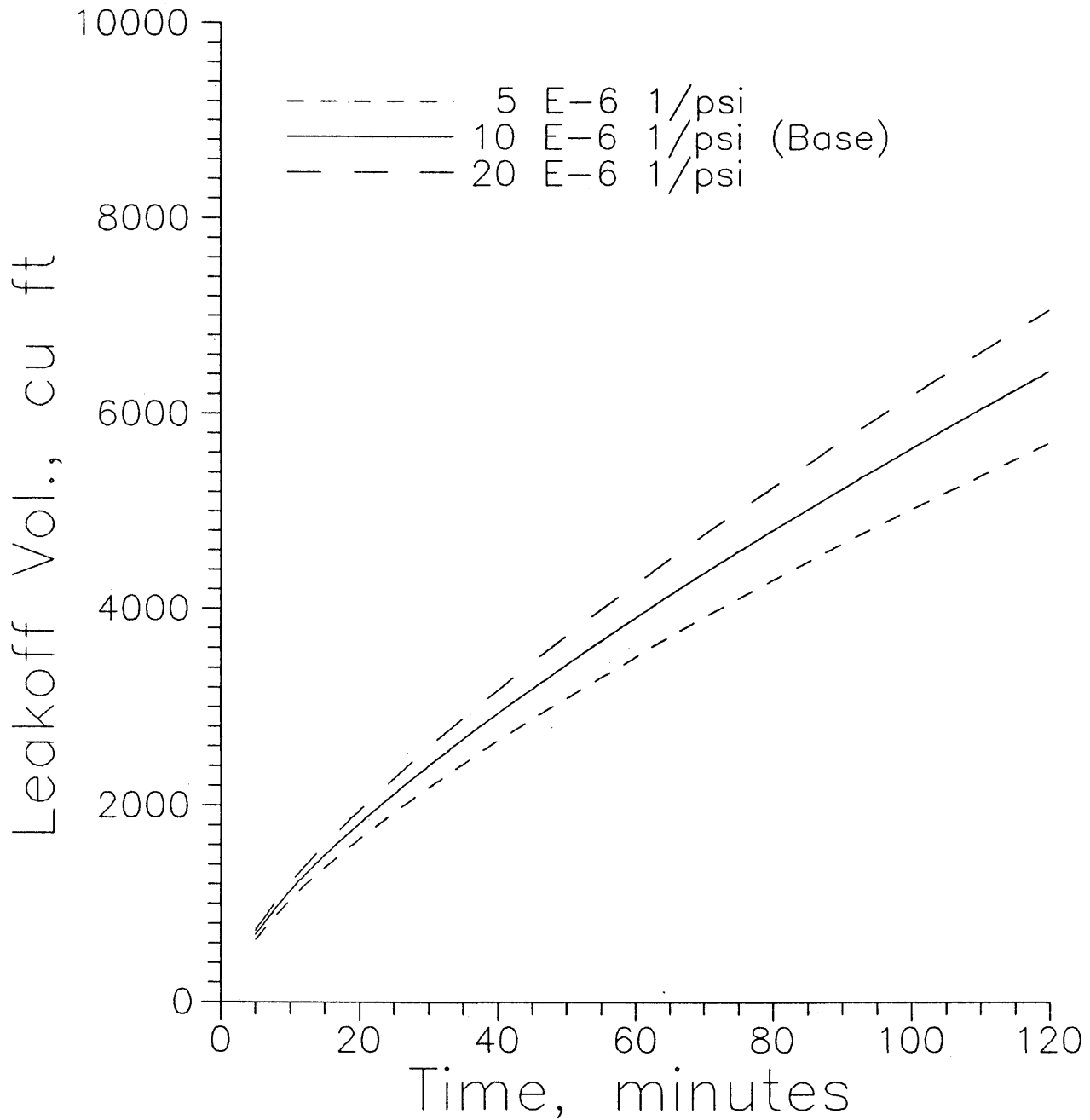


Figure 27 - Cumulative leakoff volume versus time for different values of total compressibility.

Figure 28 - Total Compressibility Effect on Pressure Wave

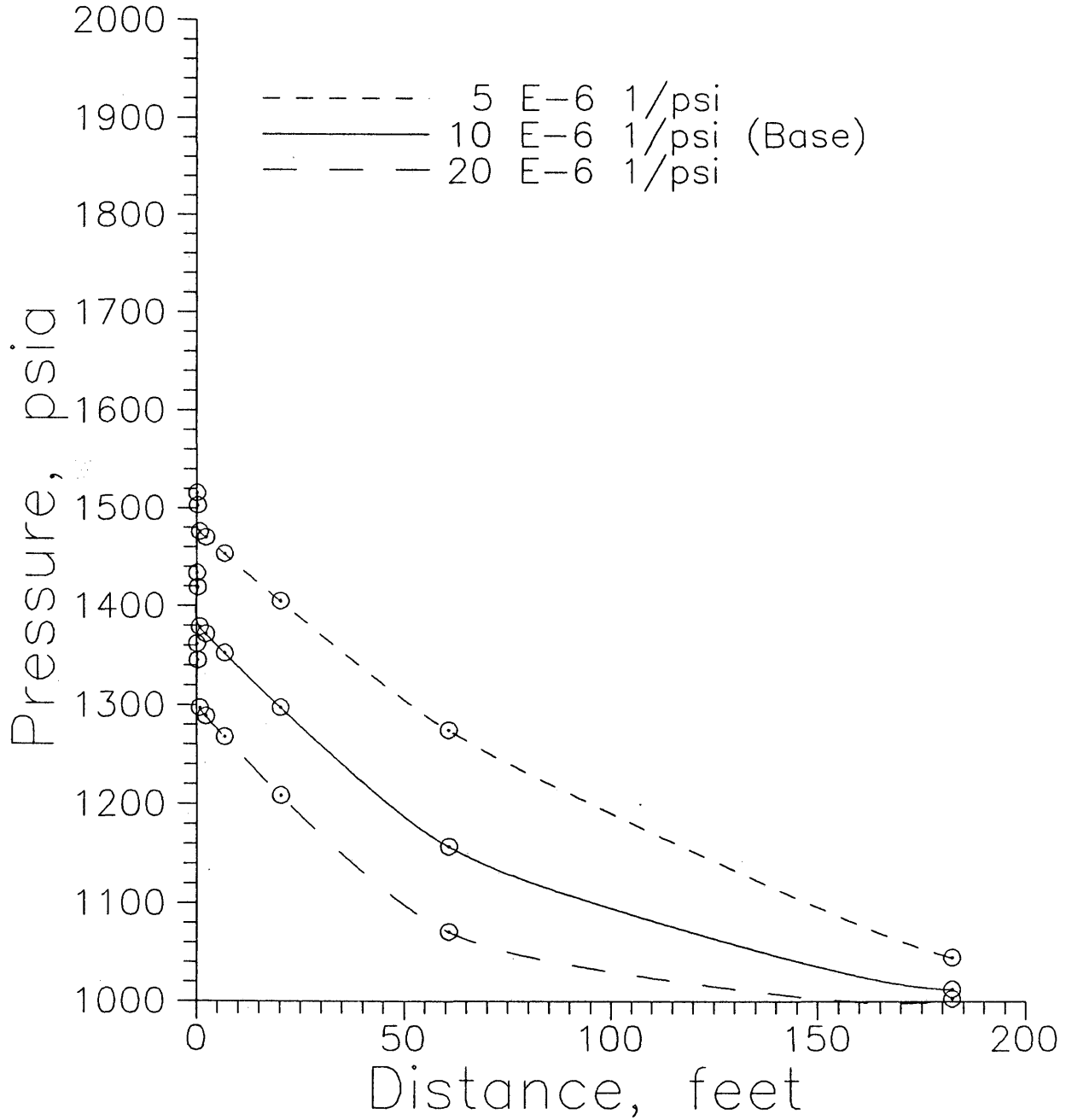


Figure 28 - Pressure versus distance for different values of total compressibility.

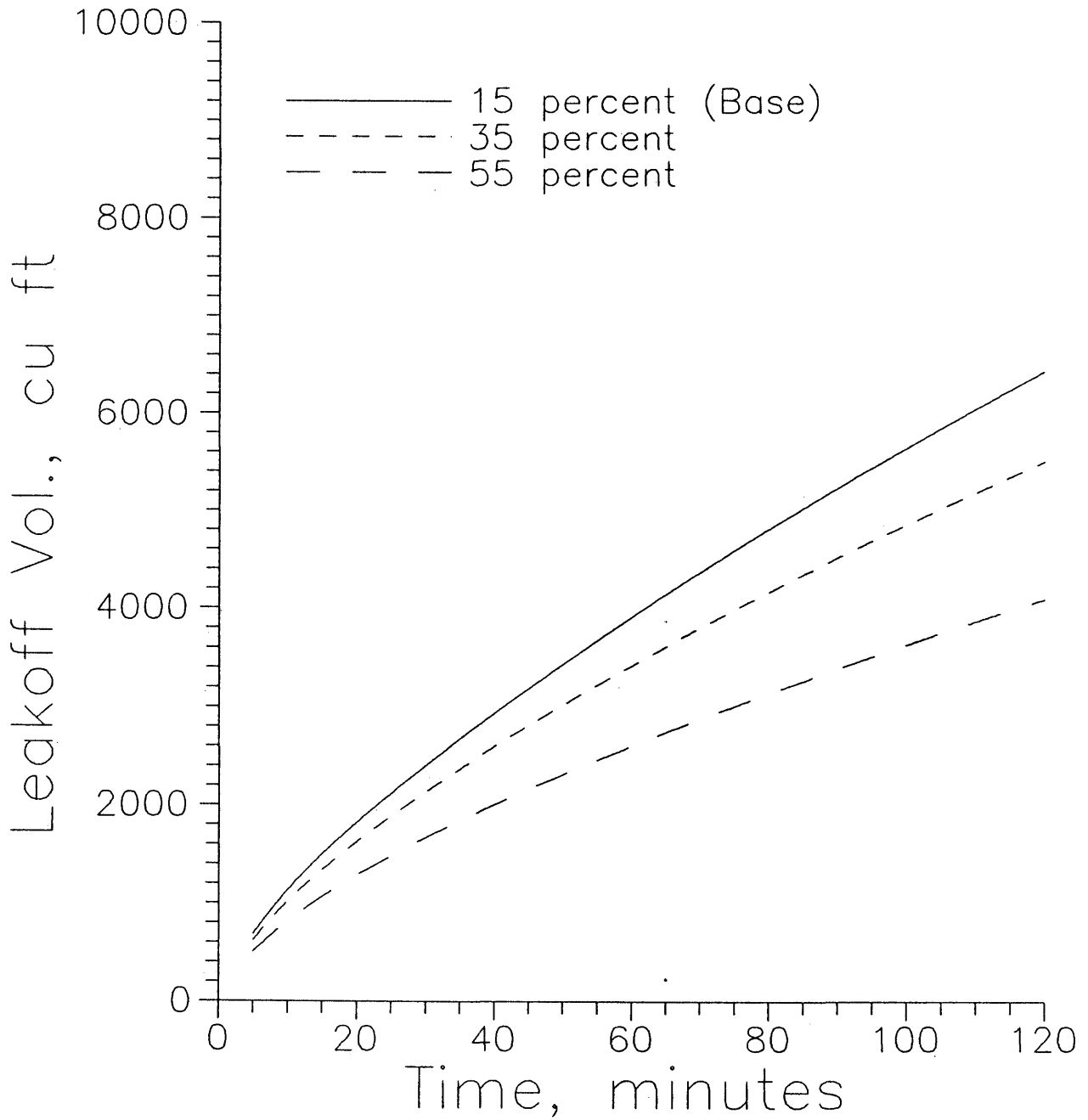
Figure 29 - Initial Water Saturation Effect on Leakoff Volume**Figure 29 - Cumulative leakoff volume versus time for different values of initial water saturation.**

Figure 30 - Initial Water Saturation Effect on Pressure Wave

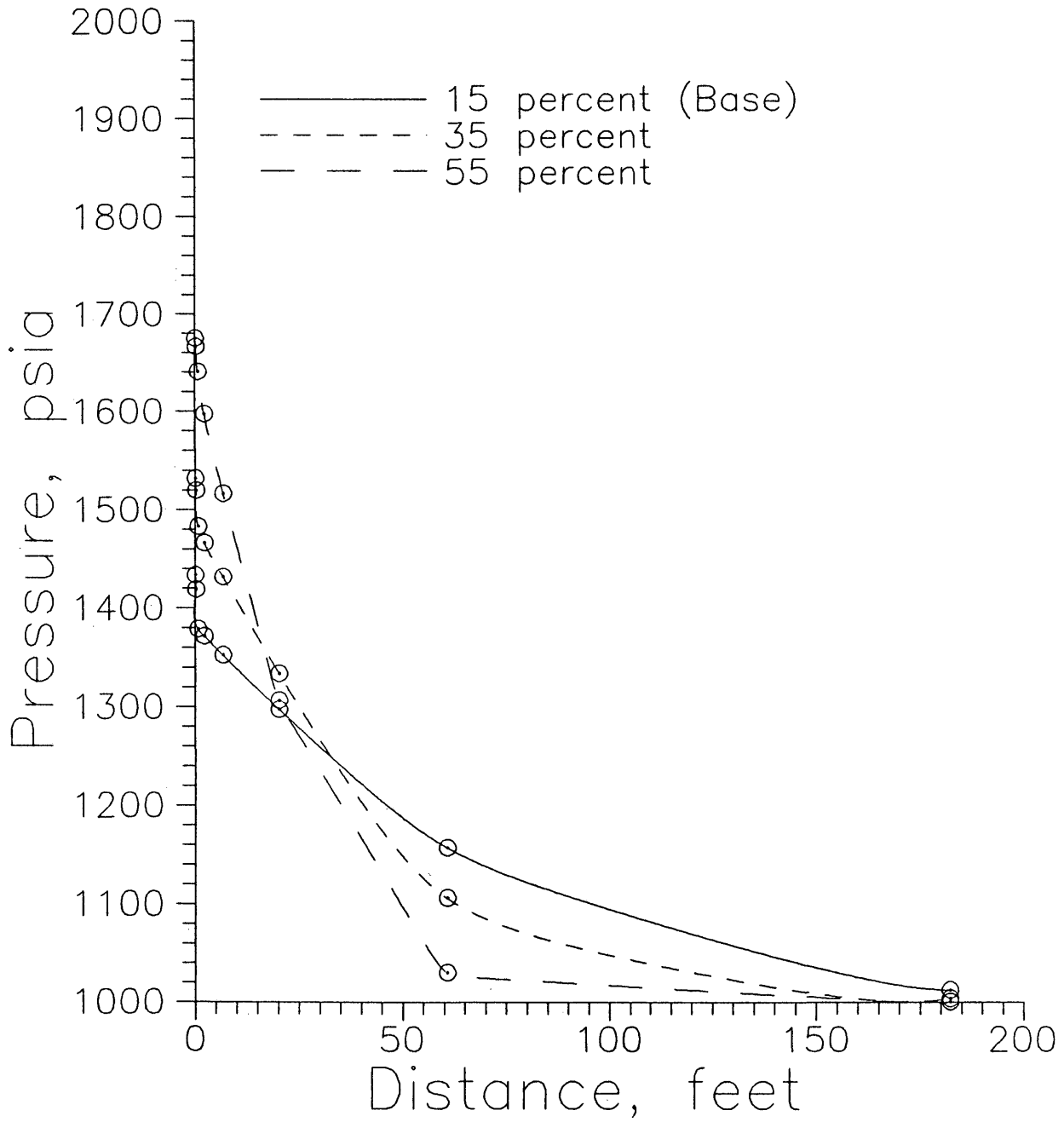


Figure 30 - Pressure versus distance for different values of initial water saturation.

water is far less mobile and less compressible than the oil, so increasing water saturation will actually impede the filtration process.

In Figures 31 and 32 it may be seen that an increase or decrease by a factor of ten in permeability may lead to a corresponding increase or decrease in the pressure wave distance and in leakoff volume. Porosity, shown in Figures 33 and 34, affects leakoff volume more than the pressure wave, but an increase or decrease of porosity leads to an increase or decrease in leakoff volume. Finally, in Figures 35 and 36, it may be seen that tripling the initial pressure drop leads to triple the pressure drop at any point in time.

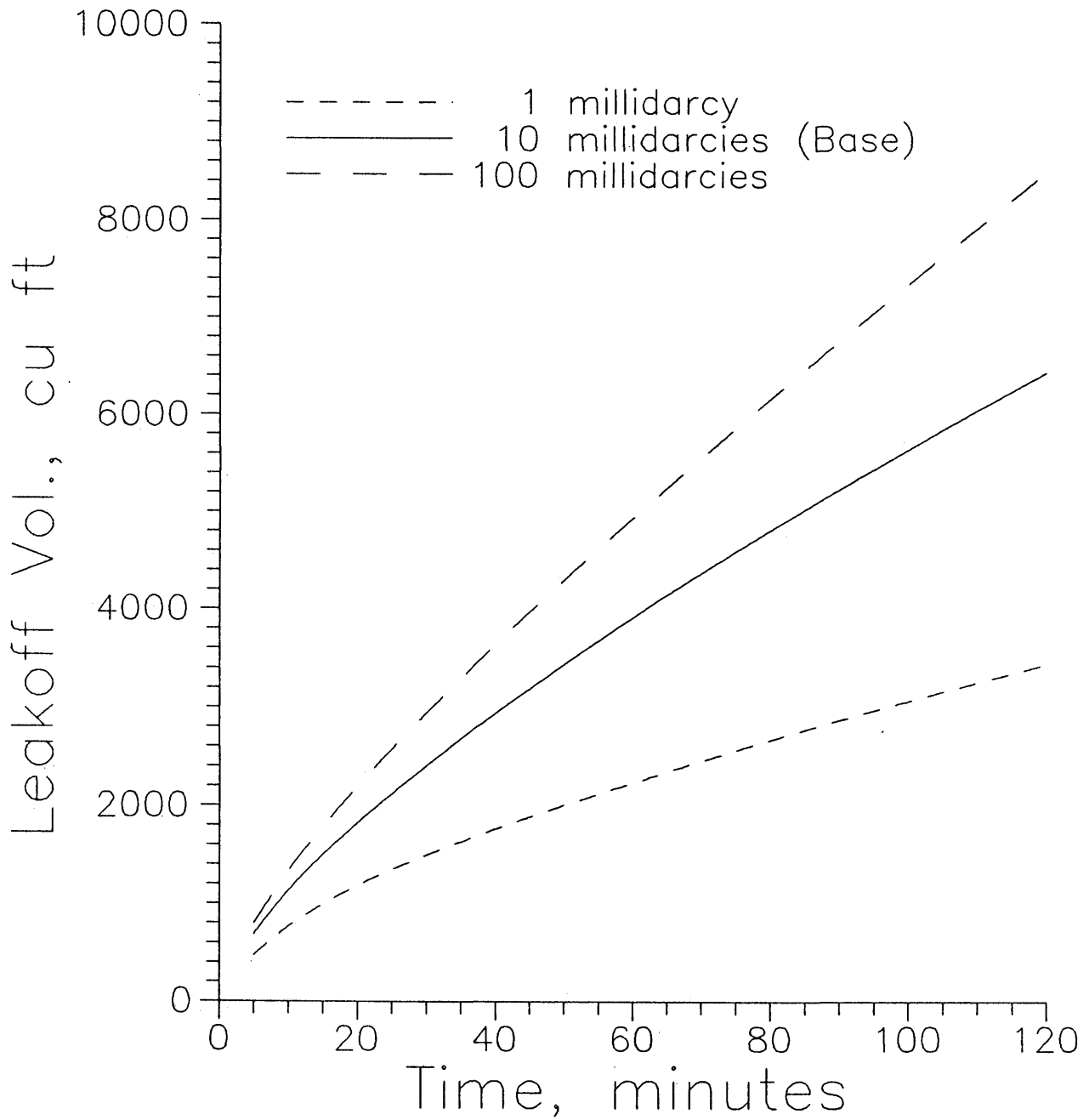
Figure 31 - Permeability Effect on Leakoff Volume**Figure 31 - Cumulative leakoff volume versus time for different values of permeability.**

Figure 32 - Permeability Effect on Pressure Wave

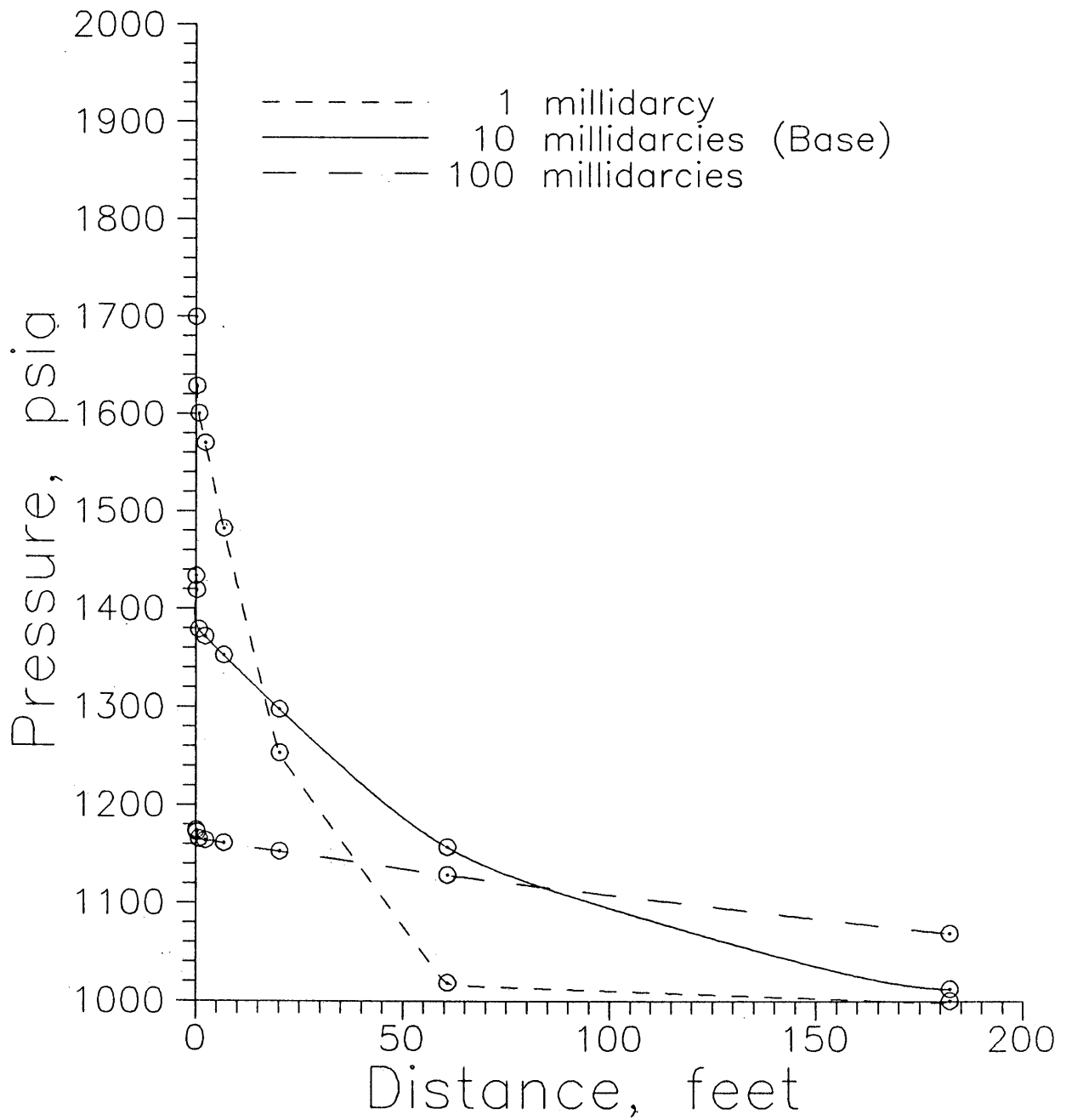


Figure 32 - Pressure versus distance for different values of permeability.

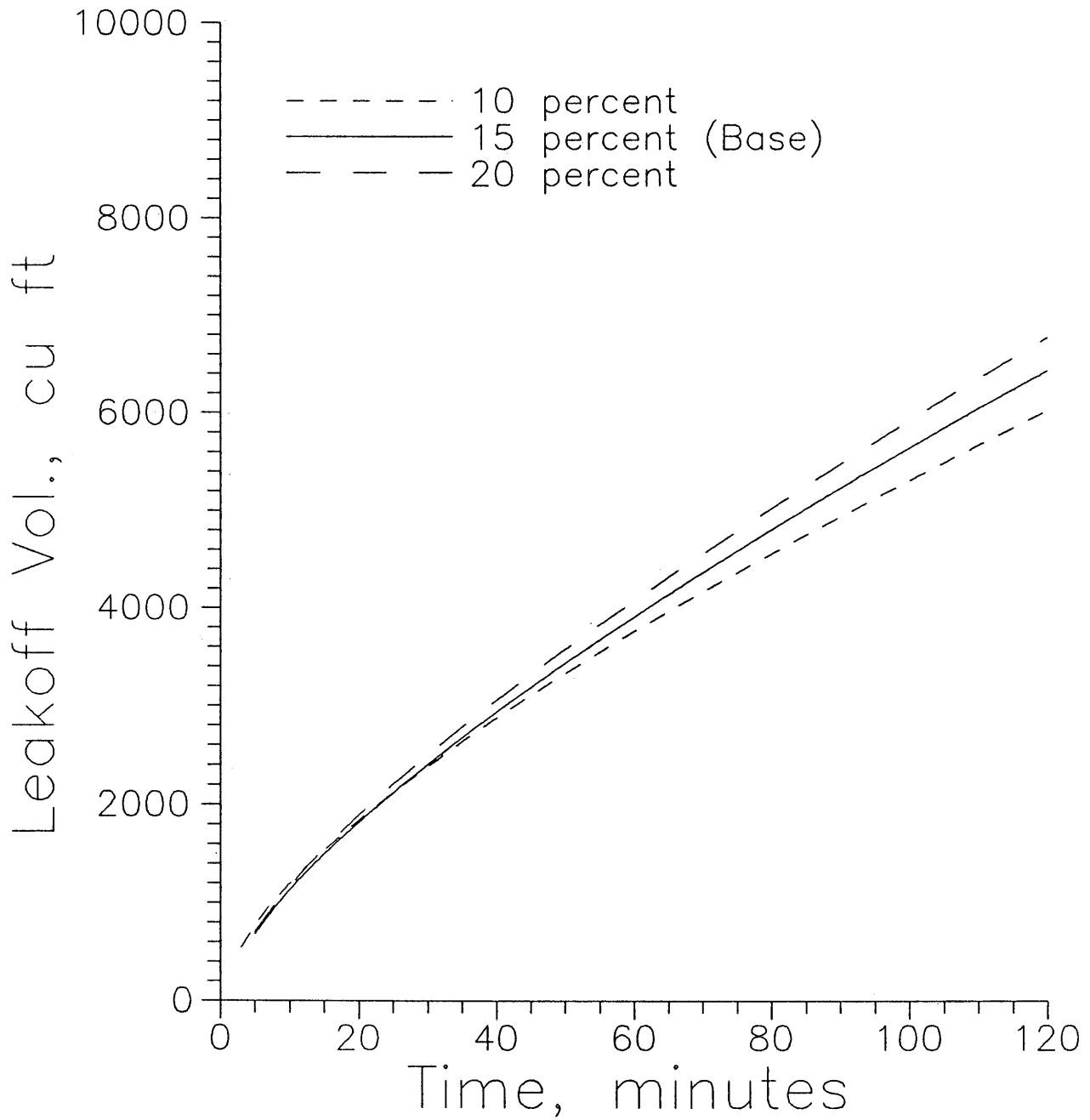
Figure 33 - Porosity Effect on Leakoff Volume

Figure 33 - Cumulative leakoff volume versus time for different values of porosity.

Figure 34 - Porosity Effect on Pressure Wave

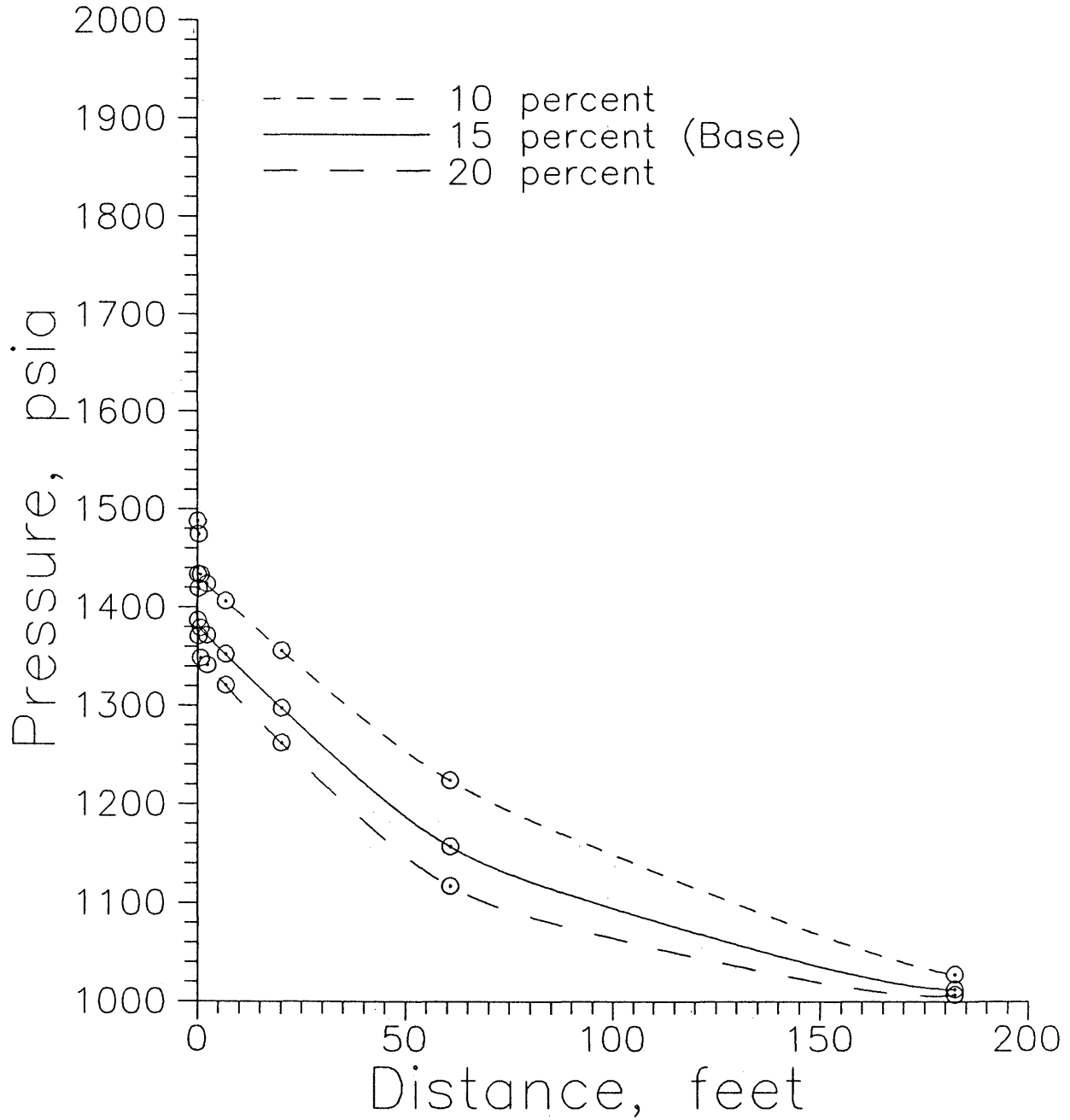


Figure 34 - Pressure versus distance for different values of porosity.

Figure 35 - Initial Pressure Drop Effect on Leakoff Volume

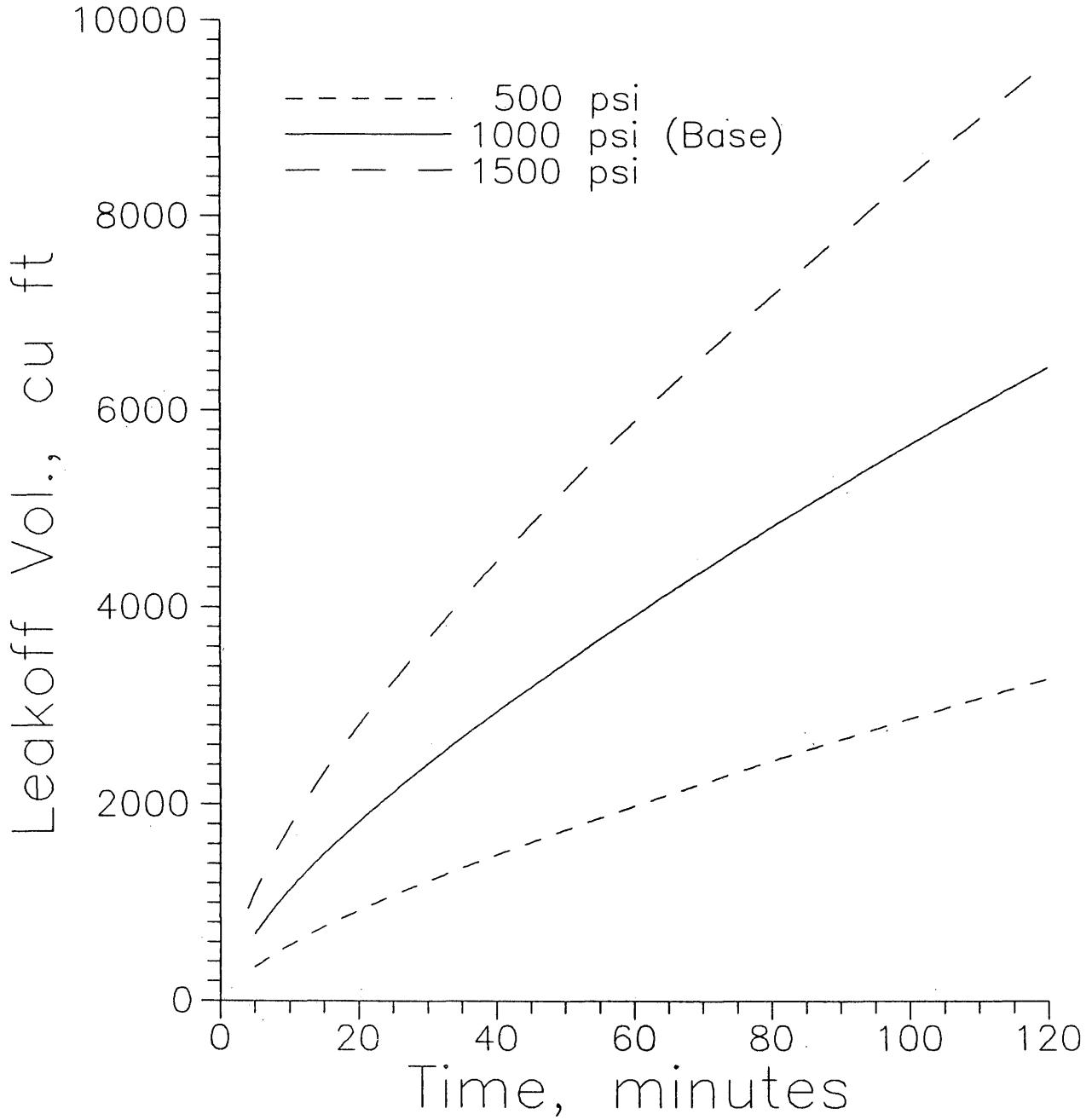


Figure 35 - Cumulative leakoff volume versus time for different values of initial pressure drop.

Figure 36 - Initial Pressure Drop Effect on Pressure Wave

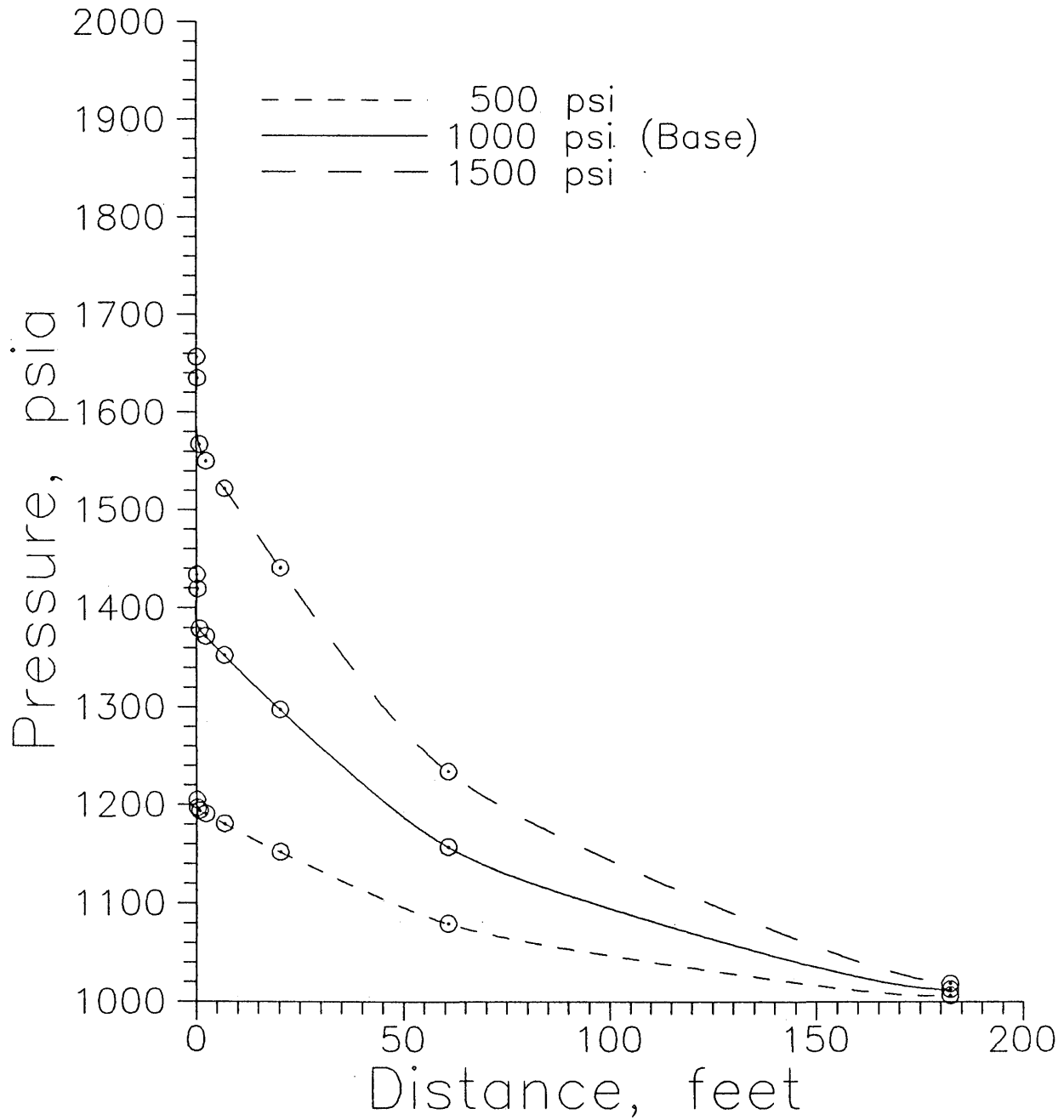


Figure 36 - Pressure versus distance for different values of initial pressure drop.

Chapter 5 - Conclusions

The new method proposed in this thesis clearly shows that filtrate leakoff is a complicated process which may not usually be modelled effectively with one simple equation. While traditional leakoff theory proposes either static or dynamic models for filtration all of the laboratory data reviewed for this paper showed evidence of a filter cake whose rate of growth had slowed, but not stopped entirely, by the end of the test. The newly derived leakoff relationship, Equation B.6, has been shown to better fit laboratory data than either the static or dynamic models. Based on the regression coefficients of Table 1 the new model fits the existing data better than a static model, hence should be more accurate in predicting field behavior. The model is superior in that it properly models the transition region between early (static) behavior and late (dynamic) behavior better than either model alone.

When compared to the only other effort at including reservoir interaction, the combined coefficient of Smith², the approach presented here projects far less leakoff. Unfortunately, the typical sandout occurs due to suspected higher leakoff than that projected by conventional methods. This may indicate that leakoff takes place in micro-fractures, either created as a byproduct of the main treatment or in a naturally fractured system.

Among the more important parameters affecting hydraulic fracture fluid leakoff are the initial pressure drop (pressure inside the fracture less the initial reservoir pressure), total system compressibility, and absolute permeability. The porosity of

the system, resident fluid viscosity, and initial water saturation all have a slightly less pronounced effect on leakoff. The least impact was produced by varying the properties of the fracture fluid itself.

Since leakoff appears to be far more complex than previously acknowledged, this work indicates the need to go beyond a simple static filtration experiment when designing a fracture treatment. It is highly recommended that laboratory filtration data be linked to a model of the reservoir so that the controllable aspects of the treatment (pressure drop and the filter cake coefficients, from Equation B.6) may be optimized. It may be possible to develop some dimensionless parameters to describe leakoff without having to resort to a simulation in each case.

Additional work should be undertaken to determine the effect of leakoff when interacting with an oil-wet system, or with gas reservoirs. In these cases leakoff may in fact be much higher than expected. Leakoff may also be unusually high in the presence of a micro-fracture system, and further study should investigate leakoff into a dual-porosity zone. Some additional insight into the invaded zone could be gained by further manipulation of the mesh space, to enable greater detail near the fracture yet allow for the depth necessary for the pressure wave. Capillary pressure effects may become highly important, particularly for gas reservoirs, and should be studied further.

Table 1 - Coefficients From Matched Filtration Data

<u>Name</u>	<u>a, min</u>	<u>u_d, cm/min</u>	<u>C, cm</u>	<u>(Sum Squared Residuals)</u>	
				<u>This Mdl</u>	<u>Static Mdl</u>
Gulbis ¹⁰	14.000	.01724098	.89745620	.0026190	.0070014
Hall and Dollarhide ⁷	8.2215	.00985819	.35906170	.0000014	.0006021
Howard and Fast ¹	5.4924	.05285336	.58875110	.0005619	.0061117
McDaniel ¹¹	22.310	.19265170	-6.285147	.1563002	1.455153
Penny ¹²	2.9250	.02002671	.00259692	.0001649	.0060427
Roodhart ¹³	20.158	.00378367	.07534383	.0001406	.0004181
Sinha ⁹	9.4400	.06165825	1.2467340	.0148067	.0825135
Williams ⁸	522.65	.00036144	.40610380	.0000259	.0009883

Table 2 - Simulation Input Data

<u>Run No.</u>	<u>μ_w, cp</u>	<u>μ_o, cp</u>	<u>k, md</u>	<u>ΔP, psi</u>	<u>Ct, 1/psi</u>	<u>ϕ, frac</u>	<u>Swi, frac</u>	<u>Figures</u>
1	4	1.0	10	1000	10 E-6	.15	.15	23 - 36
2	1	1.0	10	1000	10 E-6	.15	.15	23, 24
3	10	1.0	10	1000	10 E-6	.15	.15	23, 24
4	4	0.5	10	1000	10 E-6	.15	.15	25, 26
5	4	4.0	10	1000	10 E-6	.15	.15	25, 26
6	4	1.0	10	1000	5 E-6	.15	.15	27, 28
7	4	1.0	10	1000	20 E-6	.15	.15	27, 28
8	4	1.0	10	1000	10 E-6	.15	.35	29, 30
9	4	1.0	10	1000	10 E-6	.15	.55	29, 30
10	4	1.0	1	1000	10 E-6	.15	.15	31, 32
11	4	1.0	100	1000	10 E-6	.15	.15	31, 32
12	4	1.0	10	1000	10 E-6	.10	.15	33, 34
13	4	1.0	10	1000	10 E-6	.20	.15	33, 34
14	4	1.0	10	500	10 E-6	.15	.15	35, 36
15	4	1.0	10	1500	10 E-6	.15	.15	35, 36

Cited References

1. Howard, G.C. and Fast, C.R.: "Optimum Fluid Characteristics for Fracture Extension," Drilling and Production Practices, API (1957) pp. 261-268.
2. Smith, J.E.: "Design of Hydraulic Fracture Treatments," paper SPE 1286 presented at SPE 40th Annual Fall Meeting, Denver, Colorado, Oct. 3-6, 1965.
3. Settari, A.: "A New General Model of Fluid Loss in Hydraulic Fracturing," presented at the Symposium on Low Permeability, Denver (March 1983).
4. Krueger, R.F.: "Evaluation of Drilling Fluid Filter-Loss Additives Under Dynamic Conditions," Journal of Petroleum Technology (January 1963) p. 90.
5. Outmans, H.D.: "Mechanics of Static and Dynamic Filtration in the Borehole," Society of Petroleum Engineers Journal (September 1963) pp. 236-244.
6. Hall, C.D. and Dollarhide, F.E.: "Effects of Fracturing Fluid Velocity on Fluid-Loss Agent Performance," Journal of Petroleum Technology (May 1964) pp. 555-560.
7. Hall, C.D. and Dollarhide, F.E.: "Performance of Fracturing Fluid Loss Agents Under Dynamic Conditions," Journal of Petroleum Technology (July 1968) pp. 763-769.
8. Williams, B.B.: "Fluid Loss From Hydraulically Induced Fractures," Journal of Petroleum Technology (July 1970) pp. 882-888.
9. Sinha, B.K.: "Fluid Leak-off Under Dynamic and Static Conditions Utilizing the Same Equipment," presented at the 51st Annual Fall Technical Conference, New Orleans (October 1976).
10. Gulbis, J.: "Dynamic Fluid Loss of Fracturing Fluids," presented at the 58th Annual Fall Technical Conference, San Francisco (October 1983).
11. McDaniel, R.R., Deysarker, A.K., Callahan, M.J. and Kohlhaas, C.A.: "An Improved Method for Measuring Fluid Loss at Simulated Fracture Conditions," presented at the 56th Annual Fall Technical Conference, San Antonio (October 1981).
12. Penny, G.S., Conway, M.W. and Lee, W.S.: "The Control and Modeling of Fluid Leakoff During Hydraulic Fracturing," presented at the Formation Damage Control Symposium, Bakersfield (February 1984).
13. Roodhart, L.P.: "Fracturing Fluid, Fluid Loss Measurements Under Dynamic Conditions," presented at the Offshore Europe '83 Conference, Aberdeen, Scotland (September 1983).

14. Hagoort, J., Weatherill, B.D. and Settari, A.: "Modeling the Propagation of Waterflood-Induced Hydraulic Fractures," Society of Petroleum Engineers Journal (August 1980) pp. 293-303.
15. Veatch, R.W.: "Overview of Current Hydraulic Fracturing Design and Treatment Technology -- Part 1," Journal of Petroleum Technology (April 1983) pp. 677-687.
16. Veatch, R.W.: "Overview of Current Hydraulic Fracturing Design and Treatment Technology -- Part 2," Journal of Petroleum Technology (May 1983) pp. 853-864.
17. Crawford, H.R.: "Proppant Scheduling and Calculation of Fluid Lost During Fracturing," presented at the 58th Annual Fall Technical Conference, San Francisco (October 1983).
18. Clark, P.E. and Barkat, O.: "The Analysis of Dynamic Fluid Loss Data," Tulsa University Rheology Research Projects (TURRP), presented at the advisory meeting (November 1984).
19. Bender, M.L., Kezdy, F.J. and Wedler, F.C.: "- Chymotrypsin: Enzyme Concentration and Kinetics," Journal of Chemistry Education (1967) pp. 44,84.
20. Buell, R.S.: "Analyzing Injectivity of Non-Newtonian Fluids: An Application of the Hall Plot," Masters Thesis, Colorado School of Mines (May 1986).
21. Craig, F.F.: "The Reservoir Engineering Aspects of Waterflooding," SPE Monograph 3, (1971) p.26, Fig. 2.20.

Uncited References

1. Biot, M.A., Masse, L. and Medlin, W.L.: "A Two-Dimensional Theory of Fracture Propagation," paper SPE 11067 presented at the 57th Annual Fall Technical Conference, New Orleans (September 1982).
2. Cleary, M.P., Keck, R.G. and Mear, M.E.: "Microcomputer Models for the Design of Hydraulic Fractures," paper SPE 11628 presented at the Symposium on Low Permeability, Denver (March 1983).
3. Conway, M.W. and Harris, L.E.: "A Laboratory and Field Evaluation of a Technique for Hydraulic Fracturing Simulation of Deep Wells," paper SPE 10964 presented at the 57th Annual Fall Technical Conference, New Orleans (September 1982).
4. Cooper, G.D., Nelson, S.G. and Schopper, M.D.: "Improving Fracturing Design Through The Use of an On-Site Computer System," paper SPE 12063 presented at the 58th Annual Fall Technical Conference, San Francisco (October 1983).
5. Gall, B.L. and Raible, C.J.: "Molecular Size Studies of Degraded Fracturing Fluid Polymers," paper SPE 13566 presented at the International Symposium on Oilfield and Geothermal Chemistry, Phoenix (April 1985).
6. Geertsma, J. and Haafkens, R.: "A Comparison of the Theories for Predicting Width and Extent of Vertical Hydraulically Induced Fractures," Journal of Energy Resources Technology (March 1979) pp. 8-19.
7. Hall, B.E. and Houk, S.G.: "Fluid-Loss Control in the Naturally Fractured Buda Formation," paper SPE 12152 presented at the 58th Annual Fall Technical Conference, San Francisco (October 1983).
8. Harris, P.C.: "Dynamic Fluid Loss Characteristics of Foam Fracturing Fluids," paper SPE 11065 presented at the 57th Annual Fall Technical Conference, New Orleans (September 1982).
9. Kaspereit, D.H.: "Fracture Design for Suspended Sand Packs," paper SPE 8343 presented at the 54th Annual Fall Technical Conference, Las Vegas (September 1979).
10. McLeod, H.O.: "A Simplified Approach to Design of Fracturing Treatments Using High Viscosity Cross-Linked Fluids," paper SPE 11614 presented at the Symposium on Low Permeability, Denver (March 1983).
11. McMechan, D.E. and Conway, M.W.: "Recent Developments in Hydraulic Stimulation Treatments in the Fletcher Field in the Deep Anadarko Basin," paper SPE 11604 presented at the Symposium on Low Permeability, Denver (March 1983).

12. Medlin, W.L. and Fitch, J.L.: "Abnormal Treating Pressures in MHF Treatments," paper SPE 12108 presented at the 58th Annual Fall Technical Conference, San Francisco (October 1983).
13. Montgomery, C.T. and Steanson, R.E.: "Proppant Selection - The Key to Successful Fracture Stimulation (Revised)," paper SPE 12616 presented at the Deep Drilling and Production Symposium, Amarillo (April 1984).
14. Nghiem, L.X., Forsyth, P.A. and Behie, A.: "A Fully Implicit Hydraulic Fracture Model," Journal of Petroleum Technology (July 1984) pp. 1191-1198.
15. Nierode, D.E.: "Comparison of Hydraulic Fracture Design Methods to Observed Field Results," paper SPE 12059 presented at the 58th Annual Fall Technical Conference, San Francisco (October 1983).
16. Nolte, K.G.: "Determination of Fracture Parameters From Fracturing Pressure Decline," paper SPE 8341 presented at the 54th Annual Fall Technical Conference, Las Vegas (September 1979).
17. Nolte, K.G. and Smith, M.B.: "Interpretation of Fracturing Pressures," Journal of Petroleum Technology (September 1981) pp. 1767-1775.
18. Nolte, K.G.: "Fracture Design Considerations Based on Pressure Analysis," paper SPE 10911 presented at the Cotton Valley Symposium, Tyler, Texas (May 1982).
19. Penny, G.S.: "Nondamaging Fluid Loss Additives for Use in Hydraulic Fracturing of Gas Wells," paper SPE 10659 presented at the Formation Damage Control Symposium, Lafayette (March 1982).
20. Schlottman, B.W., Miller, W.K. and Lueders, R.K.: "Massive Hydraulic Fracture Design for the East Texas Cotton Valley Sands," paper SPE 10133 presented at the 56th Annual Fall Technical Conference, San Antonio (October 1981).
21. Settari, A.: "Simulation of Hydraulic Fracturing Processes," Society of Petroleum Engineers Journal (December 1980) pp. 487-500.
22. Settari, A. and Price, H.S.: "Simulation of Hydraulic Fracturing in Low-Permeability Reservoirs," Society of Petroleum Engineers Journal (April 1984) pp. 141-152.
23. Settari, A. and Cleary, M.P.: "Three-Dimensional Simulation of Hydraulic Fracturing," Journal of Petroleum Technology (July 1984) pp. 1177-1190.
24. Settari, A. and Cleary, M.P.: "Development and Testing of a Pseudo-Three-Dimensional Model of Hydraulic Fracture Geometry (P3DH)," paper SPE 10505 presented at the Reservoir Simulation Symposium (January/-February 1982).

25. Shah, S.N.: "Proppant Settling Correlations for Non-Newtonian Fluids Under Static and Dynamic Conditions," Society of Petroleum Engineers Journal (April 1982) pp. 164-170.
26. Smith, M.B.: "Stimulation Design for Short, Precise Hydraulic Fractures-MHF," paper SPE 10313 presented at the 56th Annual Fall Technical Conference, San Antonio (October 1981).
27. Veatch, R.W. and Crowell, R.F.: "Joint Research-Operations Programs Accelerate Massive Hydraulic Fracturing Technology," paper SPE 9337 presented at the 55th Annual Fall Technical Conference, Dallas (September 1980).
28. Zigrye, J.L., Whitfill, D.L. and Sievert, J.A.: "Fluid Loss Control Differences of Crosslinked and Linear Fracturing Fluids," paper SPE 12153 presented at the 58th Annual Fall Technical Conference, San Francisco (October 1983).

Nomenclature

a	-	filter cake "half-life," min
A	-	coefficient of new filtration equation, cm/ln(min)
A _i ,B _i ,C _i ,D _i	-	coefficients in IMPES Pressure Equation
A _w ,A _o	-	transmissibility in IMPES formulation
b _w ,b _o	-	shrinkage factor, Vol STP / Vol Res.
B _w ,B _o	-	formation volume factor, Vol Res. / Vol STP
B	-	coefficient of new filtration equation, cm/min
C	-	coefficient of new filtration equation, cm
A _c	-	core cross-sectional area, cm ²
A ₁ , B ₁	-	coefficient in equation of Bender, et al ¹⁹
b	-	exponent in equation of Bender, et al ¹⁹ and Clark, et al ¹⁸
c	-	compressibility, 1/psi
C _{eff}	-	effective fluid loss coefficient combining C _I , C _{II} & C _{III} , ft/min ^½
C _{vc}	-	effective fluid loss coefficient combining C _I & C _{II} , ft/min ^½
C _I	-	fluid loss coefficient: viscosity and relative permeability of fracture fluid, ft/min ^½
C _{II}	-	fluid loss coefficient: viscosity and compressibility of reservoir fluid, ft/min ^½
C _{III}	-	fluid loss coefficient: wall building, ft/min ^½
dP	-	pressure drop, psi
IMAX	-	number of mesh spaces in the IMPES model

k	-	permeability, md
K_r	-	relative permeability, fraction
m	-	slope of static filtration plot, $\text{cm}^3/\text{cm}^2/\text{min}^{\frac{1}{2}}$
n	-	exponent in equation proposed by Penney, et al ¹²
P	-	pressure, psi
P_c	-	capillary pressure, psi
$P_{c_{wo}}$	-	water/oil capillary pressure, psi
Q	-	injection/production from cell block, lbm/day
S	-	saturation, fraction
S_{or}	-	residual oil saturation, fraction
$S_{w_{irr}}$	-	irreducible water saturation
t	-	time, min
t_o	-	time to end of spurt loss phase, min
t_{sp}	-	time to end of spurt loss phase, min
T	-	cake thickness, cm
T_{max}	-	maximum cake thickness, cm
u_d	-	pseudo-steady state Darcy fluid velocity, cm/min
v	-	fluid velocity, cm/min
V	-	cumulative filtrate volume per unit area, cm^3/cm^2
V_{sp}	-	spurt loss, cm^3/cm^2
[V]	-	substrate concentration given by equation of Bender, et al ¹⁹

Greek Symbols

α	-	ratio of filtrate throughput to cake deposited, <u>or</u>
α	-	ratio: b_o/b_w , used in IMPES
δP	-	pressure drop, psi
Δx	-	cell block size, ft
μ	-	viscosity, cp
ϕ	-	porosity, fraction

Subscripts and Superscripts

i	-	subscript denoting the center of the cell block in question
$i+1$	-	subscript denoting the center of the next cell block
$i-1$	-	subscript denoting the center of the previous cell block
$i+\frac{1}{2}$	-	subscript denoting the face between current and next cell blocks
$i-\frac{1}{2}$	-	subscript denoting the face between current and previous cell blocks
n	-	superscript denoting current time level
$n+1$	-	superscript denoting next time level
o	-	subscript denoting oil phase
w	-	subscript denoting water phase

Appendix A - Derivation of Traditional Leakoff Formulation

Howard & Fast¹ proposed a square root of time relationship for the leakoff of a fluid through a filter cake, but gave no indication of how this was achieved. It was over 25 years later that Settari³ presented the following derivation:

Consider the cumulative throughput of leakoff fluid per unit area,

$$V = \frac{\text{cumulative filtrate volume}}{\text{unit area}} \quad (\text{A.1})$$

and assume that the volume of cake deposited is directly proportional to throughput, which implies a static filtration test with "infinite" cake buildup.

$$\alpha = \frac{\text{cumulative filtrate volume}}{\text{volume of cake deposited}} \quad (\text{A.2})$$

The filter cake thickness at any point in time may then be expressed as:

$$T = \frac{V}{\alpha}, \quad \text{cake volume per unit area} \quad (\text{A.3})$$

This expression may then be used in Darcy's law to express the velocity/pressure drop relationship across the cake:

$$u = \frac{\delta V}{\delta t} = \frac{k d P}{\mu T} = \frac{\alpha k d P}{\mu V} \quad (\text{A.4})$$

Now rearrange and integrate:

$$\int V dV = \frac{\alpha k d P}{\mu} \int dt \quad (\text{A.5})$$

$$\frac{V^2}{2} = \frac{\alpha k d P t}{\mu} \quad (\text{A.6})$$

$$V = \left[\frac{2 \alpha k d P}{\mu} \right]^{\frac{1}{2}} [t]^{\frac{1}{2}} \quad (\text{A.7})$$

If a leakoff coefficient is defined as:

$$C = \left[\frac{\alpha k d P}{2 \mu} \right]^{\frac{1}{2}} \quad (\text{A.8})$$

then,

$$V = 2C\sqrt{t} + V_{sp} \quad (\text{A.9})$$

and,

$$u = \frac{C}{\sqrt{t}} \quad (\text{A.10})$$

The leakoff coefficient may then be determined experimentally by conducting a

static filtration test and plotting cumulative filtrate throughput versus the square root of time. By Equation A.9 the coefficient is one-half the resultant slope. Equation A.10 is used in the calculation of fracture area.

Appendix B - Derivation of New Leakoff Formulation

A static filtration test does not accurately represent the dynamic conditions in a fracture. The most important error occurs in the assumption that filter cake is proportional to throughput, as this implies that the cake continues to grow linearly throughout the frac treatment. Due primarily to shear stresses exerted by the moving fluid in the fracture, in a dynamic setting the cake ceases to grow and the pressure drop across it becomes approximately constant.

In order to better model this behavior, an expression is developed in this thesis to describe a cake which grows rapidly at first, then slows until there is virtually no further growth. This approach takes the concept of Williams⁸, and uses one equation to characterize all three phases he describes. Such an equation is:

$$T = T_{\max} \left[\frac{t}{(a + t)} \right] \quad (B.1)$$

where: T_{\max} - maximum cake thickness, cm
 a - cake half life, min
 t - time, min

This satisfies the criteria that as:

$$\begin{aligned} t \rightarrow 0, T &\rightarrow 0 \\ t \rightarrow \infty, T &\rightarrow T_{\max} \end{aligned}$$

The expression is then used for the cake thickness in Darcy's equation:

$$u = \frac{\delta V}{\delta t} = \frac{k d P}{\mu T_{\max} (t/a+t)} = \frac{k d P (a+t)}{\mu T_{\max} t} = u_d \left[\left(\frac{a}{t} \right) + 1 \right] \quad (B.2)$$

where: $u_d = \frac{k d P}{\mu T_{\max}}$

Note in Equation B.2 that u_d is the Darcy velocity after the cake is fully formed. The equation makes sense also in that the initial flow before cake formation may be extremely large, exhibiting spurt loss.

$$\begin{aligned} t \rightarrow 0, u &\rightarrow \infty \\ t \rightarrow \infty, u &\rightarrow u_d \end{aligned}$$

Rearranging and integrating:

$$\int_0^V dV = u_d \int_{t_0}^t [(a/t) + 1] dt \quad (B.3)$$

$$V = u_d a \ln(t) + u_d t - u_d a \ln(t_0) \quad (B.4)$$

The term " $- u_d a \ln(t_0)$ " may be considered analogous to spurt loss in the classical formulation. Instead of representing the extrapolated volume at time zero, t_0 is the "spurt time." The value of t_0 depends on the amount of early time data taken in the experiment. In the limit:

$$\text{as } t \rightarrow 0, t \approx t_0 \text{ and } V \approx u_d t \rightarrow 0$$

This equation expresses the cumulative filtrate leakoff volume as a function of time. Note also that the Darcy velocity term contains a dP expression, so the leakoff is also a function of pressure drop across the cake. This describes the early curvature, followed by straight line pseudo-steady state behavior, seen in dynamic lab experiments. The equation may be simplified as follows:

$$\text{Let: } A = u_d a \quad (\text{B.5a})$$

$$B = u_d \quad (\text{B.5b})$$

$$C = - u_d a \ln(t_0) \quad (\text{B.5c})$$

$$\text{Then: } V = A \ln(t) + B t + C \quad (\text{B.6})$$

In this study the above relationship (Equation B.4) was used to determine the volume of fluid moved through the cake. Then the pressure drop across the cake was calculated, which in turn controls the average pressure of the first block in the simulator.

Appendix C - Derivation of IMPES Formulation

Start with the partial differential equations for water and oil:

$$\frac{\delta}{\delta x} \frac{A_w \delta P_w}{\delta x} + Q_w = \phi \frac{\delta}{\delta t} (b_w S_w) \quad (C.1)$$

$$\frac{\delta}{\delta x} \frac{A_o \delta P_o}{\delta x} + Q_o = \phi \frac{\delta}{\delta t} (b_o S_o) \quad (C.2)$$

where:

$$A_w = 0.006328 \frac{k k_{rw}}{B_w \mu_w} \quad (C.1a)$$

$$A_o = 0.006328 \frac{k k_{ro}}{B_o \mu_o} \quad (C.2a)$$

Now discretize both equations:

$$\begin{aligned} \frac{1}{\Delta x_i} A_w^{n, i+\frac{1}{2}} \frac{(P_{w_{i+1}} - P_{w_i})^{n+1}}{\Delta x_{i+\frac{1}{2}}} - A_w^{n, i-\frac{1}{2}} \frac{(P_{w_i} - P_{w_{i-1}})^{n+1}}{\Delta x_{i-\frac{1}{2}}} + Q_w^n \\ = \frac{\phi}{\Delta t} (b_w^{n+1} S_w^{n+1} - b_w^n S_w^n)_i \end{aligned} \quad (C.3)$$

$$\begin{aligned} \frac{1}{\Delta x_i} A_o^{n, i+\frac{1}{2}} \frac{(P_{o_{i+1}} - P_{o_i})^{n+1}}{\Delta x_{i+\frac{1}{2}}} - A_o^{n, i-\frac{1}{2}} \frac{(P_{o_i} - P_{o_{i-1}})^{n+1}}{\Delta x_{i-\frac{1}{2}}} + Q_o^n \\ = \frac{\phi}{\Delta t} (b_o^{n+1} S_o^{n+1} - b_o^n S_o^n)_i \end{aligned} \quad (C.4)$$

A consistent expansion of the right hand side of Equation C.3 would be:

$$(bw^{n+1}Sw^{n+1} - bw^nSw^n) \triangleq \Delta_t(bwSw) = bw^{n+1}\Delta_tSw + Sw^n\Delta_tbw \quad (C.5)$$

$$\Delta_t(bwSw) = bw^{n+1}\Delta_tSw + Sw^n \frac{bw^{n+1} - bw^n}{Pw^{n+1} - Pw^n} \Delta_tPw \quad (C.6)$$

using a chord slope for $\delta bw/\delta Pw$ (which should be adequate so long as bw doesn't change much). So,

$$\Delta_t(bwSw) = bw^{n+1}\Delta_tSw + Sw^n bw' \Delta_tPw \quad (C.7)$$

and substitute into Equations C.3 and C.4 above:

$$\begin{aligned} \frac{1}{\Delta x_i} Aw^{n_{i+\frac{1}{2}}} \frac{(Pw_{i+1} - Pw_i)^{n+1}}{\Delta x_{i+\frac{1}{2}}} - Aw^{n_{i-\frac{1}{2}}} \frac{(Pw_i - Pw_{i-1})^{n+1}}{\Delta x_{i-\frac{1}{2}}} + Qw^n_i \\ = \frac{\phi}{\Delta t} (bw^{n+1}\Delta_tSw + Sw^n bw' \Delta_tPw)_i \end{aligned} \quad (C.8)$$

$$\begin{aligned} \frac{1}{\Delta x_i} Ao^{n_{i+\frac{1}{2}}} \frac{(Po_{i+1} - Po_i)^{n+1}}{\Delta x_{i+\frac{1}{2}}} - Ao^{n_{i-\frac{1}{2}}} \frac{(Po_i - Po_{i-1})^{n+1}}{\Delta x_{i-\frac{1}{2}}} + Qo^n_i \\ = \frac{\phi}{\Delta t} (bo^{n+1}\Delta_tSo + So^n bo' \Delta_tPo)_i \end{aligned} \quad (C.9)$$

Also substitute for oil saturation,

$$S_o + S_w = 1 \quad (\text{C.10})$$

thus,

$$\Delta_t S_o = \Delta_t(1 - S_w) = \Delta_t(-S_w)' = -\Delta_t(S_w) \quad (\text{C.11})$$

and,

$$\Delta_t P_o = \Delta_t(P_w + P_{c_{wo}}) = \Delta_t P_w + \Delta_t P_{c_{wo}} \approx \Delta_t P_w \quad (\text{C.12})$$

For a slightly compressible fluid, such as water and oil, above the bubble point pressure, compressibility is related to shrinkage (and formation volume) factors by the relationships:

$$b_w = 1/B_w \quad (\text{C.13a})$$

$$b_w = 1 + c_w P_w \quad (\text{C.13b})$$

$$b_w' = c_w \quad (\text{C.13c})$$

$$b_o = 1/B_o \quad (\text{C.13d})$$

$$b_0 = 1 + c_0 P_0 \quad (C.13e)$$

$$b_0' = c_0 \quad (C.13f)$$

Substituting again, this leaves the water and oil equations in the form:

$$\begin{aligned} \frac{1}{\Delta x_i} A_w^{n_{i+\frac{1}{2}}} \frac{(P_{w_{i+1}} - P_{w_i})^{n+1}}{\Delta x_{i+\frac{1}{2}}} - A_w^{n_{i-\frac{1}{2}}} \frac{(P_{w_i} - P_{w_{i-1}})^{n+1}}{\Delta x_{i-\frac{1}{2}}} + Q_w^{n_i} \\ = \frac{\phi}{\Delta t} (b_w^{n+1} \Delta_t S_w + S_w^n c_w \Delta_t P_w)_i \end{aligned} \quad (C.14)$$

$$\begin{aligned} \frac{1}{\Delta x_i} A_o^{n_{i+\frac{1}{2}}} \frac{(P_{o_{i+1}} - P_{o_i})^{n+1}}{\Delta x_{i+\frac{1}{2}}} - A_o^{n_{i-\frac{1}{2}}} \frac{(P_{o_i} - P_{o_{i-1}})^{n+1}}{\Delta x_{i-\frac{1}{2}}} + Q_o^{n_i} \\ = \frac{\phi}{\Delta t} (-b_o^{n+1} \Delta_t S_w + S_o^n c_o \Delta_t P_w)_i \end{aligned} \quad (C.15)$$

The oil and water pressures are connected by the relationship involving capillary pressure,

$$P_o^{n+1} \approx P_w^{n+1} + P_{c_{wo}}^n \quad (C.16)$$

Thus a capillary pressure term is added to each term in the left hand side of Equation C.15, forming the new group:

$$+ \frac{1}{\Delta x_i} A_o^{n_{i+\frac{1}{2}}} \frac{(P_{c_{woi+1}} - P_{c_{woi}})^{n+1}}{\Delta x_{i+\frac{1}{2}}} - A_o^{n_{i-\frac{1}{2}}} \frac{(P_{c_{woi}} - P_{c_{woi-1}})^{n+1}}{\Delta x_{i-\frac{1}{2}}} \quad (C.17)$$

Since this is all explicit, it may be treated as a constant and placed on the right hand side of Equation C.15. Now multiply Equation C.14 by the term:

$$\alpha^{n+1}_i = \frac{b_o^{n+1}}{b_w^{n+1}} \quad (C.18)$$

and add the modified Equations C.14 and C.15. The resulting single equation (called the "Pressure Equation") may be cast in the form:

$$A_i P_{w_{i-1}}^{n+1} + B_i P_{w_i}^{n+1} + C_i P_{w_{i+1}}^{n+1} = D_i \quad (C.19)$$

, where:

$$A_i = (\alpha_i^{n+1} A_{w_{i-\frac{1}{2}}}^n + A_{o_{i-\frac{1}{2}}}^n) A / \Delta x_{i-\frac{1}{2}} \quad (C.20a)$$

$$C_i = (\alpha_i^{n+1} A_{w_{i+\frac{1}{2}}}^n + A_{o_{i+\frac{1}{2}}}^n) A / \Delta x_{i+\frac{1}{2}} \quad (C.20b)$$

$$B_i = -A_i - C_i - \frac{VP}{\Delta t} (\alpha^{n+1} S_w^n c_w + (1-S_w^n) c_o)_i \quad (C.20c)$$

$$D_i = -\frac{VP}{\Delta t} (\alpha^{n+1} S_w^n c_w + (1-S_w^n) c_o)_i P_{w_i}^n \\ - (A_o^n_{i+\frac{1}{2}} \left(\frac{A}{\Delta x_{i+\frac{1}{2}}} \right) (P_{c_{wo}}^n_{i+1} - P_{c_{wo}}^n_i) \\ - (A_o^n_{i-\frac{1}{2}} \left(\frac{A}{\Delta x_{i-\frac{1}{2}}} \right) (P_{c_{wo}}^n_i - P_{c_{wo}}^n_{i-1}) + \alpha_i^{n+1} q_{w_i}^n + q_{o_i}^n) \quad (C.20d)$$

Equation C.19 thus yields a system of "IMAX" equations for calculating the unknown water pressure at a new time level for each of the IMAX nodes. The equation is solved using a tridiagonal matrix solver. Once the updated pressures are known, the corresponding water saturations may be calculated explicitly from the "Saturation Equation,"

$$\begin{aligned}
 Sw_i^{n+1} = Sw_i^n &+ \frac{\Delta t}{VP \, bw_i^{n+1}} \left(Aw_{i+\frac{1}{2}}^n \frac{A}{\Delta x_{i+\frac{1}{2}}} (P_{w_{i+1}}^{n+1} - P_{w_i}^{n+1}) \right. \\
 &- \frac{A}{\Delta x_{i-\frac{1}{2}}} Aw_{i-\frac{1}{2}}^n (P_{w_i}^{n+1} - P_{w_{i-1}}^{n+1}) + qw_i^n \\
 &- \left. \frac{VP}{\Delta t} (Sw_i^n bw' (P_{w_i}^{n+1} - P_{w_i}^n)) \right) \quad (C.21)
 \end{aligned}$$

Appendix D - Derivation of Least Squares Regression

A least squares regression procedure for dynamic filtration data in order to solve for the constants A, B, and C in Equation B.6:

$$V = A \ln(t) + B t + C \quad (\text{B.6})$$

The sum of the squared differences may be expressed as:

$$D = \Sigma (A \ln(t_i) + B t_i + C - V_i)^2 \quad (\text{D.1})$$

The partial derivatives, with respect to each coefficient, are:

$$\delta D / \delta A = \Sigma 2(A \ln(t_i) + B t_i + C - V_i) \ln(t_i) = 0 \quad (\text{D.2a})$$

$$\delta D / \delta B = \Sigma 2(A \ln(t_i) + B t_i + C - V_i) t_i = 0 \quad (\text{D.2b})$$

$$\delta D / \delta C = \Sigma 2(A \ln(t_i) + B t_i + C - V_i) = 0 \quad (\text{D.2c})$$

Rearranging,

$$A \Sigma \ln(t_i)^2 + B \Sigma t_i \ln(t_i) + C \Sigma \ln(t_i) - \Sigma V_i \ln(t_i) = 0 \quad (\text{D.3a})$$

$$A \Sigma t_i \ln(t_i) + B \Sigma t_i^2 + C \Sigma t_i - \Sigma V_i t_i = 0 \quad (\text{D.3b})$$

$$A \sum \ln(t_j) + B \sum t_j + C N - \sum V_i = 0 \quad (\text{D.3c})$$

If we let:

$$x_1 = \sum \ln(t_j)^2, \quad x_2 = \sum t_j \ln(t_j), \quad x_3 = \sum \ln(t_j), \quad x_4 = \sum V_i \ln(t_j)$$

$$y_1 = \sum t_j \ln(t_j), \quad y_2 = \sum t_j^2, \quad y_3 = \sum t_j, \quad y_4 = \sum V_i t_j$$

$$z_1 = \sum \ln(t_j), \quad z_2 = \sum t_j, \quad z_3 = N, \quad z_4 = \sum V_i$$

Then:

$$A = \frac{[(x_2 y_3 - x_3 y_2) * (x_4 z_3 - x_3 z_4) - (x_4 y_3 - x_3 y_4) * (x_2 z_3 - x_3 z_2)]}{[(x_3 y_1 - x_1 y_3) * (x_2 z_3 - x_3 z_2) - (x_2 y_3 - x_3 y_2) * (x_3 z_1 - x_1 z_3)]} \quad (\text{D.4})$$

$$B = \frac{[(x_4 y_3 - x_3 y_4) + A(x_3 y_1 - x_1 y_3)]}{x_2 y_3 - x_3 y_2} \quad (\text{D.5})$$

$$C = [x_4 - A x_1 - B x_2] / x_3 \quad (\text{D.6})$$

This least squares regression was coded in FORTRAN and used to evaluate the coefficients from the work of Howard & Fast, Hall & Dollarhide, Gulbis, Penny, Roodhart, Kohlhaas, Sinha and Williams (see Appendix E).

Appendix E - Coefficient Regression Program Listing

```

C
C   Least Squares Fit of Leakoff Data
C
      DIMENSION T(50),V(50),SUM(8),X(4),Y(4),Z(4)
      READ(5,3) N
      DO 10 I=1,N
      READ(5,1) T(I),V(I)
10   CONTINUE
      DO 20 I=1,8
      SUM(I)=0.
20   CONTINUE
      DO 100 I=1,N
      SUM(1)=SUM(1)+T(I)
      SUM(2)=SUM(2)+T(I)**2
      SUM(3)=SUM(3)+T(I)*ALOG(T(I))
      SUM(4)=SUM(4)+ALOG(T(I))
      SUM(5)=SUM(5)+(ALOG(T(I)))**2
      SUM(6)=SUM(6)+V(I)
      SUM(7)=SUM(7)+V(I)*T(I)
      SUM(8)=SUM(8)+V(I)*ALOG(T(I))
100  CONTINUE
      X(1)=SUM(5)
      X(2)=SUM(3)
      X(3)=SUM(4)
      X(4)=SUM(8)
      Y(1)=SUM(3)
      Y(2)=SUM(2)
      Y(3)=SUM(1)
      Y(4)=SUM(7)
      Z(1)=SUM(4)
      Z(2)=SUM(1)
      Z(3)=N
      Z(4)=SUM(6)
      T1=X(4)*Y(3)-X(3)*Y(4)
      T2=X(3)*Y(1)-X(1)*Y(3)
      T3=X(2)*Y(3)-X(3)*Y(2)
      V1=X(4)*Z(3)-X(3)*Z(4)
      V2=X(3)*Z(1)-X(1)*Z(3)
      V3=X(2)*Z(3)-X(3)*Z(2)
      A=(T3*V1-T1*V3)/(T2*V3-T3*V2)
      B=(T1+A*T2)/T3
      C=(X(4)-A*X(1)-B*X(2))/X(3)
      WRITE(6,2) A,B,C
      SUM1=0.
      DO 200 I=1,N
      VV=A*ALOG(T(I))+B*T(I)+C

```

```
        SUM1=SUM1+(VV-V(I))**2
        WRITE(6,4) T(I),V(I),VV
200    CONTINUE
        SUM1=SUM1/N
        WRITE(6,5) SUM1
1     FORMAT(2F20.8)
2     FORMAT(' A = ',F15.8,' B = ',F15.8,' C = ',F15.8//)
3     FORMAT(I2)
4     FORMAT(1X,3G20.8)
5     FORMAT(///' SUM OF SQUARED RESIDUALS = ',F15.10)
        END
```

Appendix F - Leakoff Simulation Program Listing

PROGRAM LEAKOFF

C
C
C
C
C
C
C
C
C

IMPES Formulation : 1-D, 2-Phase (water/oil) System

Block 1 - Constant Rate / Injector
Block IMAX - Constant Rate / Producer

Newtonian Fluid Injection

DOUBLE PRECISION SNEW(1000),PNEW(1000),SOLD(1000),POLD(1000),
 & A1(1000),B1(1000),C1(1000),D1(1000),P1,P2,CUMINJ,XM1,
 & UW,UO,DDT,K,PF,POUT,CW,CO,A,AREA,POR,XLAMO,XLAMW,XM2,DEN,CUMOOU
 & SINIT,QOUT,AA,BB,CC,DELP,DX(1000),DT,DIFF,QI,QO,CUMWOU,VP,PIN,
 & KRW,KRO,TIM,TIME,AA1,DIST,BB1,CC1,DIFF1,MSINJ,Q2,INTER,SLOPE,
 & ALPHA,AO,AW,BO,BO1,BW,BW1,PC,QW,TERM1,DXEXP,DXI,MSINP1,MSINP2
 COMMON /PRES/POLD, /SAT/SOLD, /COMP/CW,CO
 COMMON /VIS/UO,UW, /PROP/K,A

C

READ(10,1000) UW,UO,DDT,K,PF,POUT,CW,CO,IMAX,IT,ID,A,AREA,POR
 READ(10,1000) SINIT,QOUT,AA,BB,CC,DELP
 READ(10,1000) DXI,DXEXP

C

DT=DDT/1440.
 DXI=DXI/12.
 VP=AREA*POR
 MSINP1=0.
 MSINJ=0.
 DO 100 I=1,IMAX
 DX(I)=(DXI*DXEXP**(I-1))
 POLD(I)=POUT
 PNEW(I)=POUT
 SOLD(I)=SINIT
 SNEW(I)=SINIT
 MSINP1=MSINP1+DX(I)*VP*(SOLD(I)*BW(POLD(I))+(1.-SOLD(I))*
 & BO(POLD(I),I))

100

CONTINUE
 WRITE(11,2001) MSINJ,MSINP1
 CUMINJ=0.
 CUMOOOUT=0.
 CUMWOUT=0.
 AA1=AA/DELP
 BB1=BB/DELP
 PIN=POLD(1)
 DO 10000 ITER=1,IT
 P1=PF


```

      P2=POLD(1)
C
C      RETURN POINT FOR CAKE ITERATION
C
10  CONTINUE
      DELP=PF-PIN
      BB=BB1*DELP
      AA=AA1*DELP
      TIM=ITER*DDT
      QI=(AA/TIM+BB)/30.48*AREA*1440.
      DO 150 I=1,IMAX
        A1(I)=0.
        B1(I)=0.
        C1(I)=0.
        D1(I)=0.
150  CONTINUE
      DO 200 I=2,IMAX
        A1(I)=(ALPHA(I)*AW(I-1)+AO(I-1))*AREA/((DX(I)+DX(I-1))/2.)
        B1(I)=-A1(I)
        D1(I)=(AO(I-1)*AREA/((DX(I)+DX(I-1))/2.)*(PC(I)-PC(I-1)))
200  CONTINUE
      DO 300 I=1,IMAX-1
        C1(I)=(ALPHA(I)*AW(I)+AO(I))*AREA/((DX(I)+DX(I+1))/2.)
        B1(I)=B1(I)-C1(I)
        D1(I)=D1(I)-(AO(I)*AREA/((DX(I)+DX(I+1))/2.)*(PC(I+1)-PC(I)))
300  CONTINUE
      DO 400 I=1,IMAX
        TERM1=ALPHA(I)*SOLD(I)*BW1(I)+(1.-SOLD(I))*BO1(I)
        B1(I)=B1(I)-(VP*DX(I))*TERM1/DT
        D1(I)=D1(I)-(VP*DX(I))*TERM1*POLD(I)/DT
400  CONTINUE
      D1(1)=D1(1)-ALPHA(1)*QI
      CALL TRIDIA(IMAX,B1,C1,A1,D1,PNEW)
C
C      GO BACK AND ITERATE
C
      DIFF1=(PNEW(1)-PNEW(2))/2.+PNEW(1)
      DIFF=ABS((DIFF1-PIN)/PIN)
      IF(DIFF.LE.1.E-5) GOTO 30
      SLOPE=(DIFF1-P2)/(PIN-P1)
      INTER=DIFF1-SLOPE*PIN
      P1=PIN
      P2=DIFF1
      PIN=INTER/(1.-SLOPE)
      GOTO 10
C
30  DO 700 I=1,IMAX
      SNEW(I)=SOLD(I)*CW*(PNEW(I)-POLD(I))*(VP*DX(I))/DT
      IF(I.EQ.1) GOTO 500
      SNEW(I)=SNEW(I)+AW(I-1)*AREA*(PNEW(I)-PNEW(I-1))/

```

```

      &      ((DX(I)+DX(I-1))/2.)
      IF(I.EQ.IMAX) GOTO 550
500  SNEW(I)=AW(I)*AREA*(PNEW(I+1)-PNEW(I))/
      &      ((DX(I)+DX(I+1))/2.)-SNEW(I)
      IF(I.EQ.1) SNEW(1)=SNEW(1)+QI
550  SNEW(I)=SNEW(I)*DT/(VP*DX(I))/BW(PNEW(I))+SOLD(I)
700  CONTINUE
      MSINP2=0.
      DO 800 I=1,IMAX
      POLD(I)=PNEW(I)
      SOLD(I)=SNEW(I)
      MSINP2=MSINP2+DX(I)*VP*(SOLD(I)*BW(POLD(I))+(1.-SOLD(I))*
&      BO(POLD(I),I))
800  CONTINUE
      MSINP2=MSINP2-MSINP1
      MSINP1=MSINP1+MSINP2
      TIME=TIME+DDT
      CUMINJ=CUMINJ+DT*QI
      MSINJ=DT*QI*BW(PF)
      WRITE(11,2001) MSINJ,MSINP2
      CUMWOUT=CUMWOUT+DT*QW
      CUMOOOUT=CUMOOOUT+DT*QO
      IF(ID.EQ.0) GOTO 910
      WRITE(*,1200) TIME,CUMINJ,CUMWOUT,CUMOOOUT

C
C  Write in File No. 6, for P & S
C  @ last timestep
C
      DO 900 I=1,IMAX
900  WRITE(*,2000) PNEW(I),SNEW(I)
      WRITE(*,1100)

C
C  Write in File No. 7
C  Time vs Cum Injection
C
910  QI=QI/1440./5.6148
      WRITE(*,1010) TIME,QI,CUMINJ
      WRITE(7,1010) TIME,QI,CUMINJ
      IF(TIME.EQ.5..OR.TIME.EQ.30..OR.TIME.EQ.60..OR.TIME.EQ.120.)
&  GOTO 9999
      IF(PNEW(IMAX).GT.POUT) GOTO 9999
9998  CONTINUE
10000 CONTINUE
      GOTO 9997

C
C  Write in File No. 8 & 9, for P & S respectively
C  @ last timestep
C
9999  WRITE(8,1200) TIME,CUMINJ,CUMWOUT,CUMOOOUT
      WRITE(9,1200) TIME,CUMINJ,CUMWOUT,CUMOOOUT

```

```

      DO 901 I=1,IMAX
      DIST=0.
      DO 903 J=1,I-1
903  DIST=DIST+DX(J)
      IF(I.EQ.1) DIST=0.
      DIST=DIST+DX(I)/2.
      WRITE(8,2000) DIST,PNEW(I)
      WRITE(9,2000) DIST,SNEW(I)
901  CONTINUE
      IF(PNEW(IMAX).GT.POUT) GOTO 9997
      GOTO 9998
1000 FORMAT(8F15.8/I4,2I3/3F15.8)
1010 FORMAT(1X,50G12.6)
1100 FORMAT(//)
1200 FORMAT(1X,G15.5,' MIN'/' Cum Inj - ',G15.8,' cu ft',
1/' Cum Wat - ',G15.8,' cu ft',/' Cum Oil - ',G15.8,' cu ft'/)
1500 FORMAT(1X,4G19.10)
2000 FORMAT(1X,3G15.8)
2001 FORMAT(1X,G15.5,' SCF Injected ===',G15.5,' SCF Accumulation')
9997 END
C
C
      SUBROUTINE TRIDIA(N,A,B,C,E,X)
C
C  SUBROUTINE TO SOLVE
C  TRI-DIAGONAL MATRICES
C
      DOUBLE PRECISION A(N),B(N),C(N),E(N),X(N),C1
      DO 100 I=2,N
      C1=C(I)/A(I-1)
      A(I)=A(I)-C1*B(I-1)
      E(I)=E(I)-C1*E(I-1)
100  CONTINUE
      X(N)=E(N)/A(N)
      DO 200 I=N-1,1,-1
      X(I)=(E(I)-B(I)*X(I+1))/A(I)
200  CONTINUE
      RETURN
      END
C
      FUNCTION PC(I)
      DOUBLE PRECISION SOLD(1000),K,A,PC
      COMMON /SAT/SOLD, /PROP/K,A
      PC=A*(1.25-5./3.*SOLD(I))**2
      RETURN
      END
C
      FUNCTION AW(I)
      DOUBLE PRECISION POLD(1000),K,UO,UW,A,KRW,BW,AW
      COMMON /PRES/POLD, /VIS/UO,UW, /PROP/K,A

```

```
AW=0.006328*K*KRW(I)*BW(POLD(I))/UW
RETURN
END
```

C

```
FUNCTION AO(I)
DOUBLE PRECISION POLD(1000),K,UO,UW,A,KRO,BO,AO
COMMON /PRES/POLD, /VIS/UO,UW, /PROP/K,A
AO=0.006328*K*KRO(I)*BO(POLD(I),I)/UO
RETURN
END
```

C

```
FUNCTION ALPHA(I)
DOUBLE PRECISION POLD(1000),BO,BW,ALPHA
COMMON /PRES/POLD
ALPHA=BO(POLD(I),I)/BW(POLD(I))
RETURN
END
```

C

```
FUNCTION KRW(I)
DOUBLE PRECISION SOLD(1000),KRW
COMMON /SAT/SOLD
KRW=0.2*(-0.25+5./3.*SOLD(I))**2
RETURN
END
```

C

```
FUNCTION KRO(I)
DOUBLE PRECISION SOLD(1000),KRO
COMMON /SAT/SOLD
KRO=1.0*(1.25-5./3.*SOLD(I))**2
RETURN
END
```

C

```
FUNCTION BW(P)
DOUBLE PRECISION P,CW,CO,BW
COMMON /COMP/CW,CO
BW=1.+CW*P
RETURN
END
```

C

```
FUNCTION BO(P,I)
DOUBLE PRECISION P,CW,CO,PC,BO
COMMON /COMP/CW,CO
BO=1.+CO*(P+PC(I))
RETURN
END
```

C

```
FUNCTION BW1(I)
DOUBLE PRECISION POLD(1000),P1,P2,BW,BW1
COMMON /PRES/POLD
P1=POLD(I)
```

```
P2=P1*1.01
BW1=(BW(P1)-BW(P2))/(P1-P2)
RETURN
END
```

C

```
FUNCTION BO1(I)
DOUBLE PRECISION POLD(1000),P1,P2,BO,BO1
COMMON /PRES/POLD
P1=POLD(I)
P2=P1*1.01
BO1=(BO(P1,I)-BO(P2,I))/(P1-P2)
RETURN
END
```